UNIVERSITY OF THE WITWATERSRAND, JOHANNESBURG

Synthesis and characterization of supported copper-based catalysts for thermo-catalytic hydrogenation of carbon dioxide into methanol

By

Zama Gift Duma (Student number: 717154)

Master's dissertation

Submitted in fulfilment of the requirements for the degree of MSc (Chemistry) in the School of Chemistry, Faculty of Science, University of the Witwatersrand, Johannesburg, South Africa

Supervisor(s): Dr. N. M. Musyoka, Dr. J. Moma, and Prof H. W. Langmi

August 2022

Declaration

I declare that the usage of metal-organic frameworks as supports for copper-zinc catalysts used for methanol synthesis from thermocatalytic hydrogenation of carbon dioxide is my original work, that it has not been submitted for any degree or examination in any other academic institution or university, and that all the literature sources I have utilised or quoted have been indicated and acknowledged by complete references.

Zama Gift Duma

Signed: Zama Duma 29 August 2022

Keywords

Carbon dioxide

Copper

Hydrogen

Heterogenous Catalysis

Metal-Organic Frameworks

Methanol

Thermocatalysis

Zinc

Abstract

The abatement of anthropogenic sources of carbon dioxide (CO_2) requires carbon capture and utilisation technologies which are innovative. The storage of green hydrogen (H_2) in methanol is a viable route to utilise captured CO_2. The thermocatalytic hydrogenation of CO_2 to green methanol and/or other value-added chemicals using heterogenous catalysts presents an alternative, sustainable opportunity towards carbon neutrality. The valorisation of CO_2 aims to offset the deleterious effects of greenhouse gas emissions which have already sparked global warming and climate change.

This study reports the use of heterogeneous copper-based catalysts supported on metal-organic frameworks (MOFs) for the thermocatalytic hydrogenation of CO_2 to methanol. Zirconium-based UiO-66 and aluminium fumarate MOF (AlFum MOF) were selected as supports due to their desirable physicochemical properties such as high surface area, pore-volume, and relatively high thermal stability.

Copper-based catalysts were prepared via a co-precipitation process, to form $Cu/ZnO/Al_2O_3/MgO$ (CZA) catalysts that had a similar elemental composition to a commercial-grade catalyst, and slurry phase impregnation was utilised to yield bimetallic Cu-ZnO MOF-supported catalysts. The Mg-promoted CZA catalyst prepared in this work had relatively larger CuO crystallites of 7.2 nm compared to 5.2 nm in the commercial catalyst. The latter also exhibited a larger specific surface area of 96.7 m^2/g compared to 37.9 m^2/g which is attributed to the difference in average crystallite size. In addition, despite the discrepancy in physicochemical properties, the CO_2 conversions and methanol selectivity of the Mg-promoted CZA catalyst were found to be 30.8% and 24.2% compared to 28.9% and 15% in the commercial catalyst, respectively.

Cu and Zn were supported on zirconium-based UiO-66 and AlFum MOFs via slurry phase impregnation. The crystallinity, specific surface area, and pore volume of MOF-supports were observed to decrease after metal loading and thermal activation of the catalyst precursors. The MOF-supported catalysts exhibited CO_2 conversions ranging from 0-45.6% and methanol selectivity of up to 15.7%. The Cu/ZnO/UiO-66 exhibited the greatest methanol productivity of 128 $g_{MeOH}/Kg_{cat}/h$ compared to 51.8 $g_{MeOH}/Kg_{cat}/h$ in the commercial catalyst. All the MOF-supported catalysts exhibited stability within

the 24-hour evaluation period where equilibrium CO_2 conversions were reached within 1-2 hours.

Acknowledgements and Dedication

I would like to extend my gratitude to my supervisors: Dr. Nicholas Musyoka, Dr. John Moma, and Professor Henrietta Langmi for their guidance and supervision.

I would like to thank the Royal Society-Foreign, Commonwealth & Development Office (FCDO) Africa Capacity Building Initiative (ACBI) Programme (Grant AQ150029) and CSIR for providing the funding for my bursary towards my Master's studies

The teams at Hydrogen South Africa and Carbon Capture & Utilisation, University of the Witwatersrand, University of Pretoria, and Strasbourg University for their technical and other support during my studies.

I would also like to thank God, my close friends, and my family for their continued support throughout this journey.

Contents

1 Chapter One: Introduction 1
1.1 Introduction 1
1.2 Background and motivation 1
1.3 Problem statement 3
1.4 Parent objectives 3
1.5 Outline of dissertation 4
2 Chapter Two: Literature review 5
2.1 Chapter outline 5
2.2 Carbon, capture, utilisation, and storage (CCUS) 5
2.3 Power-to-methanol 8
2.4 Carbon dioxide hydrogenation to methanol 9
2.5 Catalysts for methanol synthesis 10
2.5.1 The Reverse Water-Gas Reaction (RWGS) 13
2.6 Supports for copper-based catalysts 14
2.6.1 Metal-organic Frameworks (MOFs) as supports for catalysts 14
2.6.2 Zirconium-UiO-66 MOF 16
2.6.3 Aluminium fumarate MOF 18
2.7 Metal oxide carriers 18
2.7.1 Silicon dioxide (Silica) 18
2.7.2 Aluminium oxides 19
2.7.3 Acid-base effects of metal oxide supports on methanol synthesis 21
2.8 Chapter summary 22
3 Chapter Three: Thermocatalytic hydrogenation of CO_2 to methanol using Cu-ZnO catalysts supported on metal-organic frameworks 23
3.1 Chapter outline 23
3.2 Thermocatalytic Hydrogenation of CO_2 to Methanol Using Cu-ZnO Bimetallic Catalysts Supported on Metal–Organic Frameworks 23
3.2.1 Introduction 25
3.2.2 Results and Discussion 26
3.2.3 Materials and Methods 38
3.2.4 Conclusions 42
3.3 Chapter summary 44

4 Chapter Four: Towards high CO_2 conversions using Cu/Zn catalysts supported on aluminium fumarate metal-organic framework for methanol synthesis 45
4.1 Chapter Outline 45
4.2 Towards high CO_2 conversions using Cu/Zn catalysts supported on aluminium fumarate metal-organic framework for methanol synthesis 45
4.2.1 Introduction 46
4.2.2 Results and Discussion 48
4.2.3 Methods and Materials 57
4.2.4 Conclusions 61
4.3 Chapter summary 62
5 Chapter Five: Conclusions, Future Work and Recommendations 63
5.1 Conclusions 63
5.2 Future work and Recommendations 64
6 Appendix A 65
7 Appendix B 68
8 References 71

List of Figures

Figure 1.1. Global CO2 emissions from anthropogenic sources such as fossil fuel combustion and cement production between 1990 and 2013 (Black dots) and estimates to 2019 (Red dots). [5] 2
Figure 2.1. Schematic of the carbon capture, utilisation, and storage process.[12] 8
Figure 2.2. Methanol derived chemicals.[50] 10
Figure 2.3. Turnover frequency (TOF) of Cu-based catalysts supported and embedded in UiO-66 as well ternary Cu/ZnO/Al_2O_3. No CO was produced on Cu⊂UiO-66 at all temperatures.[101] 16
Figure 2.4. Structure and geometry of zirconium oxide-nodes and BDC linkers of UiO-66 MOF.[2] 17
Figure 2.5. Probable structure of AlFum MOF.[1] 18
Figure 3.1. (a) XRD patterns and (b) TGA profiles of commercial catalyst, Cu/ZnO/Al_2O_3/MgO catalyst, UiO-66, and Cu/ZnO/UiO-66. ♦ ZnO, ▽ CuO. ... 28
Figure 3.2. Nitrogen sorption isotherms at 77 K of (a) commercial catalyst and Cu/ZnO/Al_2O_3/MgO catalyst; (b) UiO-66 and Cu/ZnO/UiO-66; and (c) FTIR spectra of UiO-66 and Cu/ZnO/UiO-66. 31
Figure 3.3. SEM and TEM images of (a–b) UiO-66; (c–d) Cu/ZnO/UiO-66; (e–f) commercial catalyst; and (g–h) CuO/ZnO/Al_2O_3/MgO catalyst. The images were taken at different magnifications 32
Figure 3.4. XPS spectra of (a) Cu/ZnO/UiO-66 full survey, (b) Cu2p3, and (c) Zr3d. 34
Figure 3.5. H_2-TPR profiles of the prepared catalysts: (a) Commercial and Cu/ZnO/Al_2O_3/MgO catalysts; (b) UiO-66 and Cu/ZnO/UiO-66. 35
Figure 3.6. CO_2 conversions of catalysts. T = 230 °C; P = 50 bar; Qv, 0 = 40 mL·min^{-1}; GHSV = 10 000 h^{-1}. 37
Figure 3.7. Catalysts' (a) methanol selectivity; (b) CO selectivity; (c) methane selectivity and (d) space–time yield. 38
Figure 4.1. XRD patterns of (a) AlFum MOF, 7Cu/3ZnO/AlFum MOF, 15Cu/6.4ZnO/AlFum MOF; (b) 7Cu/3ZnO/AlFum MOF, 15Cu/6.4ZnO/AlFum MOF at $35^o < 2\theta < 40^o$, and (c-e) FTIR spectra of AlFum MOF, 7Cu/3ZnO/AlFum MOF, and 15Cu/6.4ZnO/AlFum MOF. CuO (♦). 49
Figure 4.2. N_2 sorption isotherms at 77 K of: (a) AlFum MOF, 7Cu/3ZnO/AlFum MOF, 15Cu/6.4ZnO/AlFum MOF; and (b) NLDFT Pore size distributions of AlFum MOF, 7Cu/6.4ZnO/AlFum MOF, and 15Cu/6.4ZnO/AlFum MOF. 50
Figure 4.3. SEM and TEM images of: (a-b) AlFum MOF; (c-d) 7Cu/3ZnO/AlFum MOF; (e-f) 15Cu/6.4ZnO/AlFum MOF; EDX elemental maps of (g) 7Cu/3ZnO/AlFum MOF, and (h) 15Cu/6.4ZnO/AlFum MOF. 52
Figure 4.4. (a) TGA profiles of AlFum MOF, 7Cu/3ZnO/AlFum MOF, 15Cu/ZnO/6.4AlFum MOF; (b) H_2-TPR profiles of: AlFum MOF, 7Cu/3ZnO/AlFum MOF, 15Cu/6.4ZnO/ AlFum MOF. 53

Figure 4.5. XPS spectra (a) Cu2p, and (b) Zn2p of 7Cu/3ZnO/AlFum MOF and, 15Cu/6.4ZnO/AlFum MOF catalysts. 54
Figure 4.6. CO_2 conversions of the catalysts. T = 230 ºC; P = 50 bar; $Q_{v,0}$ = 40 $ml.min^{-1}$; GHSV = 10 000 h^{-1}; H_2/CO_2 = 3:1 55
Figure 4.7. (a) MeOH, CO, and CH_4 selectivity and (b) MeOH space-time yield of all the tested catalysts. 57

List of tables

Table 2.1. Value-added chemicals that are produced from carbon dioxide.[12] 7
Table 3.1 Specific surface area, pore volume, and elemental loading of prepared materials..... 30
Table 4.1. Specific BET surface area, pore volume, mean pore size, and elemental loading of pristine AlFum MOF and Cu/ZnO/AlFum MOF catalysts. 50
Table 4.2. Product distribution for all the evaluated catalysts. 56

Nomenclature

AlFum MOF – Aluminium fumarate metal-organic framework

BDC – Benzene dicarboxylate

BECCS – Bioenergy with Carbon Capture and Storage

BET – Brunauer, Emmet and Teller

CO_2 – Carbon dioxide

CO – Carbon monoxide

CH_4 – Methane

CH_3OH - Methanol

EDS – Energy-dispersive X-ray spectroscopy

DMF – Dimethylformamide

Eqn - Equation

FTIR – Fourier Transform Infrared

GC – Gas chromatography

HySA&CCU – Hydrogen South Africa & Carbon Capture and Utilisation

H_2-TPR – Hydrogen temperature-programmed reduction

ICP-OES – Inductively-coupled plasma optical emission spectroscopy

MOF – Metal-organic framework

PEM – Polymer exchange membrane

PXRD – Powder X-ray diffraction

SEM – Scanning electron microscopy

SOE – Solid oxide electrolyser

TEM – Transmission electron spectroscopy

TGA - Thermogravimetric analysis

XRD -X-ray diffraction

XPS – X-ray photoelectron spectroscopy

UiO- Universitet i Oslo

Outputs

Publication(s)

- Zama G. Duma, John Moma, Xoliswa Dyosiba, Henrietta W. Langmi, Ksenia Parkhomenko, Benoit Louis, N. M. Musyoka, Thermocatalytic hydrogenation of CO_2 to methanol using Cu-Zn bimetallic catalysts supported metal-organic frameworks, *Catalysts*, **2022**, 12, 401. https://doi.org/10.3390/catal12040401 (Highly accessed article).
- Zama G. Duma, John Moma, Henrietta W. Langmi, Benoit Louis, N. M. Musyoka; Towards high CO_2 conversions using Cu/Zn catalysts supported on aluminium fumarate metal-organic framework for methanol synthesis (To be submitted).

Oral presentation(s):

- Zama G. Duma, John Moma, Xoliswa Dyosiba, Henrietta W. Langmi, Ksenia Parkhomenko, Benoit Louis, N. M. Musyoka, Thermocatalytic hydrogenation of CO_2 to methanol using Cu-Zn bimetallic catalysts supported metal-organic frameworks, 31st Catalysis Society of South Africa Conference – Virtual, 7-10 November 2021. A flash presentation was also given at the "2nd Summer School in Catalysis: from understanding to applications", Albi, France, 20-24 June 2022.
- Zama G. Duma, John Moma, Henrietta W. Langmi, Ksenia Parkhomenko, Benoit Louis, N. M. Musyoka, Towards high CO_2 conversions using Cu/Zn

catalysts supported on aluminium fumarate metal-organic framework for methanol synthesis, Gauteng Catalysis Seminar, Drakensberg, South Africa, 13-16 November 2022

Poster Presentation(s):

- Zama G. Duma, Xoliswa Dyosiba, John Moma, Henrietta W. Langmi, Ksenia Parkhomenko, Benoit Louis, N. M. Musyoka, Thermocatalytic hydrogenation of CO_2 to methanol using Cu-Zn bimetallic catalysts supported metal-organic frameworks, "2nd Summer School in Catalysis: from understanding to applications" Summer School, Albi, France, 20-24 June 2022.
- Zama G. Duma, John Moma, Henrietta W. Langmi, Ksenia Parkhomenko, Benoit Louis, N. M. Musyoka, Towards high CO_2 conversions using Cu/Zn catalysts supported on aluminium fumarate metal-organic framework for methanol synthesis, 32nd Catalysis Society of South Africa Conference, Drakensberg, South Africa, 13-16 November 2022.

Achievements during project

The following achievements were made during the study:

1. Second Runner Up: Student Oral Presentation at the 31st Catalysis Society of South Africa Conference – Virtual, 7-10 November 2021.
2. Council of Scientific and Industrial Research Best Student – Chemicals Cluster
3. Catalysis Society of South Africa national student representative 2022

Chapter One: Introduction

1.1 Introduction

This chapter outlines the purpose as well as background information for the study. It also lists the parent objectives, motivation, and problem statements associated with the project. In addition, the usage of MOFs as catalyst supports for copper-based catalysts for applications in thermocatalytic hydrogenation of carbon dioxide (CO_2) to methanol is discussed. The knowledge gaps identified in the objectives of the study are discussed as well as the synthesis of MOFs; impregnation with copper and/or promoters such as zinc; and the subsequent testing of the catalysts for methanol production via CO_2 hydrogenation.

1.2 Background and motivation

The rapid increase in the economies and population of the world has brought about a high demand for energy supply. A significant proportion of the world's energy supply comes from the combustion of non-renewable fossil fuels such as crude oil, natural gas, and coal. The use of these natural resources is associated with an alarming continuous increase in the concentration of greenhouse gases in the atmosphere.[1-4] This increase has brought about climate change, ocean acidification, and global warming which has led to an increase in mean global temperatures.[3, 5] The gradual warming of the planet has adverse effects on flora and fauna as well as the quality of human life. Levels of CO_2, a prominent greenhouse gas, in the atmosphere have been estimated to have increased by 65% since 1990. Therefore, to avert the increase in global temperatures, Carbon Capture and Utilisation (CCU) of vast amounts of anthropogenic carbon dioxide from the atmosphere is of urgent importance.[6]

Friedlingstein *et al.*[5] estimated the cumulative global CO_2 emissions between 1870 and 2014 to be 2000 ± 200 Giga tons (Gt_{CO2}) with around 25% stemming from the past 15 years alone.[5, 7] In 2013, 37 (35.2-38.9) Gt_{CO2} was released into the atmosphere (Figure 1.1). The emission of CO_2 into the atmosphere is directly proportional to the global Gross Domestic Product (GDP) due to the reliance of most economies on the combustion of non-renewable energy resources such as coal and crude oil.[8] China, the USA, EU, and India are the biggest contributors to global CO_2 emissions with 57% of the growth in global emissions emanating from China between 2013 and 2014.[5, 9]

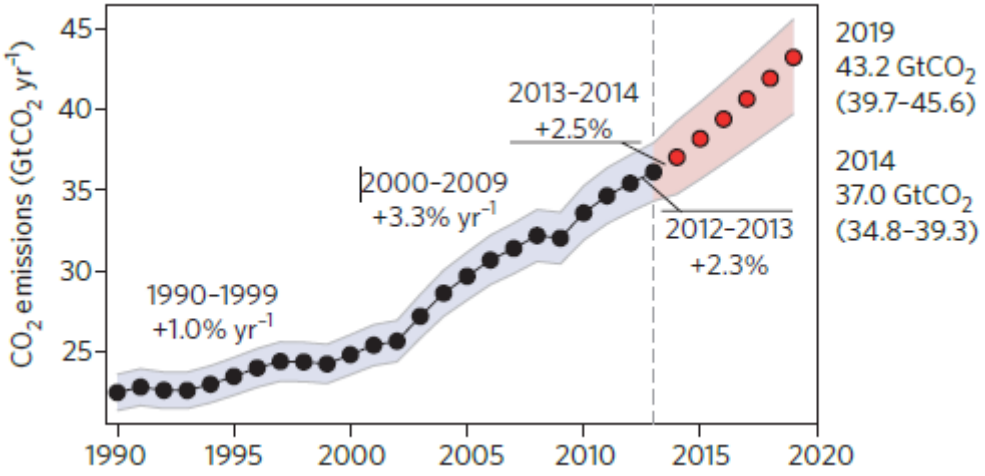

Figure 1.1. Global CO2 emissions from anthropogenic sources such as fossil fuel combustion and cement production between 1990 and 2013 (Black dots) and estimates to 2019 (Red dots). [5]

CO_2 occurs naturally as a colourless and odourless gas required in the carbon cycle for photosynthesis by plants to produce essential nutrients and comprises 0.038 % ppm (v/v) in the atmosphere. The rapid increase in CO_2 emissions globally can be ascribed to inventions of the 20th century such as cars, aeroplanes as well electricity generation from carbon-based energy sources.[10] In addition, the amount of fossil fuel sources that were made over millions of years is finite which requires a gradual transition towards sustainable, renewable, non-fossil fuel-based sources of energy.

Therefore, the rapid decline of fossil fuel reserves and detrimental effects on the planet that results from their combustion in stationary sources i.e., electric power stations and mobile sources such as cars, and trucks has given rise to mitigation strategies such as, inter alia:

- International accords amongst countries to limit the emissions of greenhouse gases to curb global warming.
- Finding alternative, greener, renewable, and sustainable sources of energy.
- Accelerated research on capture and utilisation of greenhouse gases, particularly CO_2.[11]
- The conversion of CO_2 into value-added chemicals such as methanol which can be used as a transportation fuel or as a platform molecule to produce other value-added chemicals.[12-13]

1.3 Problem statement

The sustained increase in CO_2 emissions which has existential consequences such as global warming, climate change, and ocean acidification requires technologies for its capture and utilisation. As such, the conversion of CO_2 to value-added chemicals has gained much-needed attention. One of the most prominent routes of CO_2 utilisation is the synthesis of methanol.[14] The conversion of CO_2 into value-added chemicals occurs towards the end of the CCU process which first requires the capture of a relatively pure stream of CO_2.[12] The captured CO_2 is then converted into various C1 building blocks such as urea, methanol, and formic acid, amongst others. [10, 12, 15] Therefore, the upward trend in CO_2 emissions requires urgent, innovative technologies to offset deleterious effects on the planet.

1.4 Parent objectives

The parent objective of the study is to prepare catalysts that are active for the thermocatalytic hydrogenation of CO_2 into methanol. The catalysts will encompass copper which will be loaded on supports such as metal-organic Frameworks (MOFs). The study will benchmark the supported copper-based with the conventional, promoted, ternary $Cu/ZnO/Al_2O_3$ catalysts.

The following objectives were set:

- Synthesis of high surface area and porous MOFs for optimal catalyst loading.
- Synthesis of MOF-supported copper catalysts.
- Characterisation of the synthesised MOFs and MOF-supported catalysts using techniques such as: XRD, FTIR, N_2 adsorption-desorption isotherms, TGA, microscopy, EDS, XPS, and H_2-TPR.
- Evaluation of the prepared catalysts' activity for thermocatalytic CO_2 hydrogenation into methanol.
- Comparison of the performance of the prepared catalysts and a commercial catalyst.
- Optimisation of the catalysts for methanol selectivity and CO_2 conversion.

1.5 Outline of dissertation

The dissertation reports on the available literature in the field of carbon dioxide utilisation and storage, carbon dioxide hydrogenation to methanol, typical catalysts, and key reaction in the synthesis methanol as well as conventional supports used in the carbon dioxide valorisation to methanol as outlined in Chapter Two. The first research articles, which has been published, titled is "Thermocatalytic hydrogenation of carbon dioxide to methanol using Cu-ZnO catalysts supported on metal-organic frameworks" is presented in Chapter Three in the same format in which it was published. In Chapter Four, the second manuscript from the research, which is yet to be published, titled "Towards high CO_2 conversions using Cu-ZnO catalysts supported on Aluminium fumarate metal-organic framework for methanol synthesis" is presented, including the chapter summary. The summary of the study, conclusions, summary, and future work recommendations are detailed in Chapter 5.

Chapter Two: Literature review

2.1 Chapter outline

This chapter discusses carbon dioxide capture, utilisation, and storage with a key focus on the need for the abatement of carbon dioxide emissions including technologies such as direct air capture in comparison to other capture methods. The history of carbon dioxide hydrogenation to methanol, catalysts used, key reactions, MOF-based catalysts, typical metal oxide supports, and their acid-base properties are discussed.

2.2 Carbon, capture, utilisation, and storage (CCUS)

The increase in CO_2 atmospheric emissions has brought about innovation that revolves around three global issues, the "3E's" which are: energy-environment-economy challenges. One of the most promising innovations towards combating global warming is the conversion of CO_2 into value-added chemicals such as methanol, dimethyl ether, olefins, petroleum, aromatics, and other hydrocarbons or value-added chemicals.[16] In particular, the capture and utilisation of CO_2 to form methanol has recently gained scientific and engineering scrutiny due to the benefits of methanol over hydrogen as an energy carrier.[17] CO_2, alone, can also be utilised effectively in enhanced oil recovery (EOR) as well as a solvent in supercritical or liquid states. [11, 18]

The effective utilisation of CO_2, coupled with a gradual transition towards renewable energy sources, has the propensity to reduce the increase in average global temperatures to below 2 ^oC per annum whilst limiting the usage of fossil fuels to less than 30% by 2050.[19] To date, technologies exist to convert CO_2 into value-added chemicals with the carboxylation of ammonia to form urea being the most prominent as shown in Table 2.1.[20] Salicylic acid and, most importantly, methanol for energy storage are also manufactured in considerable amounts with 100 million tons of the latter being produced per annum from CO_2.[12] Furthermore, CO_2 can be converted into other C1 compounds as well as other multi-carbon hydrocarbons such as formic acid and various carbonates. [21]

The capture of CO_2 for its valorisation first requires the successful removal of CO_2 from streams with contaminants such as biogas and flue gas. [14, 20] CO_2 can be separated from flue gas of fossil fuel-reliant power stations using proven technologies such as, inter alia: absorption using organic solvents such monoethanolamine;[22] adsorption which includes size exclusion using porous sorbents such as zeolites and activated carbons as well as;[23] cryogenic distillation at low temperatures; etc. [24] CO_2 absorption is the most mature capture methodology with regards to technology readiness in which an amine solvent absorbs CO_2 followed by its release at high temperature after which the solvent is recycled continuously.[25-26] Furthermore, the capture of CO_2 pre- or post-combustion of fossil fuels requires careful deliberation as it influences the operating cost of the process.[27] Post-combustion capture is undesirable due to the low concentration of CO_2 (4-14%) in the flue gas from coal and natural gas sources, as a result, large amounts of energy is used with little value.[28] It is therefore crucial to ensure that CO_2 capture and transportation to the site of storage and/or utilisation occurs in an economical, clean, and energy-efficient manner.[8, 26]

In addition to direct air capture (DAC) as a CO_2 source, biomass which may be obtained from waste, from industry or municipalities, is also a viable source of CO_2 and CH_4.[4, 29] As such, bio-energy with Carbon Capture and Storage (BECCS) which refers to CO_2 captured from biogenic sources also has the propensity to decrease global warming as it is part of the natural carbon cycle.[30] The utilisation of CO_2 from such sources minimizes the risk associated with CO_2 leakages from storage sites such as saline aquifers, coal bed methane (CBM), and the ocean which culminates in further global warming, eutrophication, and environmental toxicity.[8] Indeed, the major shortfall of CO_2 capture is the risk of leakage in storage sites as opposed to CO_2 utilisation.[31]

Table 2.1. Value-added chemicals that are produced from carbon dioxide.[12]

Urea (commodity)		150 million tons	112 million tons
Methanol	CH_3OH	100 million tons	2 million tons
Salicylic acid		70 thousand tons	30 thousand tons
Formaldehyde		9.7 million tons	
Formic acid		700 thousand tons	
Cyclic carbonates	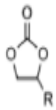	80 thousand tons	40 thousand tons
Ethylene carbonate			
Di-methyl carbonate		10 million tons	
Copolymers	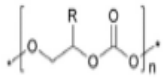		
Polymer building blocks	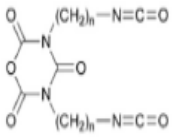		
Fine chemicals (for instance, biotin)	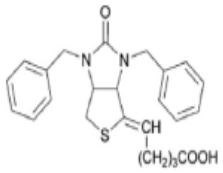		

Furthermore, as an effective alternative to CO_2 utilisation after capture, storage in geological formations is also a common approach. [27] For instance, coal bed methane (CBM) in deep coal seams can be displaced from the pores with CO_2, the latter is then subsequently converted to value-added chemicals. The process has the propensity to store up to 85 $GtCO_2$.[32] Furthermore, deep saline aquifers are also used for CO_2 storage hundreds of kilometres below the surface of Earth. The aquifers have been reported to have the highest CO_2 storage capacity of up to 10 000 Gt.[33] Therefore, the technology for CO_2 capture and storage has been demonstrated before and is a viable process as shown in the high-level CCUS schematic in Figure 2.1.

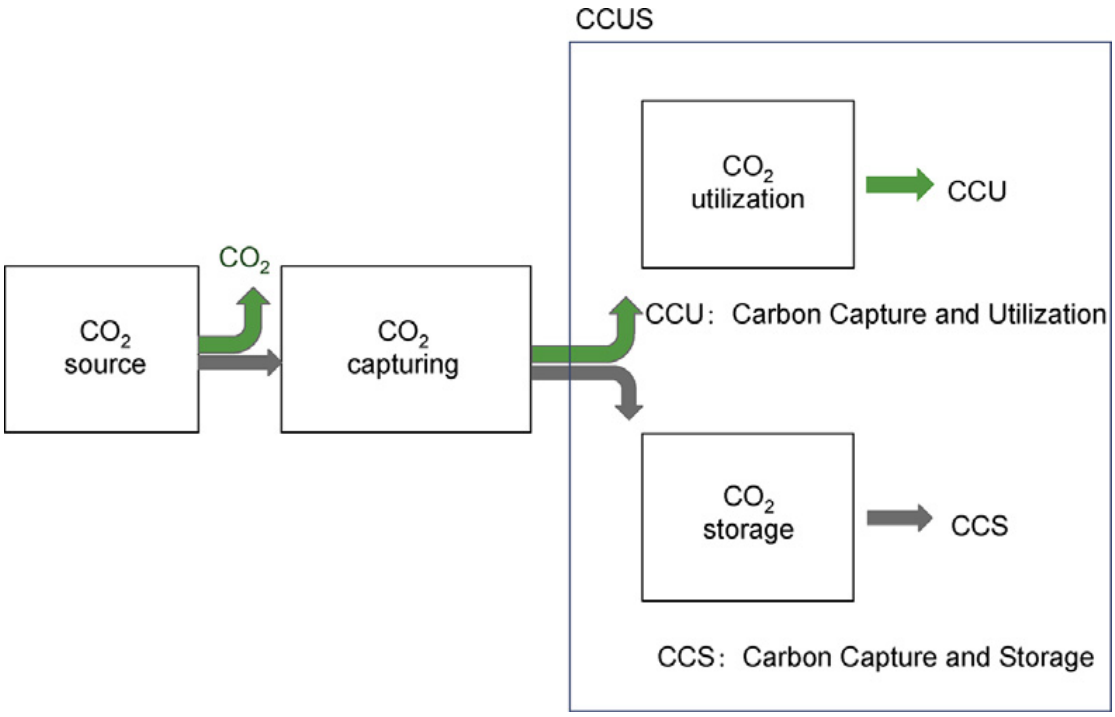

Figure 2.1. Schematic of the carbon capture, utilisation, and storage process.[12]

2.3 **Power-to-methanol**

The abatement of CO_2 emissions may also be achieved through the usage of sustainable, renewable energy sources. The usage of renewable energy i.e. wind, solar, hydroelectric, etc. to generate green hydrogen from the electrolytic splitting of water which is subsequently used to reduce CO_2 from sources such as biogas, flue gas, fossil fuel-based power stations, etc.[34] The process is conventionally referred to as Power-to-X (PtX) where X = liquid chemicals/fuels i.e. methanol or syngas. The conversion of renewable energy to value-added chemicals, electricity, etc. requires the production of green hydrogen as an energy carrier which may further be valorised to fuel hydrogen cars, energy-dense hydrogen storage compounds such as methanol, etc.[35]

Green hydrogen produced is mixed at a ratio of 3:1 with CO_2 from biogas upgrading or sequestration to produce methanol.[36] Furthermore, solid oxide electrolyser cells (SOECs), polymer-exchange membrane (PEM), and alkaline electrolysers are used to split water into oxygen and green hydrogen. The electrolysers may be powered by renewable energy sources.[35] The usage of the latter to produce value-added chemicals

has been discussed extensively where each energy and CO_2 sources are discussed with respect to techno-economics.[37-38]

2.4 **Carbon dioxide hydrogenation to methanol**

The synthesis of methanol commenced in 1923 with a catalyst prepared by Badische Anilin und Soda Fabrik (BASF) which used synthesis gas, a mixture of CO, CO_2, and H_2 produced from the gasification of coal.[39-40] The process became ubiquitous in the 1960s.[12, 39] The Zn/Cr_2O_3 catalyst had low activity and had to be run at 300-400 ºC and a pressure of 250-350 bar.[10] However, through multiple iterations and innovation as well as the relatively new technology of pure syngas production from steam reforming of methane, copper-based catalysts were developed for the synthesis of methanol from a cleaner feed of syngas i.e., the low pressure and temperature $Cu/ZnO/Al_2O_3$ catalyst developed by Imperial Chemical Industries which is active at 50-100 bar.[41] The catalyst was patented which allowed the operating conditions to be decreased to 200-300 ºC.[42]

Methanol, CH_3OH, has gained focus because it can be used as a platform molecule for the synthesis of other chemicals and can be readily produced via thermocatalytic hydrogenation.[8] Albeit homogeneous-, photocatalytic- and electrocatalytic-conversion of CO_2 is possible, heterogenous catalysis is preferred due to the ease of separation of the products and regeneration of the catalyst.[43-44] In addition, technologies exist for the conversion of methanol to olefins, MTO, and methanol to propylene, MTP, with the market demand for such products rising from 6% in 2011 to 22% in 2016 thereby making CCUS an attractive field. Furthermore, the "Methanol economy" has been cited as more practical than the "Hydrogen economy" due to the safety concerns around the handling of hydrogen. [8, 45] Methanol has the propensity to utilised directly as a fuel or fuel additive in combustion engines by increasing the octane rating to 130 and is, therefore, an ideal energy carrier that can be used at ambient conditions. [40-41, 46-47] Furthermore, methanol consists of four hydrogen atoms per molecule compared with diatomic hydrogen which consists of only two which makes it a relatively dense energy storage molecule, respectively.[48] In addition, methanol is a platform molecule for the synthesis of a wide variety of value-added chemicals such as formaldehyde, methylamines; acetic acid; and methyl *tert*-Butyl ether (MTBE), Figure 2.2, which

makes CO_2 hydrogenation to methanol a mature technology as 30-40 million tons is produced per annum.[3, 8, 39, 49] At present, majority of the methanol produced globally takes place in three rudimentary steps: (i) Synthesis gas production; (ii) catalytic methanol production for syngas conversion and; (iii) separation of the reaction products via distillation.[40]

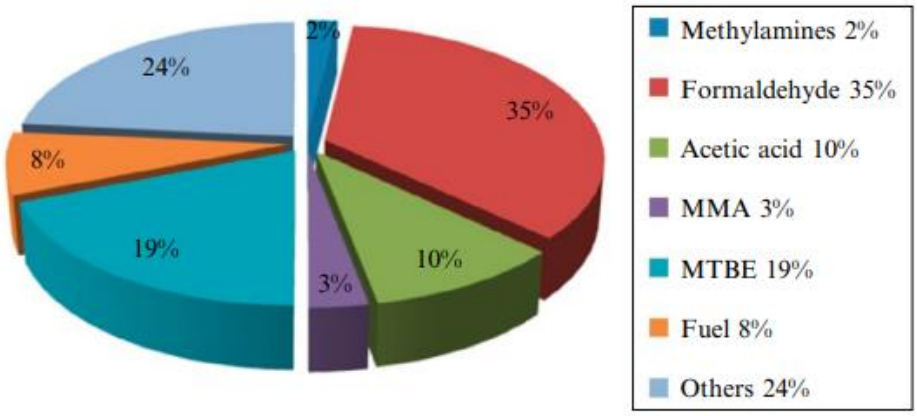

Figure 2.2. Methanol derived chemicals.[50]

Numerous green methanol demonstration plants exist globally such the pan-European mtCO_2 plants which produces green methanol using flue gas CO_2 from a coal-fired power station and green hydrogen from PEM electrolysers. The plant, located near Cologne in Germany has the propensity to produce up to 500 tons of methanol per year.[51] Other notable green methanol plant includes the George Olah plant by Carbon Recycling International (CRI) in Svartsengi, Iceland, which has the capacity to utilise up to 5600 tons of CO_2 to produce 4000 tons of methanol annually.[52] Other notable green methanol plants are located in the EU, China and Inner Mongolia.[53-54]

2.5 **Catalysts for methanol synthesis**

Currently, a significant proportion of copper-based catalysts for CO and CO_2 hydrogenation are produced via co-precipitation of metal salt precursors in a basic medium.[55-56] Metallic copper has been identified as the active site of the catalysts whereas ZnO serves multiple purposes such as: (i) Promotes the dispersion of copper

nanoparticles by preventing sintering; (ii) aids in the prevention of catalyst poisoning by impurities in the gas feed; (iii) promotes CO_2 adsorption as a basic oxide by neutralising the acidity of the catalyst.[41, 57] Furthermore, ZnO has been ascribed to act as the reservoir for atomic hydrogen as well as hydrogen spill over as it is dispersed on the Cu surfaces thereby culminating in methanol synthesis whereas the main function of Al_2O_3 is to stabilize the Cu/ZnO moiety.[17, 58-59] The proximity of Cu and Zn is vital because Cu alone reacts very poorly with CO_2.[60]

As such, the Cu/ZnO/Al_2O_3 catalyst has been in use for the industrial production of methanol from syngas since the 20th century.[60-61] The catalyst is typically prepared via hydroxycarbonate precursors viz. co-precipitation of metal nitrates in aqueous using a precipitant such as Na_2CO_3 followed by ageing in the mother liquor, filtration and washing thoroughly, drying and calcination to drive off volatile precursors and/or shaping of the catalyst.[62] After the co-precipitation step, the resultant mixture which may comprise various hydroxycarbonate precursors such as auricalcite [$(Cu,Zn)_5(OH)_6(CO_3)_2$], zincian malachite [$(Cu,Zn)_2(OH)_2CO_3$], rosasite and/or hydrotalcite-like material [$((Cu,Zn)_{1-x}Al_x)(OH)_2(CO_3)_{x/2}.mH_2O$] may be formed.[63-64] The zincian georgeite precursors [$(Cu,Zn)_7(OH)_4(CO_3)_5$] are amorphous immediately after co-precipitation, therefore, an ageing step in the mother liquor is necessary to ensure the formation of well-dispersed crystalline phases.[29, 63, 65] The amorphous hydroxycarbonate precursors transition to crystalline phases via agglomeration, re-precipitation, dissolution, and Ostwald ripening.[65] Therefore, in the design of Cu-based catalysts for catalytic hydrogenation of either CO or CO_2, the effects of the catalysts precursor morphology and crystallinity affect the crystallite size of Cu, the dispersion of Cu/Zn, and the surface area of the resultant catalyst.

The effect of Al_2O_3 as a promoter in the Cu/ZnO/Al_2O_3 catalyst has also been examined. As a refractory metal oxide, Al_2O_3 confers high activity and stability to the catalyst.[65] In addition to enhancing the thermal stability of the catalyst, Al_2O_3 also serves the purpose of a structural promoter by enhancing the distribution and specific surface area of the Cu-ZnO active phases.[66] Therefore, the addition of Al^{3+} in the Cu/Zn catalyst results in smaller Cu crystallite and consequently a high surface area.[67] Kurtz *et al.* observed that Al_2O_3-free catalysts exhibited relatively fast deactivation in the reactor which provided further evidence that Al_2O_3 also increases the stability of Cu crystallites effectively decreasing the effect of thermal sintering.[65, 68]

CO_2 is a linear, non-polar compound that is thermodynamically stable with Gibbs's free energy of -393,38 kJ/mol.[69] Therefore, in addition to the ideal catalyst, the conversion of CO_2 into methanol using hydrogen requires energy input as well as pressurisation of the reaction mixture.[39] The synthesis of methanol from CO_2 hydrogenation is characterised by three predominant reactions. Equation 2.1 is the exothermic hydrogenation of CO_2 into methanol and water.[8, 40] Based on previous observations, methanol is also produced from the hydrogenation of CO in an exothermic reaction shown by Equation 2.2.[3] CO and H_2O are produced via the reverse water-gas shift reaction (RWGS), indicated by Equation 2.3, which is characterized by the reaction of CO_2 and H_2 to yield CO and H_2O.[41, 70] There has been a lot of debate about which gas is the carbon source for methanol between CO_2 and CO, even in natural gas. However, isotopic labelling experiments have revealed that CO_2 is the main source of carbon during hydrogenation to methanol whereas the main function of CO is to maintain the active phase of Cu.[71-73]

$$CO_2 + 3H_2 \leftrightarrow CH_3OH + H_2O \qquad \Delta H = -49.47\ KJ/mol \qquad \text{Equation 2.1}$$

$$CO + 2H_2 \leftrightarrow CH_3OH \qquad \Delta H = -90.64\ KJ/mol \qquad \text{Equation 2.2}$$

$$CO_2 + H_2 \leftrightarrow CO + H_2O \qquad \Delta H = 41.14\ KJ/mol \qquad \text{Equation 2.3}$$

The formation of methanol has been widely reported to occur via the formate mechanism. In the latter, CO_2 adsorption occurs on surface metal oxides such as ZrO_2 whereas adsorption and dissociation of H_2 take place on metallic Cu sites. Thereafter, CO_2 is hydrogenated step wisely via H_2 atomic spill over with the formation and hydrogenation of the formate intermediate being the rate-determining step.[74] The formate intermediate is then hydrogenated as follows: dioxomethylene → formaldehyde → methoxy → methanol, respectively.[75] In addition, the decomposition of methanol to CO which is further hydrogenated to methanol as well the formation of carbonate surface species has also been previously described as an intermediate in CO_2 hydrogenation to methanol.[76]

2.5.1 The Reverse Water-Gas Reaction (RWGS)

The water-gas shift reaction, Equation 2.4, has long been used for ammonia synthesis as well as for the adjustment of the H_2/CO_2 ratio in the products of steam reforming of hydrocarbons.[39, 77-78] The formation of CO in the presence of Cu-based catalysts has been reported in cases where the ternary $CuO/ZnO/Al_2O_3$ has been used.[78] The RWGS, Equation 2.3, has been used over Cu-based catalysts for the conversion of CO_2 to CO and H_2O for methanol production from a pure feed of gases.[79] The mechanism of the RWGS has been under investigation for some time. The reaction has been reported to occur via a redox mechanism and a formate decomposition mechanism. The former mechanism has been cited as the most plausible for CO formation.[79] In the proposed redox mechanism, Cu^0 dissociates CO_2 into CO. The subsequent Cu_2O species is reduced to Cu^0 by H_2 forming H_2O.[39, 79-80]

$$CO + H_2 \leftrightarrow CO_2 + H_2O \qquad \Delta H = -41.14\ KJ/mol \qquad \text{Equation 2.4}$$

The other mechanistic postulate of the RWGS reaction is surface formate decomposition. Formate has been observed as a reaction intermediate in CO_2 hydrogenation to methanol using FTIR and XPS analysis.[81] The formation of CO during methanol synthesis markedly affects the selectivity of catalysts.[82] According to Le Chatelier's principle, an increase in temperature will favour the endothermic RWGS reaction which forms CO thereby decreasing selectivity to methanol.[83] Therefore, the reaction conditions such as pressure and temperature have a marked bearing on the thermodynamics of the reaction. Furthermore, the RWGS results in the formation of H_2O which deactivates the catalyst by hydrothermal sintering, via accelerated crystal growth, thereby further decreasing the activity and selectivity of the catalyst towards methanol.[84]

2.6 **Supports for copper-based catalysts**

The usage of support materials in heterogeneous catalysis, where solid particles are used to enhance liquid- or gas-phase reactions, is significant in order to markedly improve the activity, selectivity, and dispersion of active sites in the catalyst.[85-86] Support materials typically function as inert carriers or structural promoters of the active material by ensuring optimal dispersion of the active sites as well as efficient mass transfer of the reactant and products.[87-88] Supports can vary from powders to pellets with a larger particle size distribution which have a variable surface area and porosity that permit different loadings of active sites. Typical supports used include, but are not limited to: Al_2O_3; SiO_2, and TiO_2 due to their high mechanical and thermal stability which prevents the agglomeration of the active phase during catalyst evaluation in reactor runs.[89] Metal-organic frameworks (MOFs) have also gained popularity in recent years as catalyst carriers for various applications.[90-91] The usage of MOFs as porous supports for Cu-based catalysts, via strong metal-support interactions (SMSIs), for CO_2 hydrogenation to MeOH is desirable as it prevents the agglomeration/sintering which thereby decreases selectivity to methanol as the RWGS is catalysed by bulk phase Cu.[92]

2.6.1 Metal-organic Frameworks (MOFs) as supports for catalysts

MOFs are materials that are highly porous with up to 90% free volume, a high internal surface area, and exceptional crystallinity.[93] MOFs are characterised by metal inorganic clusters, nodes, or secondary building units (SBUs) that are coordinated to organic linkers and are, therefore, very tuneable in their topology.[94-96] They have a wide variety of uses ranging from the storage of energy in the form of CH_4 and H_2 as well as prospective applications in CO_2 capture post-combustion from fossil fuel-based power stations.[97] MOFs have also been under investigation for use in biogas upgrading with remarkable selectivity towards CO_2 and CH_4.[98] In addition, MOFs have been reported to have applications in heterogeneous catalysis and more interestingly, the thermocatalytic hydrogenation of CO_2 to methanol by Gutterod *et al.* who encapsulated platinum nanoparticles on a UiO-67 MOF for the synthesis of methanol from a CO_2

and H_2 mixture at 170 ^oC and 1-8 bar.[99] The catalysts were compared with platinum nanoparticles loaded on other supports such as SiO_2 and Al_2O_3. It was observed that the CO_2 conversions as well methanol selectivity were the highest for MOF-supported catalyst with Pt/SiO_2 exclusively exhibiting selectivity towards CO production. Furthermore, it was reported that the synthesis of methanol from Pt nanoparticles embedded in UiO-67 occurs via a formate intermediate with the hydrogenation of the formate species being the rate-limiting step.[99]

Zirconium-based UiO-66 MOF, characterised by Zr and ZrO_2 nodes and benzene dicarboxylic acid (BDC) linkers, as Cu support material was compared with other support materials such as ZIF-8 and MIL-101 as well as other oxidic carries including mesoporous SiO_2, Al_2O_3, ZrO_2.[59, 100-101] The prepared catalysts were tested against the conventional Cu-based catalyst for CO_2 hydrogenation viz. $Cu/ZnO/Al_2O_3$. The Cu⊂UiO-66 catalyst, Cu embedded in UiO-66, was found to have a 2-fold increase in turnover frequency for methanol production compared to any of the other supported catalysts including co-precipitated $Cu/ZnO/Al_2O_3$. In addition, Cu⊂UiO-66 catalyst was found to have a 100% selectivity towards MeOH at all temperatures ranging from 175 ^oC to 250 ^oC as shown in Figure 3. Since the RWGS reaction is endothermic, CO production anticipated at elevated reaction temperatures was not observed on Cu⊂UiO-66 catalyst compared to the $Cu/ZnO/Al_2O_3$ counterpart.[41] It was also observed that whereas Zr maintains a +4 oxidation state, Cu exists as a combination of metallic and cationic species. Cu^0 has been attributed to dissociate hydrogen molecules upon adsorption on the catalyst surface whereas cationic Cu species act to stabilise formate intermediates.[101]

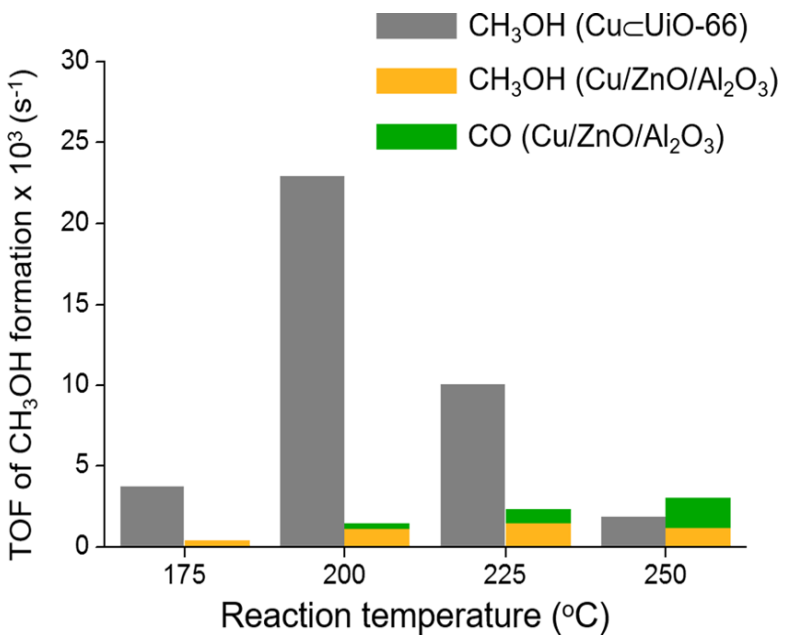

Figure 2.3. Turnover frequency (TOF) of Cu-based catalysts supported and embedded in UiO-66 as well ternary $Cu/ZnO/Al_2O_3$. No CO was produced on Cu⊂UiO-66 at all temperatures.[101]

Furthermore, An *et al.* were able to confine Cu and Zn nanoparticles in a UiO-bpy MOF support for a catalyst that exhibited high methanol activity and selectivity.[92] The study revealed that the confinement of small Cu and Zn nanoparticles on highly porous MOFs has a synergistic effect on the activity and selectivity of the catalyst. In addition, supporting Cu and Zn nanoparticles on MOFs and/or other porous materials like zeolites promotes the proximity of Cu/Zn interface which is essential for selectivity towards methanol production i.e., Cu nanoparticle growth and agglomeration on ternary $Cu/ZnO/Al_2O_3$ catalysts results in the separation of Cu and Zn.[59] The separated Cu nanoparticles then catalyse the RWGS which favours the production of CO and H_2O. It has, therefore, been demonstrated previously that it is indeed possible to load or encapsulate Cu nanoparticles in MOFs that exhibit selectivity towards methanol production from carbon dioxide hydrogenation.[92, 99, 101]

2.6.2 Zirconium-UiO-66 MOF

Zirconium-UiO-66 MOF, UiO-66, is a well-researched MOF that was first reported by the University of Oslo. UiO-66 is a zirconium-based MOF characterized by zirconium

oxide nodes or metal cluster coordinated to by 12 benzene dicarboxylate (BDC) linkers.[2] The octahedral geometry of UiO-66 is characterized by zirconium oxide clusters that are bridged by BDC linkers (Figure 2.4). UiO-66 exhibits good crystallinity, surface area, water stability and thermal stability. The latter is attributed to the Zr-O bonds in the inorganic nodes or metal cluster which have been reported to be stronger than the C-C bonds in the BDC linkers.[2, 102] In recent years, UiO-66 has been employed in catalysis for the conversion of carbon dioxide to value-added products.[103] For instance, Stawowy *et al.* observed that UiO-66-supported Cu catalyst had an enhanced activity which was attributed to unsaturated Zr sites.[104] Whereas, An *et al.* reported 100% selectivity towards methanol on UiO-bpy Cu-Zn catalysts from CO_2 hydrogenation.[92] Therefore, the usage of UiO-66 in heterogenous has been reported previously and opens up further research, particularly in the field of carbon capture, utilisation and storage.

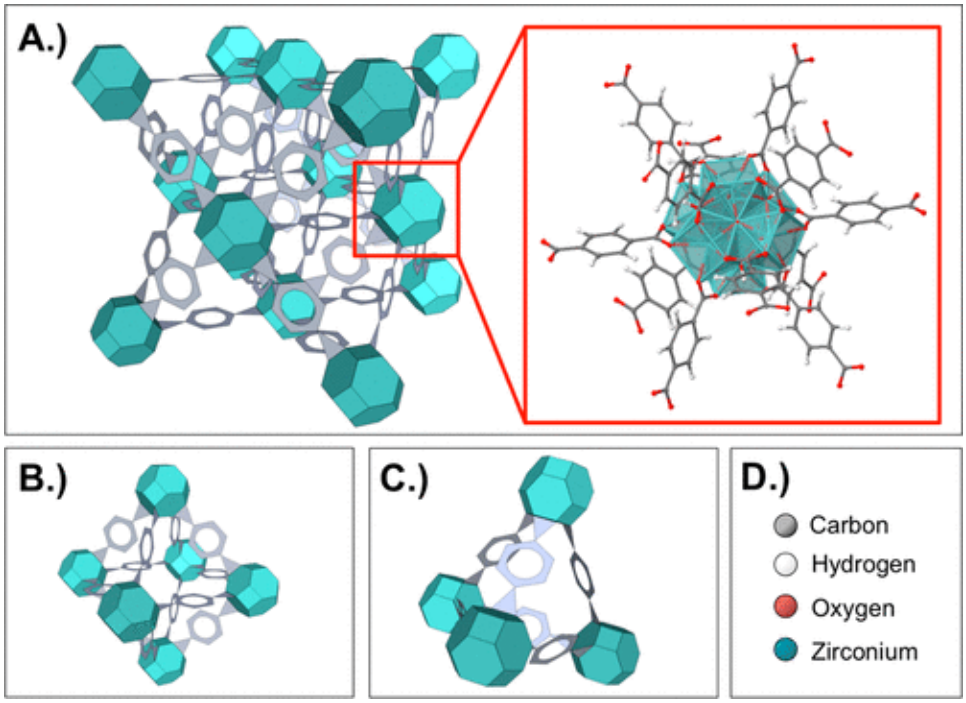

Figure 2.4. Structure and geometry of zirconium oxide-nodes and BDC linkers of UiO-66 MOF.[2]

2.6.3 Aluminium fumarate MOF

Aluminium fumarate metal-organic framework (AlFum MOF), marketed by BASF as Basolite^{TM} A520, is a robust MOF characterized by infinite Al-OH-Al chains connected by fumarate linkers (Figure 2.5).[1, 105] It has a myriad of applications including, but no limited, heat transformation, adsorbent for water purification, gas separation, gas storage, etc.[106-107] AlFum MOF presents relatively good water stability, desirable physicochemical properties such as high specific surface area and microporosity, and low-cost of synthesis via sustainable reagents.[106] AlFum MOF has not been elucidated extensively for use as catalyst support in thermocatalytic reactions, and thus, present the opportunity to design novel, AlFum MOF-supported for carbon dioxide hydrogenation to methanol.

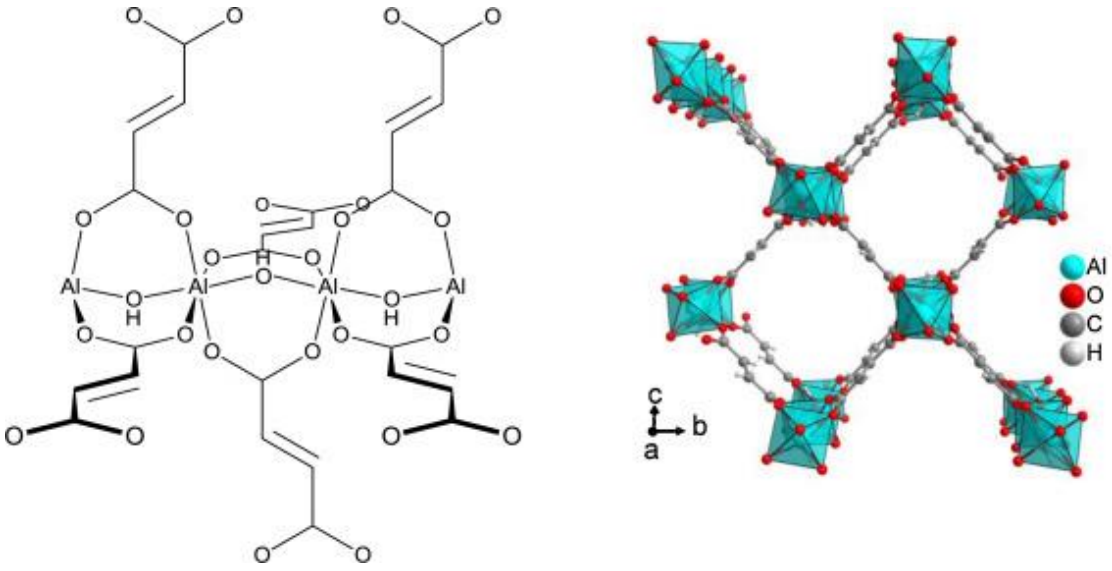

Figure 2.5. Probable structure of AlFum MOF.[1]

2.7 Metal oxide carriers

2.7.1 Silicon dioxide (Silica)

Silicon dioxide or silica (SiO_2) is a common support that is widely used in heterogeneous catalysis.[108-110] It has, therefore, also been employed in the research and development (R&D) around carbon capture and utilisation to mitigate climate change

and ocean acidification. Hengne *et al.*, for instance, synthesised Cu-Ga composites supported on mesoporous silica (SBA-15).[111] The study revealed that upon the addition of Cu and Ga to SBA-15, the surface area and pore volume decreased whilst the pore diameter remains constant. Furthermore, catalysts prepared by urea decomposition had good, homogenously dispersed, small Cu particles when matched with a catalyst prepared via wet impregnation. The addition of promoters that enhance surface acidity to silica-supported catalysts results in a beneficial two-step process where CO_2 is first hydrogenated to methanol followed by the dehydration of the latter to dimethyl ether (DME).[111-112]

Furthermore, silica is suitable as a support for the hydrogenation of CO_2 due to its relatively high surface area, good porosity, and attrition resistance.[113] In addition, the immobilisation of active phases on silica increases dispersion which lowers costs and permits for tuneable surface chemistry which can increase selectivity and activity of the catalyst.[114] The activity of the supported catalyst typically exhibits reduction at a lower temperature, high metal surface area of the active phase, and a desirable distribution of acid/base sites.[111, 115] In addition, other forms of silica, such as fumed silica, which have a high surface area can also be used as supports for the conversion of CO_2 to value-added methane via the Sabatier reaction.[116] In addition, the inert nature amorphous silica permits for the loading of active phases such as cobalt (Co) which results in catalysts that exhibit exclusive selectivity to methanol thereby suppressing the reaction pathways which results in the formation of CO and CH_4.[117]

The limitation of silica as a support in heterogenous thermocatalytic CO_2 hydrogenation is the presence of surface $Si(OH)_2$ which decreases the thermal stability of catalysts, especially in the presence of steam.[74] Furthermore, silica has the propensity to form silicide during the reduction step at elevated temperatures which further contributes to the deactivation of catalysts due to strong metal-support interactions (SMSI).[118]

2.7.2 Aluminium oxides

Aluminium oxide, alumina, or Al_2O_3, is also a prominent support material in heterogenous catalysis. It has a myriad of applications and can be used as a support or

structural promoter as in the case of co-precipitated $Cu/ZnO/Al_2O_3$ where less than 10% is incorporated into the catalysts' architecture.[41, 59] Maniecki *et al.* benchmarked various support materials for activity towards the WGS reaction as well as methanol synthesis before and after copper loading.[119] The study utilised ZnO; $ZnAl_2O_4$; $CrAlO_3$; Al_2O_3; Cr_2O_3 and $FeAlO_3$ and evaluated their physicochemical properties. It was found that after support preparation, Al_2O_3 had the highest specific surface area at 237 m^2/g which decreased with an increase in calcination temperature. The study revealed that the choice of supports has an influence on the catalytic performance with Cu supported on $ZnAl_2O_4$ exhibiting the highest activity and selectivity toward methanol synthesis from CO_2 and H_2, respectively.

In addition, the usage of gamma (γ) alumina as a support for Cu-Zn bimetallic catalyst with applications in CO_2 hydrogenation to methanol has been reported.[120] It is worth noting that calcination temperature and molar ratio of Cu/Zn have a significant impact on the surface area and reducibility of the catalysts which, in turn, affect the CO_2 conversions and selectivity to methanol. The usage of γ-alumina as a support for Cu-based catalysts is desirable for a variety of catalytic reactions such as NO_x reduction to N_2, CO oxidation, and the WGS reaction due to the high dispersion of Cu on the support.[121] Therefore, the latter may have an influence on the surface oxidation state of Cu which therefore affects the type of reaction that is catalysed i.e. Cu^0 catalyses the hydrogenation of CO_2 whereas Cu^+ has applications in photocatalysis.[122]

The use of Cu/γ-alumina also has cost benefits, due to their relatively high catalytic activity, over noble metals.[123] Due to the inherent surface acidity of alumina, Cu/γ-alumina catalysts are often promoted with alkaline and basic metallic oxides for example ZrO_2, ZnO, and MgO which increase Cu reactive surface area, dispersion as well the CO_2 conversion and methanol selectivity.[124] Therefore, the benefits of employing γ-alumina as a support for Cu-based catalysts results has numerous advantages including the emerging field of CO_2 valorisation reactions.

The drawback of alumina as a support includes poor stability of the catalyst during reactor, SMSI which leads to deactivation as well the hydrophilic nature of alumina which further decreases the performance of the catalyst, especially in water forming reaction such as CO_2 hydrogenation to methanol.[74]

2.7.3 Acid-base effects of metal oxide supports on methanol synthesis

A significant proportion of heterogeneous catalysts is characterized by reactions that occur on the surface where reactants are adsorb, oriented for reaction, and products desorbed.[125] Therefore, catalysts design requires careful attention to the surface properties of oxidic supports or active sites. Tagawa *et al.* assessed the effects of acidic and basic sites of a variety of metal oxide supports on CO_2 conversion as well as CO and methanol selectivity.[126] Through *in situ* infrared spectroscopy (IR) studies, the study was able to discern that methanol synthesis occurs via formate species intermediate that are preceded by surface bicarbonates. Therefore, acid and basic sites have the following implications on the reaction mechanism: (i) Basic sites have a high affinity towards CO_2 adsorption, which is acidic, thereby increasing bicarbonate and formate intermediates which can be hydrogenated to methanol,[127] and (ii) Acidic sites on the catalyst decrease the stability of formate intermediate species thereby decreasing selectivity to methanol. In addition, the presence of strong basic sites promotes the hydrogenation of surface carbon species to methanol instead of CO, thereby enhancing selectivity.[127-128] The basicity of Cu-based catalysts can be enhanced by basic solid oxides such as, inter alia, ZnO, ZrO_2, MgO, and La_2O_3.[17, 127-128] Surface basic sites may exist as (i) weakly basic, due to OH^- groups; (ii) moderately basic, emanating from metal-oxygen parts i.e. Zn-O, Zr-O, Mg-O, etc.; and (iii) strongly basic due low-coordination oxygen atoms or coordinatively unsaturated O^{2-} anions.[129-130]

In addition, the modification of Cu-based catalysts with basic sites such as ZrO_2 and Ga_2O_3 increases the adsorption capacity of CO_2. Therefore, the migration of H-atoms from the Cu^0 active sites to medium and strong basic sites increase CO_2 conversions, methanol selectivity and space-time yield.[131] Therefore, the modification of Cu-based catalyst for CO_2 hydrogenation with basic sites is imperative in the activity and selectivity of the catalysts.

Metal oxide supports with acidic sites such as Al_2O_3-SiO_2 have high selectivity towards dimethyl ether production whereas supports with basic sites or are neutral such as MgO and pristine SiO_2 have high selectivity towards CO and methanol production due to the RWGS reaction since both products are formed via a similar formaldehyde intermediate pathway.[111, 129] In addition, supports such as TiO_2 exhibit a high activity towards

methanol production by increasing the amount of weak basic sites in the catalyst.[127, 132] In supports like Al_2O_3, dimethyl ether is formed via the dehydration of methanol due to the presence of Lewis and Brønsted acid sites.[133] Furthermore, the CO_2 conversions of Cu-based catalysts supported on acidic metal oxides are low due to the prevention of CO_2 adsorption on the surface whereas the opposite is true for basic metal oxide supports.[126, 129] However, the basic sites stabilize the bicarbonate and formate species strongly which subsequently decompose into CO thereby resulting in low selectivity towards methanol. Therefore, the CO_2 conversions on various metal oxide supports such as Al_2O_3, TiO_2, ZrO_2, MgO, Al_2O_3-SiO_2, and SiO_2 depend on the surface acidity and basicity, respectively. Furthermore, the selectivity of the catalysts towards methanol, CO, dimethyl ether is also reliant on the surface chemistry of metal oxide supports.

2.8 **Chapter summary**

In this chapter, carbon capture, utilisation, and storage as well as the approach to each CCUS strategy was discussed. Furthermore, the valorisation of carbon dioxide to methanol, primitive and novel catalysts used, and key reactions were discussed. Power-to-Methanol concepts was discussed as well as the sources of green hydrogen and CO_2 anthropogenic sources. In addition, the usage of MOFs as catalysts support was discussed where improved methanol selectivity and turnover frequency were enhanced in MOF-supported catalysts. Metal-oxide supports were also discussed with an emphasis on their surface acid-base properties and the effect they have on the performance of the catalysts. The two MOFs employed in this study as catalyst supports, UiO-66 and AlFum MOF, were summarised.

Chapter Three: Thermocatalytic hydrogenation of CO_2 to methanol using Cu-ZnO catalysts supported on metal-organic frameworks

3.1 Chapter outline

This chapter displays the first manuscript from the project titled "Thermocatalytic hydrogenation of CO_2 to methanol using Cu-ZnO catalysts supported on metal-organic frameworks" which was published in *Catalysts* journal and can be accessed here:

Duma, Z.G.; Dyosiba, X.; Moma, J.; Langmi, H.W.; Louis, B.; Parkhomenko, K.; Musyoka, N.M. Thermocatalytic Hydrogenation of CO_2 to Methanol Using Cu-ZnO Bimetallic Catalysts Supported on Metal–Organic Frameworks. *Catalysts* **2022**, *12*, 401. https://doi.org/10.3390/catal12040401; Impact factor: 4.5.

3.2 Thermocatalytic Hydrogenation of CO_2 to Methanol Using Cu-ZnO Bimetallic Catalysts Supported on Metal–Organic Frameworks

Zama G. Duma [1,2], Xoliswa Dyosiba [1], John Moma [2], Henrietta W. Langmi [3], Benoit Louis [4], Ksenia Parkhomenko [4] and Nicholas M. Musyoka [1,*]

[1] Centre for Nanostructures and Advanced Materials (CeNAM), Chemicals Cluster, Council for Scientific and Industrial Research (CSIR), Meiring Naudé Road, Brummeria, Pretoria 0184, South Africa; zduma@csir.co.za (Z.G.D.); xdyosiba@csir.co.za (X.D.)

[2] Molecular Sciences Institute, School of Chemistry, University of the Witwatersrand, Private Bag 2001, Johannesburg, South Africa; john.moma@wits.ac.za

[3] Department of Chemistry, University of Pretoria, Private Bag X20, Hatfield 0028, South Africa; henrietta.langmi@up.ac.za

[4] Energy and Fuels for a Sustainable Environment Team, Institut de Chimie et Procédés pour l'Energie, l'Environnement et la Santé, UMR 7515 CNRS—ECPM, Université de Strasbourg, 25 rue Becquerel, 67087 Strasbourg Cedex 2 France; blouis@unistra.fr (B.L.); parkhomenko@unistra.fr (K.P.)

* Correspondence: nmusyoka@csir.co.za; Tel.: +27-12-841-4806

Abstract: The thermocatalytic hydrogenation of carbon dioxide (CO_2) to methanol is considered as a potential route for green hydrogen storage as well as a mean for utilizing captured CO_2, owing to the many established applications of methanol. Copper–zinc bimetallic catalysts supported on a zirconium-based UiO-66 metal–organic framework (MOF) were prepared via slurry phase impregnation and benchmarked against the promoted, co-precipitated, conventional ternary $CuO/ZnO/Al_2O_3$ (CZA) catalyst for the thermocatalytic hydrogenation of CO_2 to methanol. A decrease in crystallinity and specific surface area of the UiO-66 support was observed using X-ray diffraction and N_2-sorption isotherms, whereas hydrogen-temperature-programmed reduction and X-ray photoelectron spectroscopy revealed the presence of copper active sites after impregnation and thermal activation. Other characterisation techniques such as scanning electron microscopy, transmission electron microscopy, and thermogravimetric analysis were employed to assess the physicochemical properties of the resulting catalysts. The UiO-66 (Zr) MOF-supported catalyst exhibited a good CO_2 conversion of 27% and 16% selectivity towards methanol, whereas the magnesium-promoted CZA catalyst had a CO_2 conversion of 31% and methanol selectivity of 24%. The prepared catalysts performed similarly to a CZA commercial catalyst which exhibited a CO_2 conversion and methanol selectivity of 30% and 15%. The study demonstrates the prospective use of Cu-Zn bimetallic catalysts supported on MOFs for direct CO_2 hydrogenation to produce green methanol.

Keywords: CO_2 hydrogenation; bimetallic catalysts; metal–organic frameworks; catalysis; methanol economy

3.2.1 Introduction

The continuous increase in atmospheric CO_2 levels propelled by fossil fuel combustion has caused an unprecedented rise in mean global temperatures [1–4]. The increase in the atmospheric concentration of anthropogenic CO_2 contributes vastly to the greenhouse effect, which culminates in heat being trapped in the Earth's atmosphere [5]. In recent years, there has been a collective effort to research ways to capture, store, and utilise CO_2. A possible route for curbing the deleterious effects of global warming caused by greenhouse gas emissions is the conversion of CO_2 into value-added chemicals such as methanol, dimethyl ether, formaldehyde, and acetic acid [5–7]. The thermocatalytic hydrogenation of CO_2 is a proven approach towards the production of renewable methanol in substantial quantities [8–13]. Indeed, "The Methanol Economy" outlined by Olah et al. cites the advantages of CO_2 conversion to methanol where each molecule produced consists of four hydrogen atoms and is, therefore, a suitable energy storage molecule which is a liquid at ambient conditions. Furthermore, methanol may be used directly as a fuel in internal combustion engines to further curb the deleterious effects of anthropogenic CO_2 emissions [14]. Since the late 1960s, methanol has been produced from syngas (CO, CO_2, and H_2) over a coprecipitated ternary catalyst, $Cu/ZnO/Al_2O_3$, at pressures and temperatures ranging between 50 and 80 bar and 210 and 290 °C [15–17].

In recent years, $Cu/ZnO/Al_2O_3$ catalysts have been studied for the thermocatalytic hydrogenation of CO_2 to methanol [18–22]. Though the catalysts exhibit CO_2 conversion and methanol selectivity, the promoter effects conferred by ZnO_x, which induces morphological changes, and its function as a spacer for Cu active sites are diminished by the temperature and pressure conditions in the reactor with time [23–25]. The phase separation of Cu/ZnO_x results in the agglomeration, sintering, and poor dispersion of Cu nanoparticles, which consequently decreases activity towards methanol production due to a decrease in the metallic surface area of the Cu active sites. In addition, the deactivation attributed to the phase separation and sintering of Cu nanoparticles can catalyse the reverse water–gas shift reaction (RWGS), which produces carbon monoxide (CO) and water (H_2O) from the CO_2/H_2 inlet gas mixture, thereby decreasing the catalysts' selectivity to methanol [23,26,27]. The phase separation of Cu-based catalysts can be circumvented by the deposition and/or

encapsulation of Cu/ZnO_x nanoparticles into metal–organic frameworks (MOFs) [28,29]. MOFs are a class of highly crystalline, nanoporous materials prepared via the self-assembly of metal ion clusters and multidentate organic linkers [30,31]. Recently, MOFs have been identified as prospective supports for Cu-based CO_2 hydrogenation catalysts. Rungtaweevoranit et al., for instance, encapsulated and deposited Cu nanoparticles on a Zr-based MOF (UiO-66) and observed that the latter exhibited an 8-fold increase in turnover frequency when compared to the conventional Cu/ZnO/Al_2O_3 catalyst [4]. In addition to the confinement of Cu nanoparticles by strong support–metal interactions (SMSI), MOFs such as UiO-66 exhibit chemical promotion by charge transfer from Cu to the MOF, which significantly enhances the activity of the hybrid catalysts towards CO_2 hydrogenation [32]. Therefore, the purpose of this study is to elucidate the performance of novel Cu-Zn bimetallic catalysts supported on a zirconium-based MOF, UiO-66(Zr), prepared via slurry-phase impregnation compared with conventional ternary promoted Cu/ZnO/Al_2O_3 catalysts.

3.2.2 Results and Discussion

3.2.2.1 Characterisation

XRD and Thermogravimetric Analysis (TGA)

The XRD analytical results of the co-precipitated commercial and CuO/ZnO/Al_2O_3/MgO catalysts are shown in Figure 3.1a, where the crystalline phase of CuO is observed at $35° < 2\theta < 39°$ whilst that of ZnO can be seen at 31, 33, and 37° [5,18,33–35]. The average crystallite sizes of CuO at $2\theta = 38.7°$ in the commercial and CuO/ZnO/Al_2O_3/MgO catalysts, calculated using the Debye–Scherrer equation, were found to be 5.2 and 7.8 nm, respectively. The smaller CuO crystallite sizes in the commercial catalyst can be attributed to a high Cu dispersion [36,37]. The XRD results of the pristine UiO-66 support and Cu/ZnO/UiO-66 also shown in Figure 3.1a are typical of the crystalline phase with peaks at $2\theta = 7.4$, 8.5 and 14.1, 14.7, 17, 18.6, and 19.1° [38,39]. Neither the copper nor zinc phases (Cu^0, CuO, Cu_2O, or ZnO) could be observed in Cu/ZnO/UiO-66, potentially attributed to the high Cu and Zn dispersion over the framework or low metal loading [3].

The thermal stabilities of the commercial and Cu/ZnO/Al_2O_3/MgO catalysts as well as the MOF-supported catalyst were determined using thermogravimetric analysis in comparison to the commercial catalyst shown in Figure 3.1b. The commercial and Cu/ZnO/Al_2O_3/MgO catalysts were observed to exhibit thermal stability up to 900 °C. The mass loss observed in UiO-66 and Cu/ZnO/UiO-66 from 100 to 350 °C is attributed to the removal of dimethylformamide (DMF), ethanol, H_2O, and residual carboxylic acid groups (Figure 3.1b) [38,40]. The almost linear weight loss of UiO-66 and Cu/Zn/UiO-66 between 300 and 500 °C is indicative of the high thermal stability of the Zr-based MOF, after which ZrO_2 is formed due to the degradation of the organic linkers [41]. Furthermore, the thermal stability of UiO-66 decreases after impregnation and thermal activation at 350 °C. The thermal stability of the catalysts is essential for the stability under reactor conditions at 230 °C and 50 bar to prevent catalyst deactivation due to thermal degradation and MOF-support structural collapse. Therefore, all the as-prepared catalysts are anticipated to be relatively stable over time on stream while the reactor operates continuously for CO_2 hydrogenation. Furthermore, it can be seen that the commercial and Cu/ZnO/Al_2O_3/MgO catalysts are relatively more thermally stable than UiO-66 and the Cu/ZnO/UiO-66 catalyst, respectively.

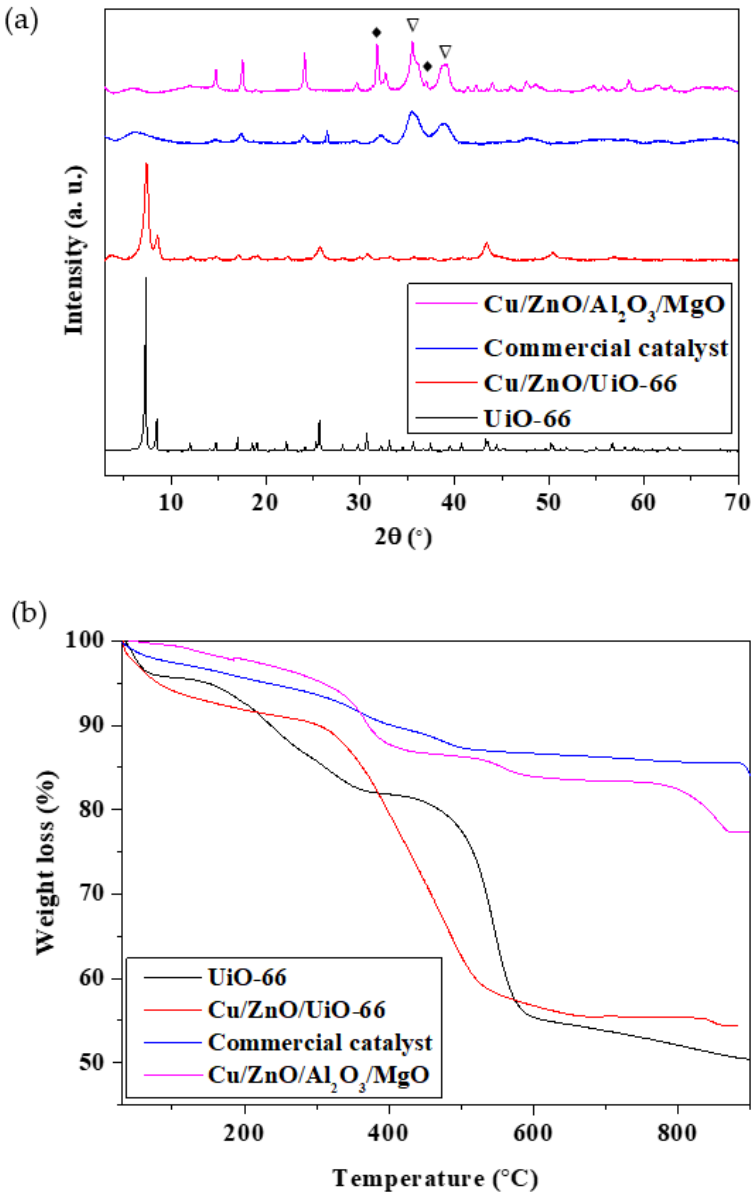

Figure 3.1. (**a**) XRD patterns and (**b**) TGA profiles of commercial catalyst, $Cu/ZnO/Al_2O_3/MgO$ catalyst, UiO-66, and Cu/ZnO/UiO-66. ♦ ZnO, ▽ CuO.

N_2 Physisorption, Fourier Transform Infrared Spectroscopy (FTIR), and Metal Loading

The surface area and pore volume of the catalysts and pristine UiO-66 were characterised using nitrogen adsorption–desorption isotherms where the results are listed in Table 3.1. The Brunauer–Emmett–Teller (BET) surface area of UiO-66 was 1238 m^2/g with a pore volume of 0.47 cm^3/g. The reported values are consistent with

data previously reported for UiO-66 [38,40]. The nitrogen sorption isotherms of pristine UiO-66, Cu/ZnO/UiO-66, Cu/ZnO/Al_2O_3/MgO, and commercial catalysts are shown in Figure 3.2. It is clear from Figure 3.2b that both pristine and impregnated MOFs exhibit type-I sorption isotherms owing to their microporous structure. Furthermore, the decrease in specific surface area (SSA) observed in Cu/ZnO/UiO-66 can be attributed to the presence of Cu and Zn nanoparticles which occupy available surface sites of the UiO-66 support [3,32]. The commercial catalyst had a higher SSA compared to the CuO/ZnO/Al_2O_3/MgO catalyst. The effect of larger crystallite sizes, corroborated by the XRD derived data in Figure 3.1a, culminates in a relatively low SSA when compared to the commercial catalyst [33,42]. The functional groups of the organic linkers present in the samples were studied using FTIR (Figure 3.2c). The peak at 656 cm^{-1} is attributed to the vibration of μ_3-O in the $Zr_6O_4(OH)_4(CO_2)_{12}$ nodes of UiO-66, whereas the peak at 550 cm^{-1} is due to asymmetric Zr-(OC) vibrations which further indicate successful coordination of the Zr secondary building units (SBUs) to the organic benzene dicarboxylate (BDC) linkers [3,40,43]. The stretching symmetric and asymmetric vibrations of the carboxylate group can be observed at 1572 and 1392 cm^{-1}, whereas the π C=C vibration in the aromatic benzene ring in the linker can be observed at 1508 cm^{-1} [40,44]. The decrease in the intensity of peaks can be observed in the Cu/ZnO/UiO-66 catalyst, which may be attributed to the decrease in the amount of the functional groups, due to partial degradation, associated with UiO-66 after impregnation and thermal treatment, which is corroborated by the decrease in crystallinity and SSA seen in Figures 3.1a and 3.2b [45].

The inductively coupled plasma-optical emission spectroscopy (ICP-OES) results showed that the concentration of Cu in the Cu/ZnO/UiO-66 catalyst was 12 wt%, which confirms successful Cu impregnation although it was slightly higher than the nominal loading of 7 wt%. The amount of Zn was also found to be 4.2% compared to a loading of 3%. The discrepancy in nominal loading may be due to inhomogeneous dispersion over the UiO-66 framework, albeit scanning electron microscopy-electron dispersive X-ray spectroscopy (SEM-EDS) elemental maps revealed a good dispersion of both Cu and Zn (Appendix A, Figure 6.1). The amount of Cu, Zn, Al, and Mg in the Cu/ZnO/Al_2O_3/MgO catalysts was found to be 61.7/27.7/10.6/0.1 weight% (wt%) compared with the nominal loading of 64.2/24.5/9.8/1.3 wt%. In addition, the elemental map shows good dispersion of all the elements, and Mg was not observed in the analysis,

most likely due to its low loading (Appendix A, Figure A2). Similarly, the EDS results of the commercial catalyst showed a good dispersion as seen in Figure A3 and a loading of 59.9, 27.5, 10.1, and 2.54 wt%, which corresponds to the certificate of analysis issued by the supplier, reporting a loading of 64.2/24.5/9.8/1.3 wt%. The elemental loading in each catalyst is summarised in Table 3.1.

Table 3.1 Specific surface area, pore volume, and elemental loading of prepared materials.

Sample	**SSA (m^2/g)**	**Pore Volume (cm^3/g)**	**Cu wt%**	**Zn wt%**
Commercial catalyst	97	0.188	59.9	27.5
$Cu/ZnO/Al_2O_3/MgO$	38	0.103	61.7	27.7
UiO-66	1238	0.471	-	-
Cu/ZnO/UiO-66	561	0.200	12	4.2

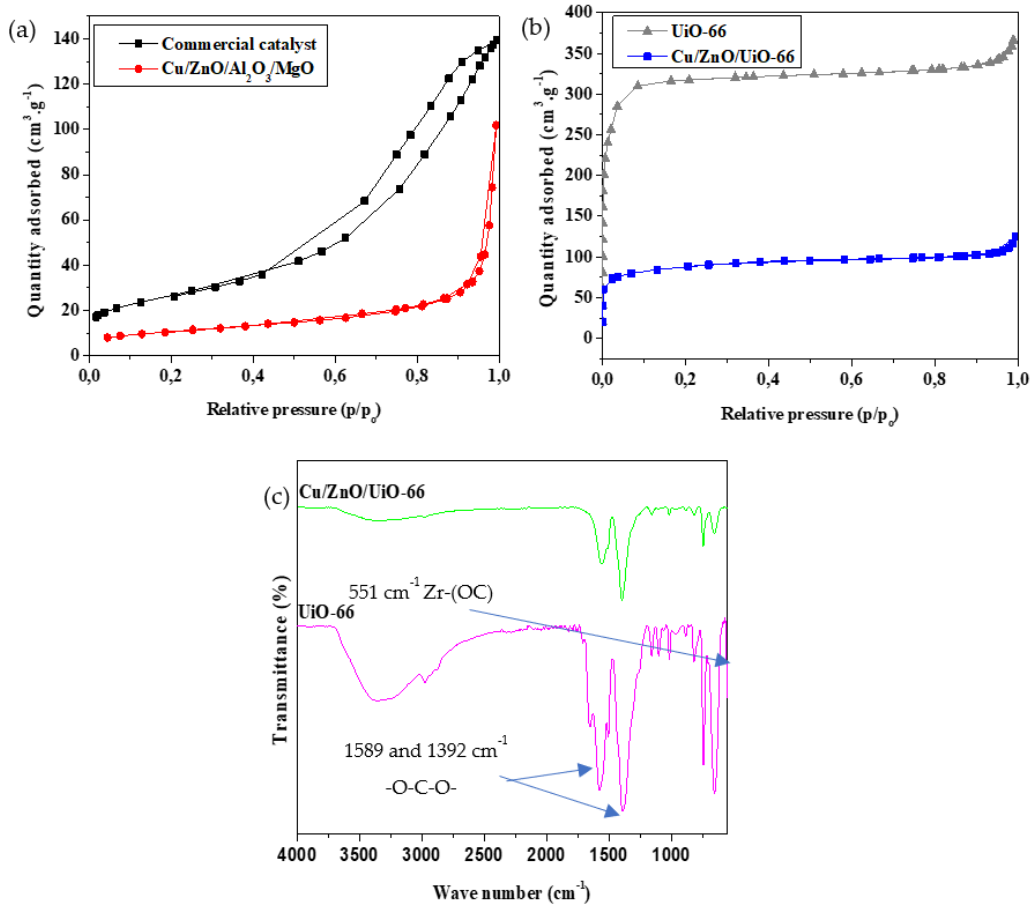

Figure 3.2. Nitrogen sorption isotherms at 77 K of **(a)** commercial catalyst and Cu/ZnO/Al_2O_3/MgO catalyst; **(b)** UiO-66 and Cu/ZnO/UiO-66; and **(c)** FTIR spectra of UiO-66 and Cu/ZnO/UiO-66.

Microscopy

The scanning and transmission electron microscopy (SEM and TEM) images of the samples are shown in Figure 3.3. The morphology of pristine UiO-66 (Figure 3.3a,b) is typical of octahedral-shaped crystals with a homogeneous particle size distribution [15,21,25]. The octahedral shape of UiO-66 is also preserved after impregnation with Cu and Zn (Figure 3.3c-d). The commercial catalyst (Figure 3.3e-f) exhibited irregular shapes which are typically observed when the ageing time in the mother liquor after co-precipitation is too short [46]. The CuO/ZnO/Al_2O_3/MgO catalyst (Figure 3.3g-h) exhibited a needle-like morphology similar to those observed by Mota et al., being characteristic of catalysts prepared via the zincian malachite precursor as were prepared in this study [34].

The TEM images of the pristine UiO-66 and Cu/ZnO/UiO-66 catalyst shown in Figure 3.3b, d corroborate the octahedral shape of UiO-66 particles seen in Figure 3.3a, b. Furthermore, on the surface of the UiO-66 particles in the Cu/ZnO/UiO-66 catalyst, small spherical nanoparticles can be seen which are indicative of CuO/ZnO nanoparticles [4,28]. These nanoparticles are well dispersed on the surface of UiO-66 particles as indicated by SEM-EDS (Appendix A, Figure A1). The micrographs confirm the successful dispersion of Cu and Zn in the Cu/ZnO/UiO-66 catalyst.

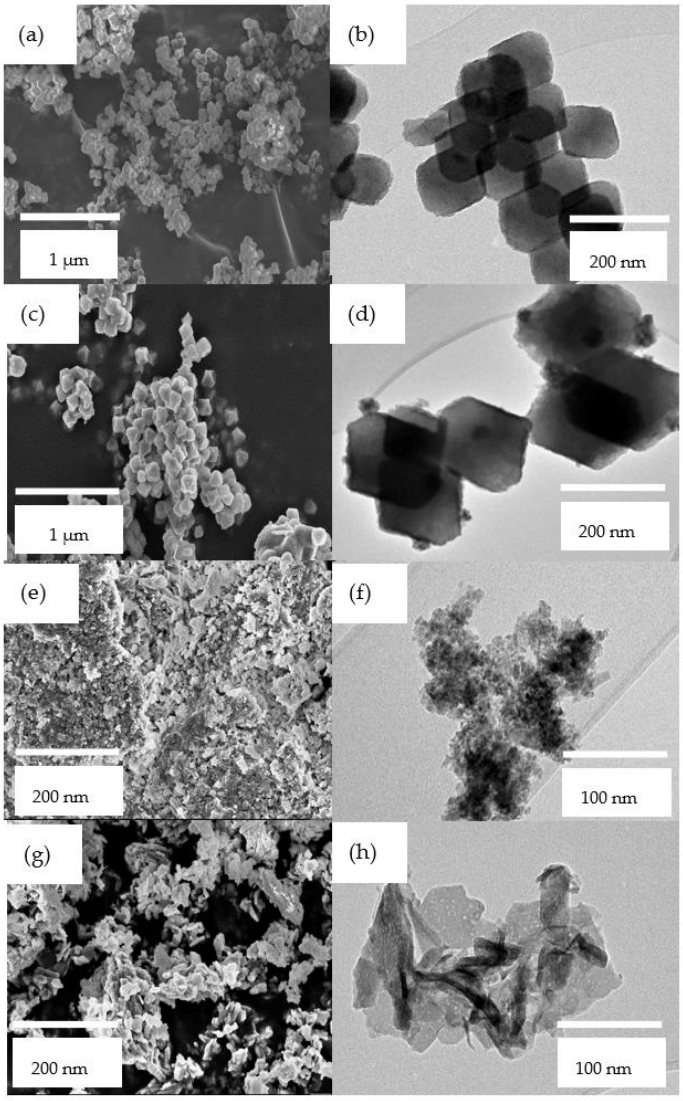

Figure 3.3. SEM and TEM images of (**a**–**b**) UiO-66; (**c**–**d**) Cu/ZnO/UiO-66; (**e**–**f**) commercial catalyst; and (**g**–**h**) CuO/ZnO/Al_2O_3/MgO catalyst. The images were taken at different magnifications

X-ray Photoelectron Spectroscopy (XPS)

The XPS results revealed that Cu was indeed successfully loaded on the surface of the UiO-66 support (Figure 3.4a,b). Cu was present as cupric hydroxide ($Cu(OH)_2$) after drying at 160 °C in air. Furthermore, the $2p_{1/2}$ and $2p_{3/2}$ peaks at 934.5 and 953.6 3eV, and the satellite peak at 943 ± 0.2 eV, corroborate the presence of Cu^{2+} species (Figure 4b) [47,48]. Therefore, to ensure the preferential formation of the Cu^{2+} precursor to the copper active phase precursor, Cu^0, the dried pre-catalyst was activated by thermal treatment under a constant flow of argon at 350 °C. CuO is desired as it is the precursor phase to the metallic Cu active phase formed by reduction with H_2 at temperatures between 200 and 300 °C [15]. Furthermore, Zr was present as ZrO_2 as revealed by the peak at Zr $3d_{5/2}$ at 182.1 eV and the Zr $3d_{3/2}$ peak at 185.2 eV, respectively (Figure 3.4c) [45]. XPS analysis did not detect any Zn, probably due to its low loading or high dispersion [3]. It is also likely that the analysis depth of the X-rays used in the XPS analysis are beyond the penetration depth of the Zn nanoparticles [4]. Furthermore, near ambient pressure XPS would be required to ascertain the surface and subsurface oxidation states of nanoparticles smaller than 4 nm [49]. Zn was, however, observed using SEM-EDS with a good dispersion due to the relatively high analysis depth of SEM-EDS which extends to 1–3 μM, whereas XPS is limited to up to 10 nm of the surface (Figure 6.1) [50,51]. The XPS results of the pristine UiO-66 support are shown in Figure A3, Appendix A.

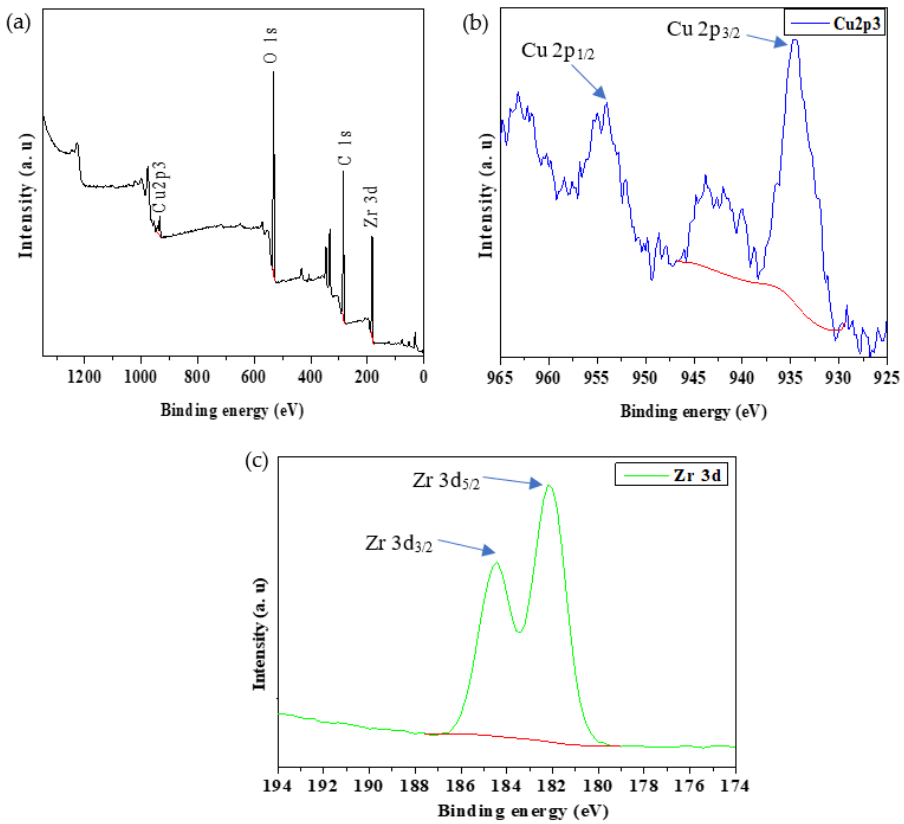

Figure 3.4. XPS spectra of (**a**) Cu/ZnO/UiO-66 full survey, (**b**) Cu2p3, and **(c)** Zr3d.

Hydrogen Temperature-Programmed Reduction (H_2-TPR)

The reducibility of the catalysts was studied using hydrogen temperature-programmed reduction (H_2-TPR) where the reduction profiles are shown in Figure 3.5. All the Cu-loaded catalysts exhibited hydrogen uptake. The commercial and Cu/ZnO/Al_2O_3/MgO catalysts showed reduction peaks at T_{max} = 195 °C and 223 °C (Figure 3.5a). The reduction peaks are indicative of CuO crystallite formed after calcination. The broader curve of the Cu/ZnO/Al_2O_3/MgO may be due to the larger CuO crystallite size of 7.8 nm compared to 5.2 nm in the commercial catalyst [5,34]. The H_2-TPR profiles of UiO-66 and Cu/ZnO/UiO-66 are in Figure 3.5b, where no Cu reduction peak was seen for pristine UiO-66. H_2 uptake, conversely, was observed in Cu/ZnO/UiO-66 at T_{max} = 209 °C; the reduction peak further corroborates the presence of H_2-active copper species on the surface of UiO-66 [45]. The peaks at T_{max} = 446 °C in Figure 3.5b indicate the reduction of Zr species in the metal centre or clusters of the UiO-66 framework. It can also be seen that the loading of Cu and Zn on UiO-66 shifts the T_{max}

of the ZrO_2 reduction peak to 446 °C, which may be due to the ease of reduction facilitated by H_2 spillover from Cu and Zn, respectively [45,52].

3.2.2.2 Catalyst Testing and Evaluation

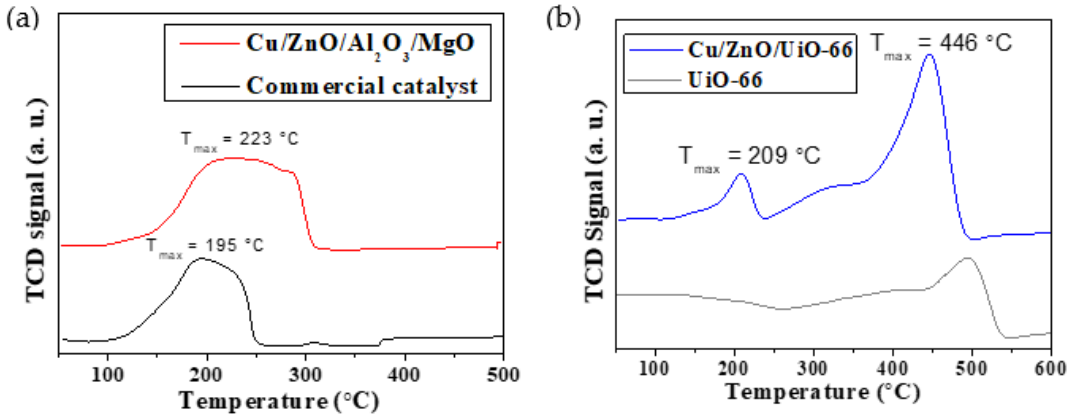

Figure 3.5. H_2-TPR profiles of the prepared catalysts: (**a**) Commercial and $Cu/ZnO/Al_2O_3/MgO$ catalysts; (**b**) UiO-66 and Cu/ZnO/UiO-66.

Conversion, Selectivity, and Productivity

The CO_2 conversion results of all catalysts are shown in Figure 3.6. In the study, it was predominantly CO, MeOH, and methane (CH_4) that were formed as products in addition to H_2O. The reaction progresses through the exothermic CO_2 hydrogenation reaction shown in Equation 3.1. CO is formed via the endothermic reverse water–gas shift reaction in which CO_2 is reduced to CO and H_2O, Equation 3.2 [4,10,15,26]. In addition, CH_4 was presumably formed via the Sabatier reaction, in which CO_2 methanation takes place to form CH_4 and H_2O, Equation 3.3 [53]. The highest average CO_2 conversion after 24 h online was exhibited by the $Cu/ZnO/Al_2O_3/MgO$ catalyst (30.6%) followed by the commercial catalyst (29.8%) and the Cu/ZnO/UiO-66 catalyst (26.7%). Furthermore, all the catalysts tested exhibited a good stability within the 24 h evaluation period.

$$CO_2 + 3H_2 \leftrightarrow CH_3OH + H_2 \qquad \Delta H = -49.47\ KJ/mol \qquad \text{Equation 3.1}$$

$$CO_2 + H_2 \leftrightarrow CO + H_2O \qquad \Delta H = 41.14\ KJ/mol \qquad \text{Equation 3.2}$$

$$CO_2 + 4H_2 \leftrightarrow CH_4 + 2H_2O \qquad \Delta H = -165\ KJ/mol \qquad \text{Equation 3.3}$$

The selectivity of the catalysts towards methanol was also evaluated, where the Cu/ZnO/Al_2O_3/MgO catalyst exhibited the highest selectivity towards methanol (24%) followed by the Cu/ZnO/UiO-66 catalyst (16%), whereas the commercial catalyst had the lowest selectivity of 15.0% (Figure 3.7a). Furthermore, owing to the competing RWGS in thermocatalytic CO_2 hydrogenation, the selectivity of the catalysts towards CO was evaluated [54]. As can be seen in Figure 3.7b, the selectivity of the catalysts towards CO was very high for all catalysts with the highest, at 84%, exhibited by the commercial catalyst, despite small CuO crystallites and a high SSA, which are anticipated to suppress CO selectivity [23,26]. In contrast, the Cu/ZnO/Al_2O_3/MgO and Cu/ZnO/UiO-66 catalysts had relatively lower CO selectivities of 74 and 83%, respectively. In addition, CH_4 was also observed in the product streams of all the catalysts, which is presumably from the Sabatier reaction in which CO_2 methanation occurs [53]. As such, the Cu/ZnO/UiO-66 and Cu/ZnO/Al_2O_3/MgO catalysts had the most selectivity towards CH_4 at 1.6% and 1.7%, respectively, with the lowest observed in the commercial catalyst (0.9%). The methanol productivity, space–time yield (STY), of the Cu/ZnO/UiO-66 catalyst commercial catalyst was 128 $g_{MeOH}/Kg_{cat}/h$, followed by the commercial catalyst at 52 $g_{MeOH}/Kg_{cat}/h$ (Figure 3.7d). The Cu/ZnO/Al_2O_3/MgO catalyst had the lowest methanol productivity at 37 $g_{MeOH}/Kg_{cat}/h$, which may be attributed to the relatively large CuO crystallite size and consequently low SSA [54].

In comparison to An et al., who observed a 100% methanol selectivity, the Cu/ZnO/UiO-66 catalyst showed a relatively low methanol selectivity of 15.7%. However, they also reported relatively low CO_2 conversions of 3.3% at a GHSV of 18 000 h^{-1} compared to 10,000 h^{-1}, as high GHSV results in low per-pass conversion [55]. Furthermore, the commercial and Cu/ZnO/Al_2O_3/MgO co-precipitated catalysts also

exhibit superior CO_2 conversion when compared to the 11% observed by Portha et al., although their catalyst, with a copper–zinc–alumina composition, exhibited a methanol selectively of 43% compared to the 24% of the $Cu/ZnO/Al_2O_3/MgO$ catalyst in this work [56]. These results highlight the promise of using Cu-based MOF-supported catalysts for CO_2 hydrogenation to methanol due to the relatively good catalytic performance of Cu/ZnO/UiO-66 despite having ten times less the Cu loading compared to the $Cu/ZnO/Al_2O_3/MgO$ and commercial catalysts. The high CO_2 conversion and relative methanol STY may be attributed to the good dispersion of Cu over UiO-66, the high SSA, and the enhancement of the active sites by the ZrO_2 secondary building units [4,57].

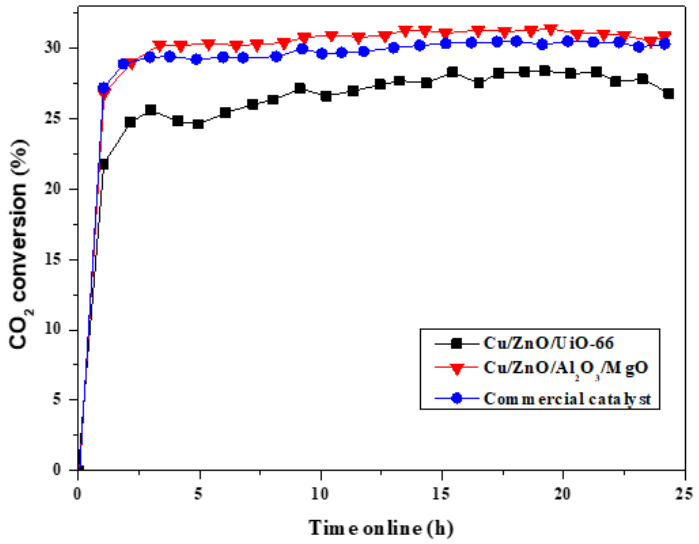

Figure 3.6. CO_2 conversions of catalysts. T = 230 °C; P = 50 bar; Qv, 0 = 40 mL·min^{-1}; GHSV = 10 000 h^{-1}.

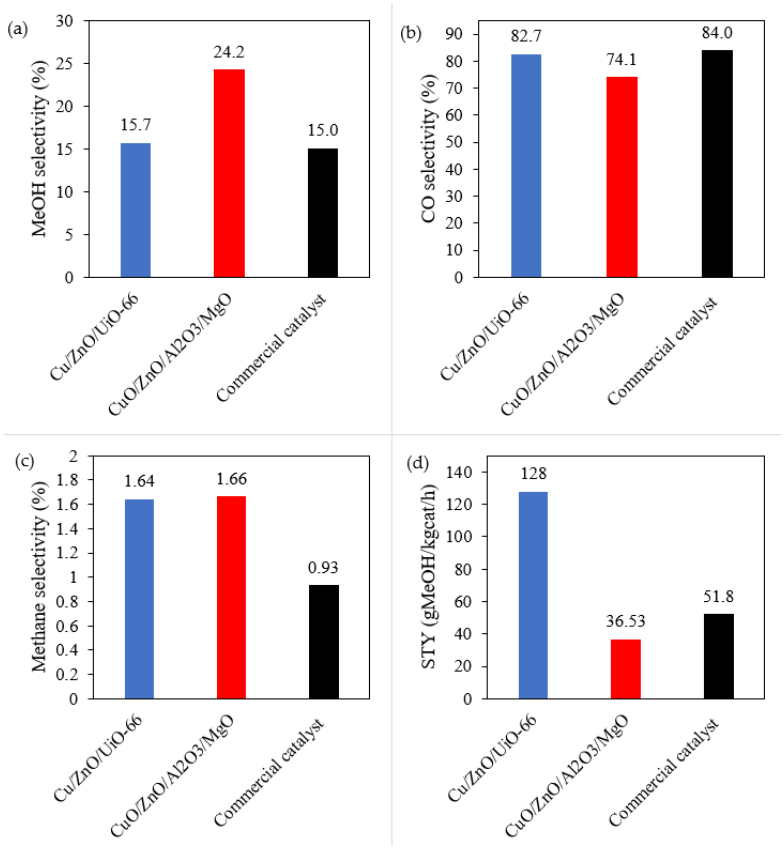

Figure 3.7. Catalysts' (**a**) methanol selectivity; (**b**) CO selectivity; (**c**) methane selectivity and (**d**) space–time yield.

3.2.3 Materials and Methods

3.2.3.1 Reagents and Chemicals

Ethanol (Associated Chemical Enterprises, 95%), *N*,*N*-dimethyl formamide (Associated Chemical Enterprises, 99.5%), cupric nitrate trihydrate ($Cu(NO_3).3H_2O$, Associated Chemical Enterprises, 99.9%), magnesium nitrate hexahydrate ($Mg(NO_3)_2.6H_2O$, Associated Chemical Enterprises, 98%), zinc nitrate hexahydrate ($Zn(NO_3)_2.6H_2O$, Associated Chemical Enterprises, 99.9%), zirconium tetrachloride ($ZrCl_4$, Sigma-Aldrich, 99.5%), terephthalic acid (Sigma-Aldrich, 98%), and aluminium nitrate nonahydrate ($Al(NO_3).9H_2O$, Sigma-Aldrich, ≥98%) were commercially sourced from Associated Chemical Enterprises Pty Ltd. (Johannesburg, South Africa) and Merck KGaA (Darmstadt, Germany),and used without further purification. De-ionised water was sourced from a water demineralisation system

(Instrubal, Zeneer Power II) located on-site. A copper-based methanol synthesis catalyst was procured from Alfa Aesar, Thermo Fischer Scientific (Kandel, Germany). The pelletised catalyst with a percentage composition of 64.2/24.5/9.8/1.3 (Cu/Zn/Al/Mg) was ground to a powder with a pestle and mortar before any use.

3.2.3.2 Catalysts' Synthesis

Cu/ZnO/Al_2O_3/MgO Catalyst

The Cu/ZnO/Al_2O_3/MgO catalyst was prepared via a co-precipitation method. In the procedure, a catalyst with a mass percentage loading of 64.2/24.5/9.8/1.3 (Cu/Zn/Al/Mg) was prepared by dissolving 50.5 mmol of $Cu(NO_3).3H_2O$, 11.9 mmol of $Zn(NO_3)_2.6H_2O$, 10.3 mmol of $Al(NO_3).9H_2O$, and 1.55 mmol of $Mg(NO_3)_2.6H_2O$ in demineralised water (90 mL) followed by acidification with 20 mL of 65% HNO_3 to give a 1 M metal nitrates' solution. The solution, maintained at 60 °C, was dosed with 1 M Na_2CO_3 solution at a rate of 3 mL/min whilst stirring at 400 rpm. Once the solution reached a pH of 6.5 ± 0.5, it was left to age for 1 h. The solution was then filtered, and the precipitates were washed several times with demineralised water and then dried overnight at 90 °C. The dried precursors were then calcined in open air at 330 °C for 3 h.

UiO-66 (Zr) MOF Synthesis

UiO-66 MOFs were prepared via a modified solvothermal method reported by Ren et al. (2014) [38]. In the procedure, terephthalic acid (4.54 mmol) and $ZrCl_4$ (4.54 mmol) were dissolved in 500 mL of dimethylformamide (DMF) and dissolved by magnetic stirring in a beaker at room temperature. After dissolution, 171.3 mL of formic acid (0.453 mmol) was added as a modulator. The crystallisation of UiO-66 was carried out at a constant reaction temperature of 120 °C under static reflux for 4 h. The white precipitate was recovered by vacuum filtration, washed by immersing in a round-bottom flask with hot ethanol at 60 °C overnight, vacuum filtered, and dried at 90 °C for 24 h.

UiO-66 (Zr) MOF-Supported Catalyst Synthesis

$Cu((NO_3)_2.3H_2O$ (9.97 mmol) and $Zn(NO_3)_2.6H_2O$ (4.06 mmol) were dissolved in 14 mL of ethanol. Thereafter, UiO-66 (8.005 g) was added slowly to the metal nitrate ethanolic solution with continuous stirring. The mixture was then dried overnight at ambient temperature. The dried, light blue, catalyst precursor was thermally treated at 350 °C for 4 h under a constant flow of argon and a heating rate of 5 °C/min to furnish a 7/3/90 wt% Cu/ZnO/UiO-66 catalyst.

3.2.3.3 Characterisation

Powder X-ray diffraction (PXRD), for phase identification, was conducted with a Rigaku Ultima IV diffractometer with a Ni-filtered radiation of 0.154 nm, a voltage of 40 kV, and a current of 30 mA at room temperature (Akishima-shi, Tokyo, Japan). A scanning range of $2\theta = 3–90°$ at a rate of $0.01° \ s^{-1}$ was used for all the samples.

The thermal stability of the precursors and catalysts was measured using thermogravimetric analysis (TGA) using the Mettler, Toledo TGA/SDTA 851^e instrument (Mettler Toledo, Greifensee, Switzerland). In the procedure, 10 mg of the sample was heated to 1000 °C at a rate of 10 °C min^{-1} in nitrogen.

Surface area and porosity measurements were performed with an ASAP 2020 HD analyser (Micromeritics Instrument Corporation, Georgia, United States of America), and high purity (99.999%) grade nitrogen (N_2) gas. The Brunauer–Emmett–Teller (BET) surface area and pore volume were determined using N_2 gas sorption isotherms at 77 K and relative partial pressures (p/p_o) of up to 1. Prior to each analysis, the samples (>0.2 g) were degassed under vacuum using a Micromeritics SmartVac with heating to no more than 200 °C.

Fourier transform infrared spectroscopy (FTIR) was recorded on a PerkinElmer Spectrum 100 FTIR spectrometer at a mid-IR range of 4000–550 cm^{-1} (PerkinElmer, Waltham, United States of America).

The powder skeletal density of the samples was determined using a Micromeritics AccuPyc II 1340 pycnometer and helium gas at 135 kPa (Micromeritics Instrument Corporation, Georgia, United States of America).

The morphology of the samples was imaged using an Auriga Cobra focused-ion beam scanning electron microscope coupled with energy-dispersive X-ray spectroscopy (Zeiss, Oberkochen, Germany) . Prior to imaging and elemental mapping, the samples were mounted on an adhesive carbon tape loaded on a sample holder and coated with carbon to prevent charging. An FEI Tecnai T12 transmission electron microscope (Thermo Fischer Scientific (Kandel, Germany) was used to image the Cu/ZnO/UiO-66 catalyst. The sample was crushed to a fine powder, dispersed in ethanol by ultrasonication, and a drop was placed on a carbon-coated copper grid which was loaded into the microscope. Elemental analyses were done using EDS for the commercial and Cu/ZnO/Al_2O_3/MgO catalysts, whereas inductively coupled plasma-optical emission spectroscopy was used for the MOF-supported catalyst. The latter was digested in aqua regia using a microwave, the digest made up to 50 mL with deionised water and analysed using ICP-OES PlasmaQuant 9100 (Analytik Jena GmbH, Jena, Germany).

Temperature-programmed reduction was used for reducibility testing using a Micromeritics Autochem II analyser (Micromeritics Instrument Corporation, Georgia, United States of America). Each sample, placed between two pieces of glass wool in a U-tube, was degassed at 150 °C at a heating rate of 10 °C/min under a constant flow of helium for 30 min and then cooled to 50 °C. Thereafter, the sample was heated to 900 °C at 10 °C/min under a 50 mL/min flow of 5% H_2/Ar. The hydrogen consumption was measured using a thermal conductivity detector.

The surface oxidation state of Cu, chemical composition of the SBUs, and metal oxide bonds were characterised using X-ray photoelectron spectroscopy (XPS). A Thermo Scientific ESCALAB 250Xi instrument was used with a monochromatic X-ray Al source with an energy of 1486.7 eV, which was operated at 300 W and a pass energy of 100 eV. The analysis was conducted under an ultrahigh vacuum of $<10^{-8}$ mbar (Thermo Fischer Scientific (Kandel, Germany).

3.2.3.4 Catalyst Testing

Synthesised catalysts were tested in a fixed-bed reactor. The reactor was 21 cm in length with an internal and external diameter of 1.01 cm and 1.27 cm. Typically, the catalyst

was sieved to a 50–125 µM size fraction, weighed and packed between two pieces of inert glass wool, and positioned at the centre of the reactor. Before each run, the catalyst was reduced under a stream of pure hydrogen for approximately 2 h at 40 mL/min, 250 °C, and 20 bar. Thereafter, the reactor was cooled to 50 °C, and a pre-mixed gas consisting of 3:1:0.2 H_2/CO_2/Ar was introduced into the reactor and left for 12 h to stabilise. A CO_2 hydrogenation reaction was then carried out at 230 °C, 50 bar, and a flow rate of 40 mL/min with a constant GHSV of 10,000 h^{-1} for 24 h. The analysis of the outgoing products was carried out using an Agilent 7890B gas chromatograph instrument (Agilent Technologies Inc, California, United States of America) equipped with an FID (CH_3OH, CH_4) and two TCDs (Ar, CO, CO_2, CH_4, and H_2). Online analysis was carried out for all the outlet gases, whereas the liquid products were condensed in a trap maintained at 0 °C and injected into the GC. The conversions of CO_2 were calculated according to Equation 3.4.

$$X_{CO_2} = = 1 - \left[\left(\frac{CO_{2,out}}{co_{2,in}}\right) \times \left(\frac{Ar_{in}}{Ar_{out}}\right)\right] \qquad \text{Equation 3.4}$$

The selectivity for methanol, CO, and CH_4 were calculated using Equations 3.5-3.7:

$$S_{CH_3OH} = \frac{n_{CH_3OH}}{n_{CH_3OH} + n_{CH_4} + n_{CO}} \qquad \text{Equation 3.5}$$

$$S_{CO} = \frac{n_{CO}}{n_{CH_3OH} + n_{CH_4} + n_{CO}} \qquad \text{Equation 3.6}$$

$$S_{CH_4} = 1 - (S_{CO} + S_{CH_3OH}) \qquad \text{Equation 3.7}$$

3.2.4 Conclusions

In this study, a Zr-based MOF, UiO-66, was used as a support to prepare catalysts via slurry phase impregnation with Cu as well as Zn and tested for the thermocatalytic conversion of CO_2 to methanol. The catalyst was benchmarked against the conventional, co-precipitated, MgO-promoted ternary catalyst, and a CZA commercial catalyst.

Hydrogen uptake shown by TPR revealed the presence of active Cu species for H_2 uptake and a good dispersion of Cu and Zn over the UiO-66 support was observed from SEM-EDS elemental maps. Furthermore, the performance of Cu/ZnO/UiO-66 displayed a good CO_2 conversion, selectivity towards methanol, and the highest methanol space–time yield, making MOF-supported Cu-based catalysts promising for their utilisation in the thermocatalytic hydrogenation of CO_2 to methanol.

Supplementary Materials: The following supporting information can be downloaded at www.mdpi.com/xxx/s1 and also found in Appendix A. Figure A1: Elemental maps of Cu/ZnO/UiO-66; Figure A2: Elemental maps of Cu/ZnO/Al_2O_3/MgO catalyst; Figure A3: Elemental maps of commercial catalyst; Figure A4: XPS results of UiO-66: (a) full survey, (b) Zr3d, and O1s scans.

Author Contributions: Conceptualization, Z.G.D., B.L., K.P., and N.M.M.; methodology, Z.G.D., B.L., and K.P.; investigation, Z.G.D.; resources, N.M.M., H.W.L., and J.M.; writing—original draft preparation, Z.G.D.; writing—review and editing, Z.G.D., H.W.L., J.M., N.M.M., X.D., and B.L.; supervision, N.M.M., H.W.L., and J.M.; formal analysis, X.D.; funding acquisition, N.M.M., B.L., and H.W.L. All authors have read and agreed to the published version of the manuscript.

Funding: This research was funded by Royal Society Foreign, Commonwealth & Development Office (FCDO) Africa Capacity Building Initiative (ACBI) Programme (grant AQ150029) and the South African Department of Science and Innovation (DSI) for research activities under HySA Infrastructure (grant No. CNMH20X).

Institutional Review Board Statement: Not applicable.

Informed Consent Statement: Not applicable.

Data Availability Statement: Not applicable.

Acknowledgments: The authors would like to acknowledge financial support from the Royal Society Foreign, Commonwealth & Development Office (FCDO) Africa Capacity Building Initiative (ACBI) Programme (grant AQ150029), the Council for Scientific and Industrial Research (CSIR), and the South African Department of Science and Innovation (DSI) for research activities under HySA Infrastructure (grant No. CNMH20X) and the South Africa–France PROTEA Programme, which is a

bilateral incentive programme dedicated to strengthening research collaborations between the two countries (project No. CNMH02X).

Conflicts of Interest: The authors declare no personal or financial conflict of interest.

3.3 Chapter summary

Chapter Three presents the first peer-reviewed, published manuscript from the project. The article presented the usage of UiO-66 as support of Cu-ZnO catalysts for carbon dioxide hydrogenation to methanol. The manuscript exhibited that the catalytic performance of the MOF-supported catalyst in comparison to co-precipitated catalysts has good activity, carbon dioxide conversions and relative methanol selectivity.

Chapter Four: Towards high CO_2 conversions using Cu/Zn catalysts supported on aluminium fumarate metal-organic framework for methanol synthesis

4.1 Chapter Outline

This chapter displays the second manuscript from the project titled "Towards high CO_2 conversions using Cu/Zn catalysts supported on aluminium fumarate metal-organic framework for methanol synthesis" which is planned for publication.

4.2 Towards high CO_2 conversions using Cu/Zn catalysts supported on aluminium fumarate metal-organic framework for methanol synthesis

Zama G. Duma [a, b], Nicholas M. Musyoka [a*], John Moma [b], Henrietta W. Langmi [c*], Ksenia Parkhomenko [d] , Benoit Louis [d]

[a] Centre for Nanostructures and Advanced Materials (CeNAM), Chemicals Cluster, Council for Scientific and Industrial Research (CSIR), Pretoria, South Africa; zduma@csir.co.za

[b] Molecular Sciences Institute, School of Chemistry, University of the Witwatersrand, Johannesburg, South Africa; John.moma@wits.ac.za

[c] Department of Chemistry, University of Pretoria, Private Bag X20, Hatfield 0028, South Africa; henrietta.langmi@up.ac.za

[d] Fuels for a Sustainable Environment Team, Institut de Chimie et Procédés pour l'Energie, l'Environnement etla Santé, UMR 7515 CNRS – ECPM, Université de Strasbourg, France; blouis@unistra.fr (B.L.); parkhomenko@unistra.fr (K.P.)

**Corresponding author. Tel: +27 128414806. Email: NMusyoka@csir.co.za; Tel: +27 12 420 2800, Email: henrietta.langmi@up.ac.za*

Abstract

Green methanol is a viable alternative for the storage of hydrogen and may be produced from captured anthropogenic sources of carbon dioxide. The latter was hydrogenated over Cu-ZnO catalysts supported on an Aluminium fumarate metal-organic framework (AlFum MOF). The catalysts, prepared via slurry phase impregnation, were assessed for thermocatalytic hydrogenation of CO_2 to methanol. PXRD, FTIR, and S_{BET} exhibited a decrease in crystallinity of the AlFum MOF support after impregnation with Cu-Zn active sites. SEM, SEM-EDS, and TEM revealed that the morphology of the support is preserved after metal loading where H_2-TPR confirmed the presence of active sites for hydrogen uptake. The catalysts exhibited good activity with a double in Cu and Zn loading over the AlFum MOF resulting in a four-fold increase in CO_2 conversions from 10.8% to 45.6% as well as an increase in methanol productivity from 34.4 $g_{MeOH}/Kg_{cat}/h$ to 56.5 $g_{MeOH}/Kg_{cat}/h$. The catalysts exhibited comparatively high CO selectivity and high yields of H_2O thereby favouring the reverse water-gas shift reaction. The selectivity of the catalysts towards methanol was found to be 12.9% and 6.9%. The performance of the catalyst supported on AlFum MOF further highlights the potential use of MOFs as supports in the heterogeneous thermocatalytic conversion of CO_2 to value-added products.

Keywords: CO_2 hydrogenation, methanol, reverse water-gas shift reaction, metal-organic frameworks, catalysis.

4.2.1 Introduction

It is evident that the continuous increase in anthropogenic CO_2 levels in the atmosphere has resulted in global warming which leads to higher average temperatures on Earth as well as an increase in the acidity of oceans [3, 16, 134]. As such, driven by the large-scale combustion of carbonaceous fossil fuel sources such as coal, natural gas, and oil, CO_2 concentrations have increased by 20% in the past four decades [135]. Therefore, to abate climate change, the mitigation of CO_2 emissions is required via capture, storage, and utilisation. The latter includes the chemical conversion of CO_2 into value-added

chemicals such as, inter alia, methanol, dimethyl ether, organic acids, higher alcohols, and hydrocarbons [135-136]. The valorised products have a myriad of applications as chemical feedstocks as well as direct usage, and in the case of methanol, as fuel sources in internal combustion engines which makes it an ideal energy carrier [40-41].

The chemical conversion of CO_2 to methanol is predominantly carried out over a ternary co-precipitated $Cu/ZnO/Al_2O_3$ catalysts, which are typically used for methanol production from synthesis gas (CO, CO_2, H_2), at industrial conditions of 210-300 ºC and 50-80 bar [137-140]. However, the deactivation of the catalysts driven by thermal sintering of the Cu particles, phase segregation of ZnO and Al_2O_3 from Cu active sites, and decreased dispersion, result in poor performance concerning selectivity to methanol thereby facilitating CO production [62, 141-142]. Furthermore, zinc has been reported to react with the Al_2O_3 promoter to form zinc aluminates which further deactivates the catalyst [142]. As such, the preparation of supported catalysts that favour good Cu dispersion, high activity toward CO_2 hydrogenation, and methanol selectivity may prevent the aforementioned catalyst deactivation mechanisms [143]. Therefore, the usage of metal-organic frameworks (MOFs), which are a class of very crystalline and porous materials with a large surface area, as supports for Cu-based catalysts promises to circumvent poor performance inherent to ternary, co-precipitated Cu-based catalysts [101, 104].

The application of MOFs, characterized by metal-ion clusters coordinated to multidentate ligands, as catalyst supports have been reported to increase methanol selectivity and turnover frequency [144-145]. Therefore, the ability of MOFs as supports that have high metallic active phase dispersion makes them attractive in heterogeneous catalysis [146]. In this study we present, according to our knowledge, for the first time the loading of Cu-ZnO on Aluminium Fumarate MOF (AlFum MOF) for the thermocatalytic hydrogenation of CO_2 to methanol.

4.2.2 Results and Discussion

4.2.2.1 Characterisation

The XRD patterns of the catalysts supported on AlFum MOF are shown in Fig. 4.1a. The 7Cu/3ZnO/AlFum MOF catalyst exhibits the diffraction pattern typical of AlFum MOF, with characteristic peaks at 2θ = 10.2, 14.9, 21.1, 31.8 and 42.7 º, with no Cu or Zn peaks observed which may be due to low metal loading, and good dispersion [104, 147]. Fig. 4.1a also shows the diffraction pattern of the pristine AlFum MOF whereas Fig. 4.1b, zooms into the 35º < 2θ < 40 º region of Cu/ZnO/AlFum MOF catalysts. In comparison to 7Cu/3ZnO/AlFum MOF, 15Cu/6.4ZnO/AlFum MOF has double the loading of Cu and Zn and, as a result, the CuO peak at 35º < 2θ < 39 º can be observed [41, 120]. Furthermore, it can be seen that the crystallinity of the AlFum MOF in the supported catalysts decreases which may be due to the high thermal treatment temperature of 350 ºC under a constant flow of argon during thermal activation.

The FTIR spectra of the pristine AlFum MOF and Cu/ZnO/AlFum MOF catalysts are shown in Fig. 4.1c-e. The broad peak at 3400-3600 cm^{-1} is attributed to O-H vibrations from physisorbed or intercrystalline water and/or absorbed moisture [1, 103, 148]. The symmetric and asymmetric vibrations of the fumarate carboxylate group can be seen at 1403 and 1591 cm^{-1} [1, 147]. Furthermore, it can be seen in the Cu/ZnO/AlFum MOF catalysts, Fig 4.1c-d, that after impregnation and thermal treatment the intensity of the peaks decreases which corroborates the decrease in crystallinity observed in the XRD diffractograms, Fig 4.1a-b.

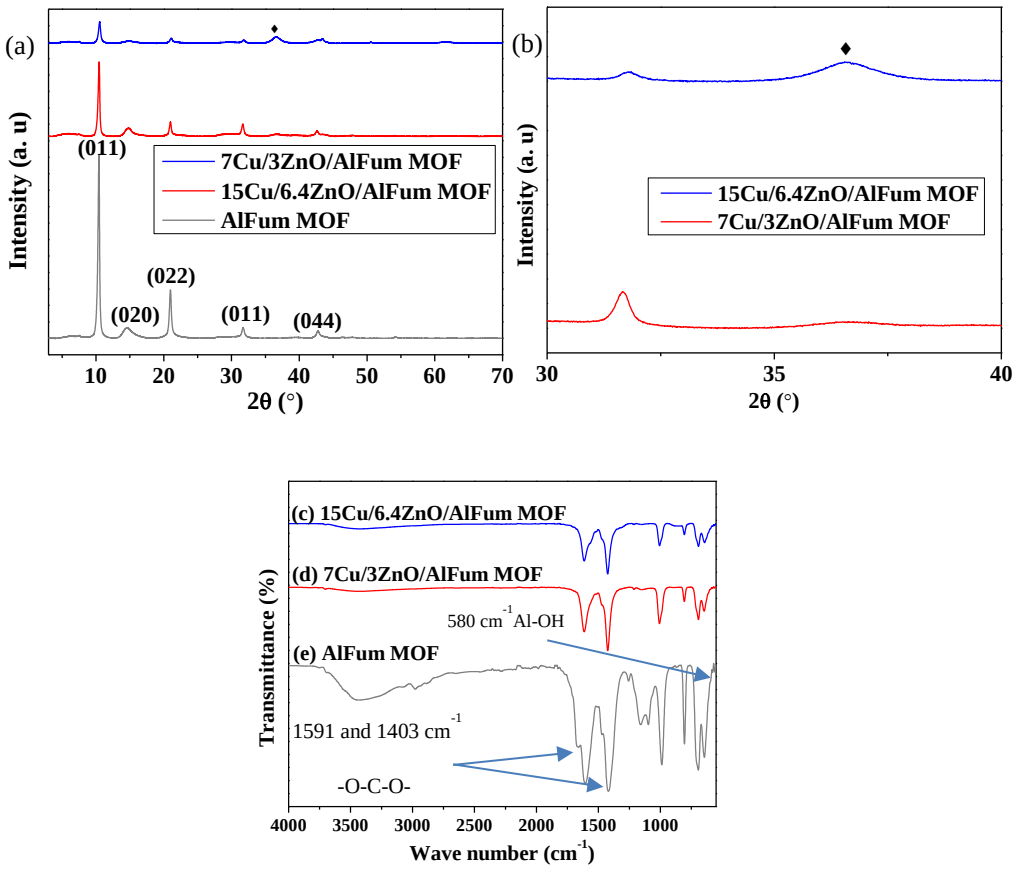

Figure 4.1. XRD patterns of **(a)** AlFum MOF, 7Cu/3ZnO/AlFum MOF, 15Cu/6.4ZnO/AlFum MOF; **(b)** 7Cu/3ZnO/AlFum MOF, 15Cu/6.4ZnO/AlFum MOF at $35^{o} < 2\theta < 40^{o}$, and **(c-e)** FTIR spectra of AlFum MOF, 7Cu/3ZnO/AlFum MOF, and 15Cu/6.4ZnO/AlFum MOF. CuO (♦).

The pristine AlFum MOF exhibited a BET surface area (S_{BET}) of 910 m^2/g which is consistent with previously reported values [149]. The nitrogen sorption isotherms of the pristine and AlFum MOF-supported catalysts are shown in Fig. 4.2a whereas the H-K pore volumes and NLDFT PSDs are summarised in Table 4.1. It can be observed that the pristine MOF and catalysts exhibit type-I sorption isotherms which are indicative of their microporous structure [104]. In addition, the PSDs, shown in Fig. 2b, displays that the majority of the pores in the AlFum MOF-support and catalysts are in the micropore range with a median pore diameter below 20 Å, Table 4.1 [1, 147]. Furthermore, the decrease in S_{BET} observed in the impregnated MOFs to 757 and 416 m^2/g can be attributed to the presence of Cu and Zn nanoparticles as well as thermal treatment [104, 150]. The decrease in S_{BET} observed in both the AlFum MOF-supported catalysts is consistent with the decrease in intensity of the XRD and FTIR peaks in Fig. 4.1. In addition, a decrease in pore volume, 0.344 cm^3/g in pristine AlFum MOF, upon

impregnation to 0.300 cm^3/g and 0.148 cm^3/g in the 7Cu/3ZnO/AlFum MOF and 15Cu/6.4ZnO/AlFum MOF catalysts is observed in Table 4.1. Furthermore, SEM-EDX elemental analysis revealed a Cu loading of 11.2 wt% and 18.2 wt% compared with a theoretical composition of 7 wt% and 15 wt% shown in parenthesis. In addition, the Zn content was 3.12 wt% and 5.77 wt% in the Cu/ZnO/AlFum MOF and 7Cu/3ZnO/AlFum MOF catalysts, respectively. The discrepancy may be attributed to high Cu dispersion in the framework of the AlFum MOF support with regions of surface enrichment, potentially leading to higher Cu content [151-152].

Table 4.1. Specific BET surface area, pore volume, mean pore size, and elemental loading of pristine AlFum MOF and Cu/ZnO/AlFum MOF catalysts.

Sample	S_{BET} (m^2/g)	Pore volume (cm^3/g)	d (Å)	Elemental loading (weight %)	
				Cu	Zn
AlFum MOF	910	0.344	12.7	-	-
7Cu/3ZnO/AlFum MOF	757	0.300	12.3	11.2 (7)	3.12 (3)
15.4Cu/6.4ZnO/AlFum MOF	416	0.148	13.0	18.2 (15)	5.77 (6.4)

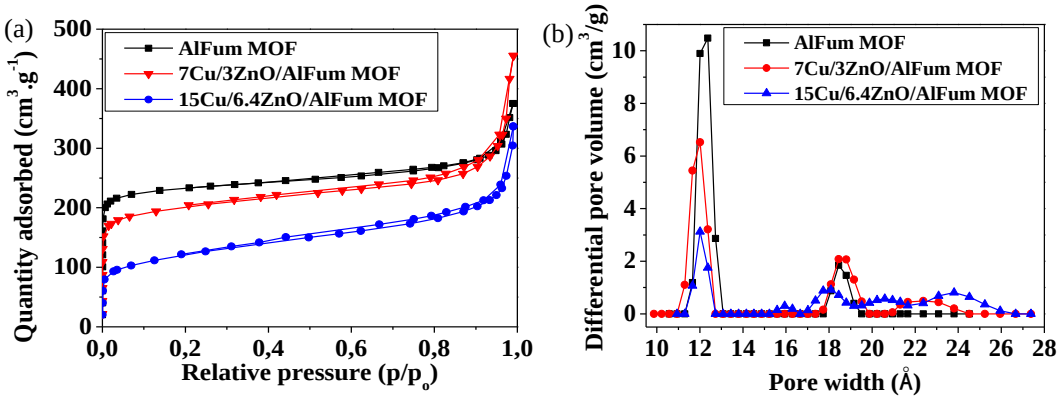

Figure 4.2. N_2 sorption isotherms at 77 K of: **(a)** AlFum MOF, 7Cu/3ZnO/AlFum MOF, 15Cu/6.4ZnO/AlFum MOF; and **(b)** NLDFT Pore size distributions of AlFum MOF, 7Cu/6.4ZnO/AlFum MOF, and 15Cu/6.4ZnO/AlFum MOF.

The morphology imaged using SEM and TEM, of the pristine AlFum MOF support and Cu/ZnO/AlFum MOF catalysts are shown in Fig. 4.3. The AlFum MOF support particles exhibit a lozenge, quadrilateral shape characterized by a geometry of Al-octahedra coordinated to by fumarate linkers [1, 105]. The AlFum MOF particles exhibit some degree of agglomeration which is consistent with literature reports [149]. The Cu/ZnO/AlFum MOF catalysts, Fig. 4.3c-f, have a similar quadrilateral morphology as the pristine AlFum MOF prepared via the solvothermal method, Fig 4.3a-b [153]. Therefore, it can be seen that the morphology of the AlFum MOF support is preserved after impregnation, drying, and thermal treatment. This may be attributed to the good relative thermal stability of the support [106].

The SEM-EDX elemental maps of 7Cu/3ZnO/AlFum MOF and 15Cu/6.4ZnO/AlFum MOF catalysts are shown in Fig. 4.3g-h. In both catalysts, a uniform, homogenous distribution of Cu and Zn is observed which is indicative of successful impregnation. In addition, the micrographs show that in contrast to the pristine AlFum MOF support in Fig. 4.3a-b, tiny spherical nanoparticles can be observed on the surface of the MOF support in the catalysts which may be attributed to Cu and Zn nanoparticles, Fig 4.3c-f. The individual SEM-EDX elemental maps of each metal in the 7Cu/3ZnO/AlFum MOF and 15Cu/6.4ZnO/AlFum MOF catalysts are shown in Figs. A5 and A6 in Appendix B where the homogenous, uniform dispersion of Cu and Zn over the AlFum MOF support observed in Figs. 4.3g-h are further corroborated.

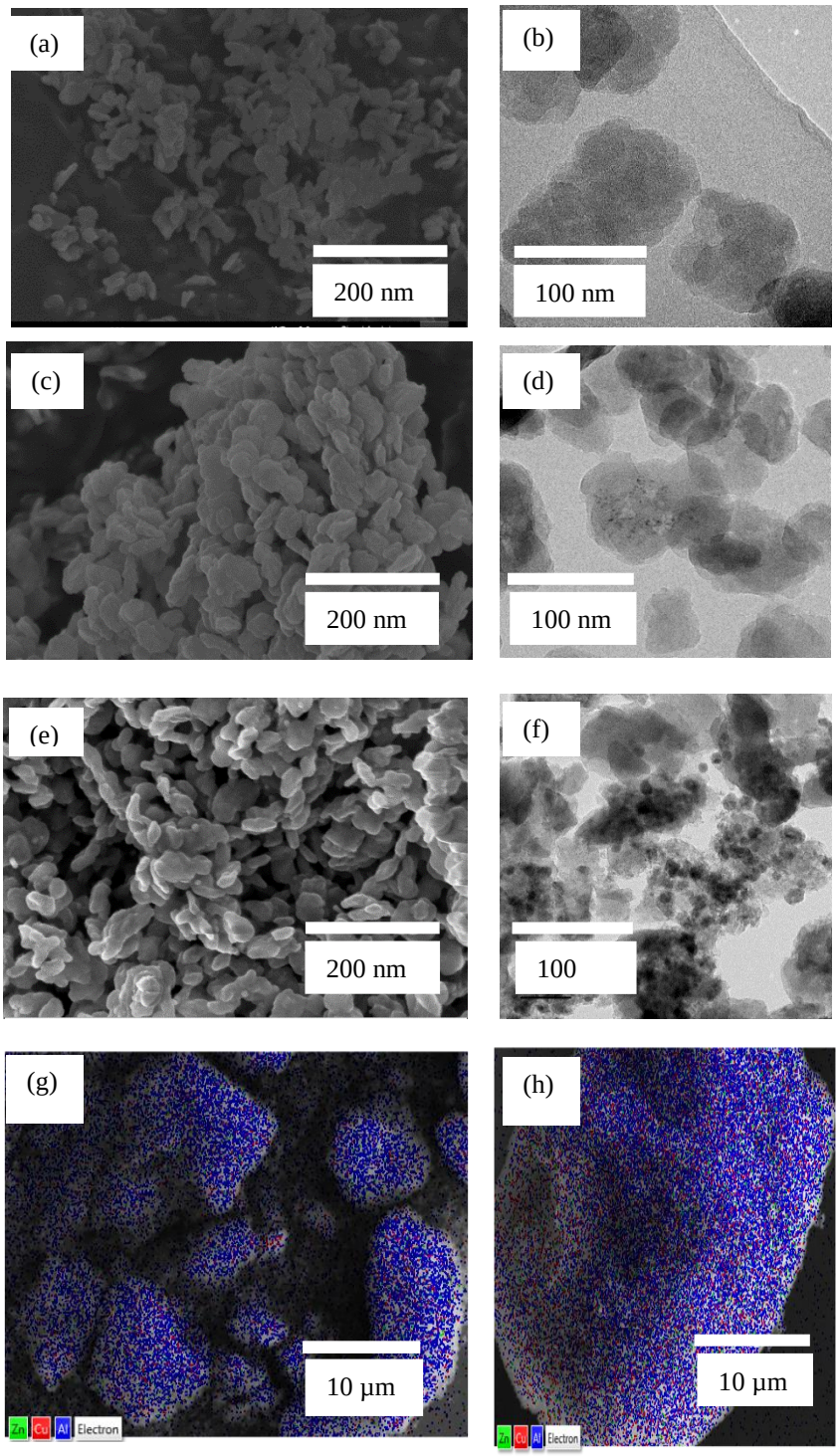

Figure 4.3. SEM and TEM images of: (a-b) AlFum MOF; (c-d) 7Cu/3ZnO/AlFum MOF; (e-f) 15Cu/6.4ZnO/AlFum MOF; EDX elemental maps of (g) 7Cu/3ZnO/AlFum MOF, and (h) 15Cu/6.4ZnO/AlFum MOF.

The TGA profiles of the pristine AlFum MOFs and Cu/ZnO/AlFum MOF catalysts are shown in Fig. 4.4a whereas the derivative TGA plots are shown in Figs A7-A9 (Appendix B). The TGA profile of the pristine AlFum MOF is consistent with previously reported literature results where the initial mass loss below 100 ^{o}C is

attributed to physisorbed water, which is in accordance with the -OH bending vibration FTIR peak at 3300-3600 cm^{-1} in FTIR, Fig. 4.1c-e [147-148]. The weight loss peak at 172 ^{o}C is due to the removal of residual solvents such as DMF, acetone, and methanol used during the synthesis and washing steps, Fig. 4.4a [148]. The derivative TGA plot of the pristine AlFum MOF is shown in Fig. A7 (Appendix B) where an additional weight loss peak at 469 ^{o}C indicates the thermal degradation of the fumarate organic linkers [147]. In addition, the TGA profiles and derivative TGA plots (Appendix B) reveal that the thermal stability in the catalysts decreases after impregnation and thermal activation where the weight loss of fumarate organic linkers temperatures shifts from 469 ^{o}C in the pristine AlFum MOF to 375 ^{o}C and 370 ^{o}C in the 7Cu/3ZnO/AlFum MOF and 15Cu/6.4ZnO/AlFum MOF catalysts (Appendix B, Figs A7-A9). The rapid weight loss indicates the decomposition of the organic linkers followed by the formation of relatively thermally stable metal oxides [147, 154].

The H_2-TPR profiles of 7Cu/3ZnO/AlFum MOF and 15Cu/6.4ZnO/AlFum MOF catalysts exhibit α reduction peaks indicative of CuO presence at T_{max} = 213 ^{o}C and 229 ^{o}C, Fig. 4.4b. The β peaks at T_{max} = 339 ^{o}C and 340 T_{max} = 340 ^{o}C indicate the presence of a second phase of CuO formed after thermal treatment [155]. The α peaks indicate the reduction of Cu ions or CuO clusters that are in close contact with the AlFum MOF whereas the β peaks indicate the reduction of "bulk-like" CuO particles [156]. Furthermore, the α peaks indicate the reduction of finely dispersed CuO particles over the surface of the AlFum MOF support [157]. The H_2-reduction peaks further corroborate the successful loading of Cu as well the formation of the desired CuO species after thermal treatment. The pristine peak AlFum MOF did not show any reduction peaks due to the absence of Cu active sites.

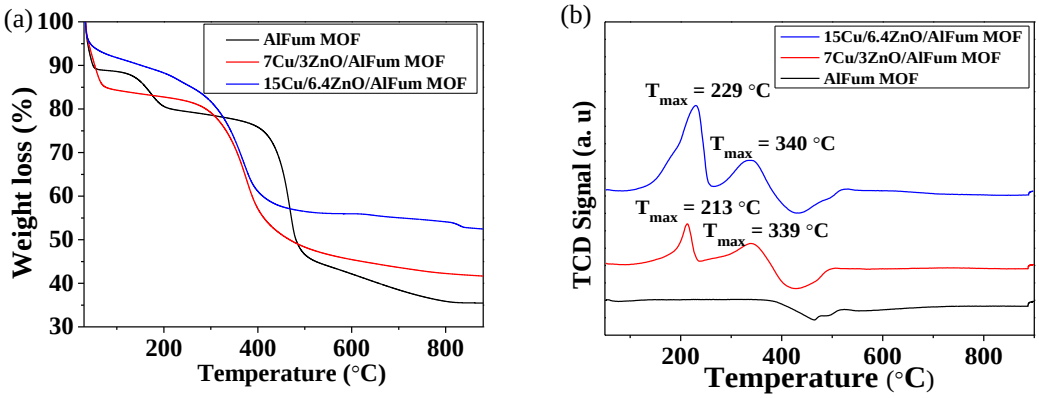

Figure 4.4. (a) TGA profiles of AlFum MOF, 7Cu/3ZnO/AlFum MOF, 15Cu/ZnO/6.4AlFum MOF; **(b)** H_2-TPR profiles of: AlFum MOF, 7Cu/3ZnO/AlFum MOF, 15Cu/6.4ZnO/ AlFum MOF.

The surface oxidation states of Cu and Zn in the catalysts are shown in Fig. 4.5. Conventionally, the Cu^{+} $2p_{3/2}$ and $2p_{1/2}$ peaks are typically observed at 932.5 ± 0.2 eV and 952.3 ± 0.2 eV whereas the Cu^{2+} $2p_{3/2}$ and $2p_{1/2}$ peaks are located at 933.7 ± 0.2 eV and 953.6 ± 0.2 eV, respectively [158-159]. In addition, a satellite peak at 943.2 eV is indicative of Cu^{2+} [159]. In both catalysts, the peaks at 935 eV and 954 eV are indicative of Cu^{2+} species which is further corroborated by the satellite peak at 944 eV, respectively [92]. The XPS spectra confirm the presence of CuO in both the catalysts. Fig. 5b shows the spectrum of Zn 2p which indicates the presence of Zn^{2+} $2p_{3/2}$ and $2p_{1/2}$ peaks at 1022 eV and 1046 eV [160].

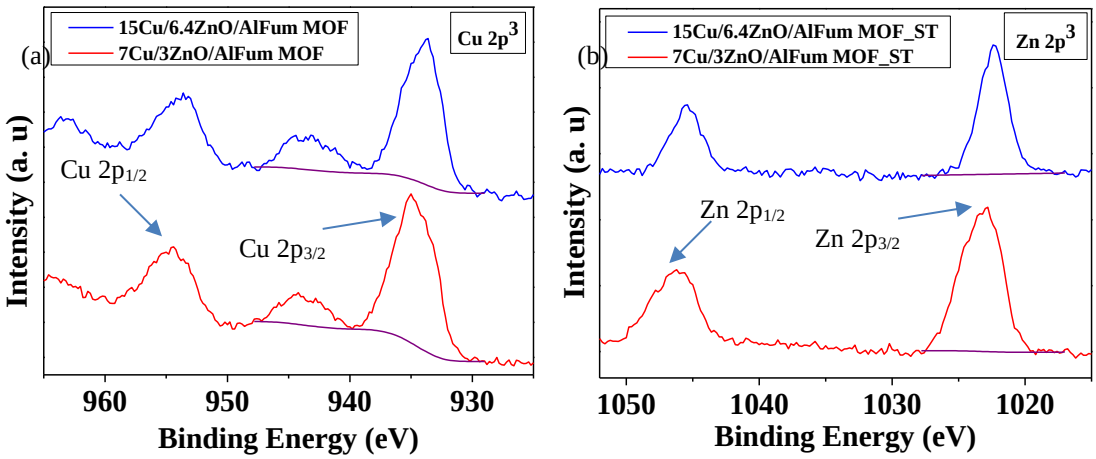

Figure 4.5. XPS spectra **(a)** Cu2p, and **(b)** Zn2p of 7Cu/3ZnO/AlFum MOF and, 15Cu/6.4ZnO/AlFum MOF catalysts.

4.2.2.2 Catalyst performances

The CO_2 conversion results of all tested catalysts, including a commercial catalyst, are shown in Fig. 4.6. The main reaction of interest is the exothermic, direct CO_2 hydrogenation to methanol shown in equation 4.1. In addition to methanol, the catalysts formed CO, H_2O, and CH_4 with no other products observed. CO is formed via the endothermic reverse water-gas shift reaction in which CO_2 is hydrogenated to CO and H_2O, equation 4.2 [101, 137, 141, 161]. In addition, CH_4 was a by-product that was formed in the reactor presumably from the Sabatier reaction in which CO_2 methanation takes

place to form CH_4 and H_2O, equation 4.3 [162]. The highest average CO_2 conversion after 24 h online was exhibited by the 15Cu/6.4ZnO/AlFum MOF catalyst (45.6%), followed by the commercial catalyst (29.8%), and the Cu/ZnO/AlFum MOF catalyst (10.8%), respectively. In addition, the catalysts showed relatively good stability over the 24-hour testing period.

$$CO_2 + 3H_2 \leftrightarrow CH_3OH + H_2O \qquad \Delta H = -49.47\ KJ/mol \qquad \text{Equation 4.1}$$

$$CO_2 + H_2 \leftrightarrow CO + H_2O \qquad \Delta H = 41.14\ KJ/mol \qquad \text{Equation 4.2}$$

$$CO_2 + 4H_2 \leftrightarrow CH_4 + 2H_2O \qquad \Delta H = -165\ KJ/mol \qquad \text{Equation 4.3}$$

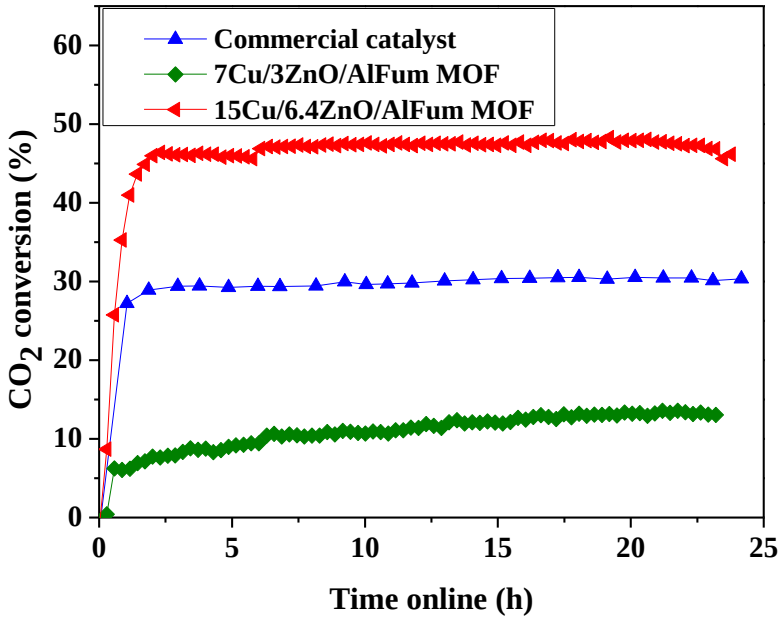

Figure 4.6. CO_2 conversions of the catalysts. T = 230 ºC; P = 50 bar; $Q_{v,0}$ = 40 ml.min^{-1}; GHSV = 10 000 h^{-1}; H_2/CO_2 = 3:1

The methanol selectivity of the catalysts was also investigated. The commercial catalyst exhibited the highest selectivity (15.0%) whereas 7Cu/3ZnO/AlFum MOF and 15Cu/6.4ZnO/AlFum MOF exhibited relatively lower methanol selectivity of 12.9% and 6.90%, Fig. 4.7a. In addition, CO was produced by all the evaluated catalysts due to the competing RWGS [163]. The selectivity of the catalysts towards CO was very high in all catalysts with the highest at 88% exhibited by the 15Cu/6.4ZnO/AlFum MOF

catalyst followed by the 7Cu/3ZnO/AlFum MOF catalyst (85.2%) whereas the commercial catalyst had the lowest comparative CO selectivity of 84%, Fig. 4.7a. In addition, all the catalysts produced methane which is attributed to the Sabatier reaction in which CO_2 methanation occurs [162]. As such, the 15Cu/6.4ZnO/AlFum MOF and 7Cu/3ZnO/AlFum MOF catalysts had the most selectivity towards CH_4 at 5.17% and 1.82%, respectively, with the lowest observed in the commercial catalyst at 0.93%. Furthermore, the mole product distribution, Table 4.2, indicates that the catalysts form a significantly larger amount of CO and H_2O which further corroborates the high selectivity towards CO which is attributed to the RWGS. Furthermore, all the catalysts produced 48-50% of H_2O due to both the RWGS and the CO_2 to methanol reaction shown in equation 5 and 6, respectively.

In contrast, Bonura *et al.* observed methanol selectivity of 48.7% using copper-zinc-zirconia catalysts at 240 °C, 30 bar, and a GHSV of 10 000 h^{-1}. However, the catalysts had relatively low CO_2 conversions of 16.8% compared to the 15Cu/6.4ZnO/AlFum MOF catalyst (45.6%), respectively [164]. Furthermore, An *et al.* also reported comparatively high methanol selectivity of 100% albeit the CO_2 conversion was 3.3% at 250 ° C, 40 bar and GHSV of 6000 h^{-1} [92]. As such, even though the 15Cu/6.4ZnO/AlFum MOF catalyst showed relatively low selectivity toward methanol it exhibited superior CO_2 conversions.

Table 4.2. Product distribution for all the evaluated catalysts.

Product distribution (mol%)				
Catalyst	**MeOH**	**CO**	**CH_4**	**H_2O**
Commercial	12.8	36	2.5	48.8
7Cu/3ZnO/AlFum MOF	6.5	42.8	0.92	48.9
15Cu/6.4ZnO/AlFum MOF	11.4	38.4	0.25	50

The methanol space-time yield (STY) of the 15Cu/6.4ZnO/AlFum MOF catalyst was found to be 56.5 $g_{MeOH}/Kg_{cat}/h$ followed by the commercial catalyst at 51.8 $g_{MeOH}/Kg_{cat}/h$ whereas the 7Cu/3ZnO/AlFum MOF catalyst had the lowest STY of 34.4

$g_{MeOH}/Kg_{cat}/h$, Fig. 4.7b. The methanol STY increases with an increase in Cu loading: 11.2% (7Cu/3ZnO/AlFum MOF); 18.2% (15Cu/6.4ZnO/AlFum MOF), and 64.2% (Commercial catalyst). It is evident that loading and increasing the amount of Cu on high surface area materials such as MOFs enhances catalytic activity, with respect to CO_2 conversions and methanol productivity, due to the high dispersion conferred by the porous supports [101, 165].

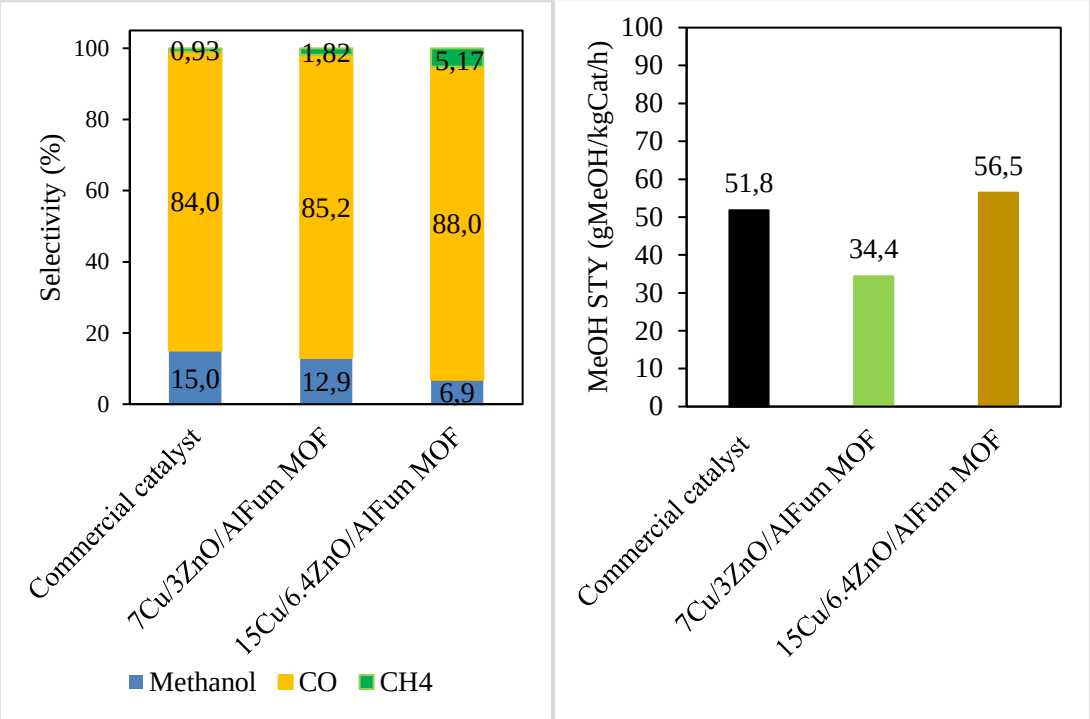

Figure 4.7. **(a)** MeOH, CO, and CH_4 selectivity and **(b)** MeOH space-time yield of all the tested catalysts.

4.2.3 Methods and Materials

Reagents

Aluminium chloride hexahydrate ($AlCl_3.6H_2O$, Associated Chemical Enterprises), cupric nitrate trihydrate ($Cu(NO_3)_2.3H_2O$, Associated Chemical Enterprises, 99.9%), *N*,*N*-dimethyl formamide (DMF, Associated Chemical Enterprises, 99.5%), sodium hydroxide (NaOH, Associated Chemical Enterprises), and fumaric acid ($C_4H_4O_4$, Sigma-Aldrich, 99.9%) were procured and used directly without any purification. De-ionized water from a water demineralization system, Thermo Fischer Barnstead

Smart2Pure, located in the laboratory was used. A copper-based methanol synthesis catalyst was procured from Alfa Aesar. The pelletized catalyst with a weight percentage composition of 64.2/24.5/9.8/1.3 wt% (Cu/Zn/Al/Mg) was ground to a powder with a pestle and mortar before any use.

Synthesis of AlFum MOF

The solvothermal synthesis of AlFum MOF was carried out at ambient pressure. In the procedure, 19.62 g $AlCl_3.6H_2O$ and 14.76 g of fumaric acid were simultaneously added to 400 mL of DMF in a round-bottom flask. Thereafter, the resultant mixture was stirred at 250 rpm and 130 °C for 4 days. The suspension was then washed twice with acetone and methanol, collected using centrifugation, and dried in an oven at 80 °C. The samples were activated at 90 °C, under vacuum, using a rotary evaporator [107]. Before impregnation with Cu and Zn, the AlFum MOF support was sieved to a size fraction of 50-125 µm.

Synthesis of AlFum MOF-supported catalysts

$Cu(NO_3)_2.3H_2O$ (5.50 mmol) and $Zn(NO_3)_2.6H_2O$ (2.33 mmol) were dissolved in 30 mL of deionized water in a round bottom flask. Thereafter, the Cu and Zn-nitrate solution was added slowly to 4.50 g AlFum MOF whilst stirring continuously. The obtained slurry was continuously mixed at 90 ^oC, 50 rpm at ambient pressure for 2 hours in a rotary evaporator. Thereafter, the temperature was decreased to 65 ^oC, the vacuum was activated and maintained for 4 hours to furnish a dry, free-flowing powder. The catalyst was labelled 7Cu/3ZnO/AlFum MOF. A similar procedure was followed to produce a catalyst with double the loading of Cu and Zn by mixing $Cu(NO_3)_2.3H_2O$ (9.44 mmol) and $Zn(NO_3)_2.6H_2O$ (4.00 mmol) with AlFum MOF (3.16 g). The catalyst was labelled 15Cu/6.4ZnO/AlFum MOF.

The dried catalyst precursors were heated at 350 ^oC under the constant flow of argon. The precursors were heated at a rate of 5 ^oC/min with a hold time of 4 hours to furnish catalysts with a theoretical weight percent (wt%) composition of 7/3/90 (7Cu/3ZnO/AlFum MOF) and 15/6.4/78.6 (15Cu/6.4ZnO/AlFum MOF), respectively.

Characterization

Powder X-Ray diffraction (PXRD) was used for phase identification. The Rigaku Ultima IV diffractometer was used with Ni-filtered radiation of 0.154 nm, a voltage of 40 kV, and a current of 30 mA at room temperature. A scanning range of $2\theta = 3\text{-}90^{o}$ at a rate of $0.01^{o}\ s^{-1}$ was used for all the samples. The thermal stability of the precursors and catalysts was measured by thermogravimetric analysis (TGA) using the Mettler, Toledo, TGA/SDTA 851^{e} instrument. In the procedure, 10 mg of the sample was heated to 1000 ^{o}C at a rate of 10 ^{o}C min^{-1} in nitrogen. Surface area and porosity measurements were performed with an ASAP 2020 HD analyser and high purity (99.999%) grade nitrogen (N_2) gas. The Brunauer-Emmett-Teller (BET) surface areas were determined using N_2 gas sorption isotherms at 77 K and relative partial pressures (p/p_o) of up to 1 whereas pore size distributions (PSD) were estimated using the non-linear density functional theory (NLDFT) and pore volumes using H-K isotherms. Before each analysis, the samples (>0.2 g) were degassed under vacuum using Micromeritics SmartVac with heating to no more than 200 ^{o}C. Fourier Transform Infrared Spectroscopy (FTIR) analysis was recorded on a PerkinElmer Spectrum 100 FTIR spectrometer at a mid-IR range of 4000-550 cm^{-1}. The powder skeletal density of the samples was determined using a Micromeritics AccuPyc II 1340 pycnometer and helium gas at 135 kPa. Morphology of the samples was imaged using an Auriga Cobra focused-ion beam scanning electron microscope (SEM) coupled with energy-dispersive X-ray spectroscopy (EDS). Prior to imaging and elemental mapping, the samples were mounted on an adhesive carbon tape loaded on a sample holder and coated with carbon to prevent charging. Transmission Electron Microscope (TEM) imaging was carried out using a JEOL-Jem 2100 model where prior to analyses, each sample was dispersed in ethanol via ultrasonication for 20 minutes, transferred to a carbon-coated copper grid, and left to dry overnight. The samples were then mounted onto the stage and analysed under vacuum. Elemental analyses were done using EDS for all the catalysts. Hydrogen temperature-programmed reduction (H_2-TPR) was used for reducibility tests using a Micromeritics Autochem II 2920 analyser. Each sample, placed between two pieces of glass wool in a U-tube, was degassed at 150 ^{o}C at a heating rate of 10 ^{o}C/min under a constant flow of helium for 30 minutes and then cooled to 50 ^{o}C. Thereafter, the sample was heated to 900 ^{o}C at 10 ^{o}C /min under a 50 ml/min flow of 5% H_2/Ar. Hydrogen consumption was measured using a thermal conductivity detector (TCD). The surface

oxidation state of Cu, chemical composition of the SBUs, and metal oxide bonds were characterised using X-ray photoelectron spectroscopy (XPS). A Thermo Scientific ESCALAB 250Xi instrument was used with a monochromatic X-ray Al source with an energy of 1486.7 eV, which was operated at 300 W and a pass energy of 100 eV. The analysis was conducted under an ultrahigh vacuum of $<10^{-8}$ mbar (Thermo Fischer Scientific).

Catalyst testing

Synthesised catalysts were tested in a fixed-bed tubular reactor. The reactor was 27 cm in length with an internal and external diameter of 1.01 cm and 1.27 cm. Typically, each catalyst was sieved to a 50-125 µm size fraction, weighed and packed between two pieces of inert glass wool, and positioned at the centre of the reactor. Before each run, catalysts were reduced under a stream of pure hydrogen for approximately 2 hours at 40 mL/min, 250 ºC, and 20 bar. Thereafter, the reactor was cooled to 50 ºC, and a pre-mixed gas consisting of 3:1:0.2 H_2/CO_2/Ar was introduced into the reactor and left for 12 hours to stabilize. CO_2 hydrogenation reaction was then carried out at 230 ºC, 50 bar, and a flow rate of 40 ml/min with a constant GHSV of 10 000 h^{-1} for 24 hours. The analysis of the outgoing products was carried out using an Agilent gas chromatography equipped with a flame ionization detector (FID) for analyses of CH_3OH and CH_4 whereas two TCDs were used for Ar, CO, CO_2, CH_4, and H_2, respectively. Online analysis was carried out for all the outlet gases whereas the liquid products were condensed in a trap maintained at 0 ºC and injected into the GC. The conversions of CO_2, *X*, were calculated according to equation 4.4.

$$X_{CO_2} = = 1 - \left[\left(\frac{CO_{2,out}}{co_{2,in}}\right) \times \left(\frac{Ar_{in}}{Ar_{out}}\right)\right] \qquad \text{Equation 4.4}$$

Whereas selectivity to methanol, CO, and CH_4 were calculated using equations 4.5, 4.6, and 4.7:

$$S_{CH_3OH} = \frac{n_{CH_3OH}}{n_{CH_3OH} + n_{CH_4} + n_{CO}} \qquad \text{Equation 4.5}$$

$$S_{CO} = \frac{n_{CO}}{n_{CH_3OH} + n_{CH_4} + n_{CO}}$$ Equation 4.6

$$S_{CH_4} = 1 - (S_{CO} + S_{CH_3OH})$$ Equation 4.7

4.2.4 Conclusions

In this work, Cu-based catalysts supported on AlFum MOF were, for the first time, successfully prepared and evaluated for thermocatalytic hydrogenation of CO_2. The catalyst preparation method results in homogenous, uniform dispersion of Cu and Zn active sites. Doubling the copper loading resulted in a four-fold increase in CO_2 hydrogenation from 10.8% to 45.6% as well as an enhancement in methanol productivity. The catalysts exhibited relatively high selectivity toward CO and low selectivity toward methanol when benchmarked with a commercial-grade catalyst. Furthermore, the evaluated catalysts favoured the reverse water-gas shift reaction and thereby formed considerable amounts of CO and H_2O at the catalyst testing conditions employed in this study.

Supplementary Materials: The following supporting information for Chapter Four is reported in Appendix B. Figure A5: Individual elemental maps of 7Cu/3Zn/AlFum MOF. (a) Al Kα1; (b) Cu Kα1; and (c) Zn Kα1; Figure A6: Individual elemental maps of 15Cu/6.4Zn/AlFum MOF of (a) Al Kα1; (b) Cu Kα1; and (c) Zn Kα1. Figure A7: Derivative TGA plot of AlFum MOF; Figure A8: Derivative TGA plot of 7Cu/3ZnO/AlFum MOF; Figure A9: Derivative TGA plot of 15Cu/6.4ZnO/AlFum MOF.

Declaration of competing interests

The authors declare no competing financial interests. The authors declare that they have no known competing financial interests or personal relationships that could have appeared to influence the work reported in this paper.

Acknowledgements

This research was funded by Royal Society Foreign, Commonwealth & Development Office (FCDO) Africa Capacity Building Initiative (ACBI) Programme (Grant AQ150029) and the South African Department of Science and Innovation (DSI) for research activities under HySA Infrastructure (grant No. CNMH20X).

4.3 Chapter summary

In this chapter, the second manuscript from the project titled "Towards high CO_2 conversions using Cu/Zn catalysts supported on aluminium fumarate metal-organic framework for methanol synthesis" which is under review and is yet to be published. It was found that increasing the copper and zinc loading on a AlFum MOF-supported catalyst by a factor two resulted in a four-fold increase in CO_2 conversions. In addition, the tested catalysts were observed to favour the reverse water-gas shift reaction shown by the relatively high selectivity towards CO. In addition, the use of AlFum MOF as a catalyst is feasible as it is currently available commercially as Basolite A520 which has the propensity to employed in large-scale catalyst preparation. The study highlights the potential of MOFs as high surface area support material in heterogenous catalysis.

Chapter Five: Conclusions, Future Work and Recommendations

5.1 Conclusions

In this study, Cu-based catalysts were prepared via the conventional co-precipitation method using sodium carbonate as a precipitant. The Mg-promoted CZA catalysts were benchmarked with a commercial catalyst of similar composition and metal loading. In addition, supported catalysts were successfully prepared in which Cu and Zn were loaded on UiO-66 and AlFum MOF via slurry phase impregnation. The prepared catalysts were evaluated for thermocatalytic hydrogenation of CO_2 to MeOH.

The following conclusions may therefore be drawn:

- Cu-based catalysts were successfully prepared via slurry phase impregnation and conventional co-precipitation with sodium carbonate;
- A decrease in crystallinity and S_{BET} was observed for the MOF-supported catalysts after thermal treatment;
- The morphology of the MOF-supported catalysts was preserved after Cu and Zn loading as well as after heat treatment;
- The co-precipitated Cu/ZnO/Al_2O_3/MgO catalyst exhibited a lower specific surface area and larger CuO average crystallites when compared to the commercial catalyst of similar composition;
- The Cu/ZnO/Al_2O_3/MgO catalyst had higher CO_2 conversions and MeOH selectivity than the commercial catalyst which had a higher productivity/STY of MeOH;
- In the MOF-supported catalysts with 7 wt% of Cu, the Cu/ZnO/UiO-66 catalyst had the highest CO_2 conversion, MeOH selectivity, and STY;
- Doubling the Cu and Zn loading such as in the 15Cu/6.4ZnO/AlFum MOF_ST catalyst increases CO_2 conversions by a factor of four;
- At the testing conditions, the catalysts exhibited the most selectivity towards CO thereby favouring the reverse water-gas shift reaction.

5.2 Future work and Recommendations

The recommendations for future work are as follows:

- Preparation and testing of co-precipitated catalysts where Al_2O_3 is replaced with ZrO_2 in the conventional, promoted ternary catalysts;
- Investigation of effect of different Cu and Zn loadings on MOF-supported catalysts' performance;
- Effect of temperature, pressure, flow rate, GHSV, gas partial pressures on the performance of MOF-supported catalysts;
- Green synthesis of AlFum MOF for use as supports for CO_2 hydrogenation;
- Usage of UiO-66 and AlFum MOF-derived carbons (MDC) as supports for preparation of Cu-ZnO catalysts;
- Incorporation of promoters such that enhance structural and electronic properties of MOF-supported catalysts;
- Investigation of other MOFs as catalyst supports as well as their acid-base surface properties using temperature-programmed desorption studies. Furthermore, the effect of surface acidity and basicity of the various MOF supports on the kinetics of the catalysts;
- The use of density functional theory (DFT), and *operando* or *in situ* catalyst characterisation techniques to study the reaction mechanism as well as intermediate molecules formed during CO_2 hydrogenation.

Appendix A

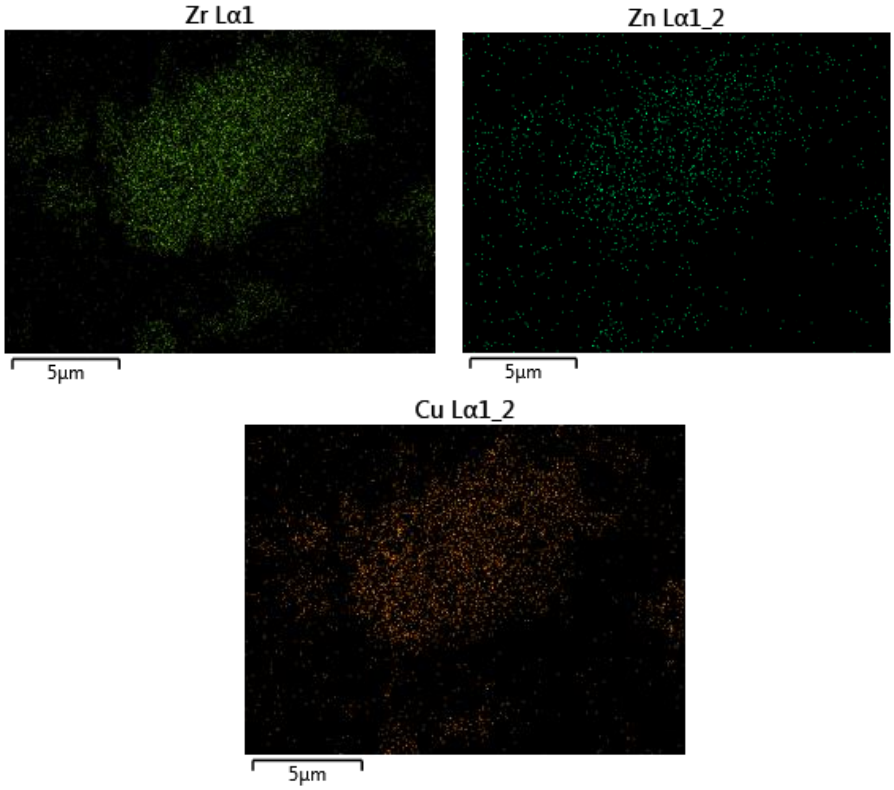

Figure A1. Elemental maps of Cu/ZnO/UiO-66.

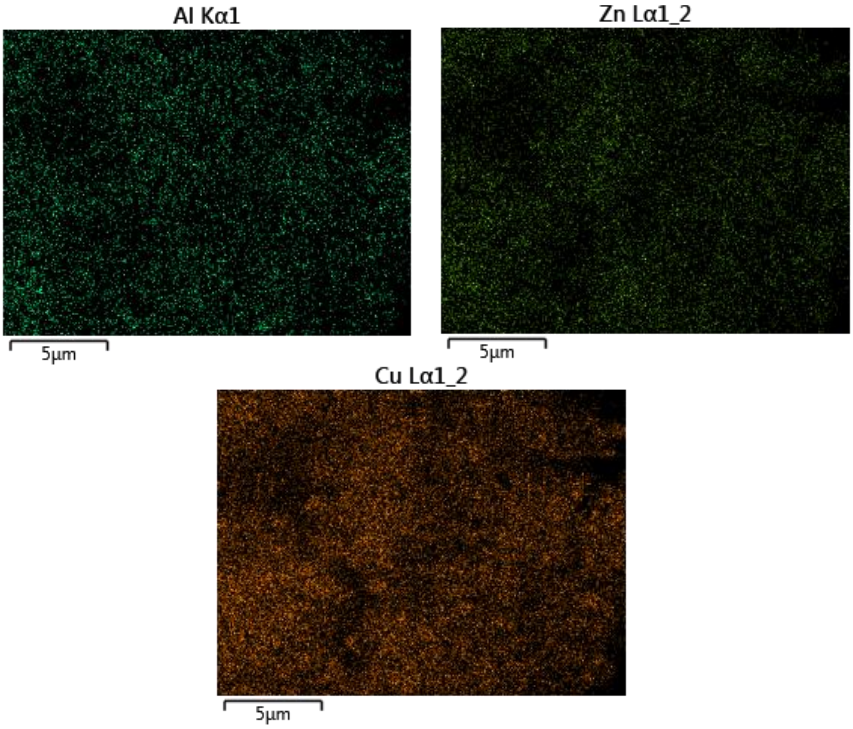

Figure A2. Elemental maps of Cu/ZnO/Al2O3/MgO catalyst.

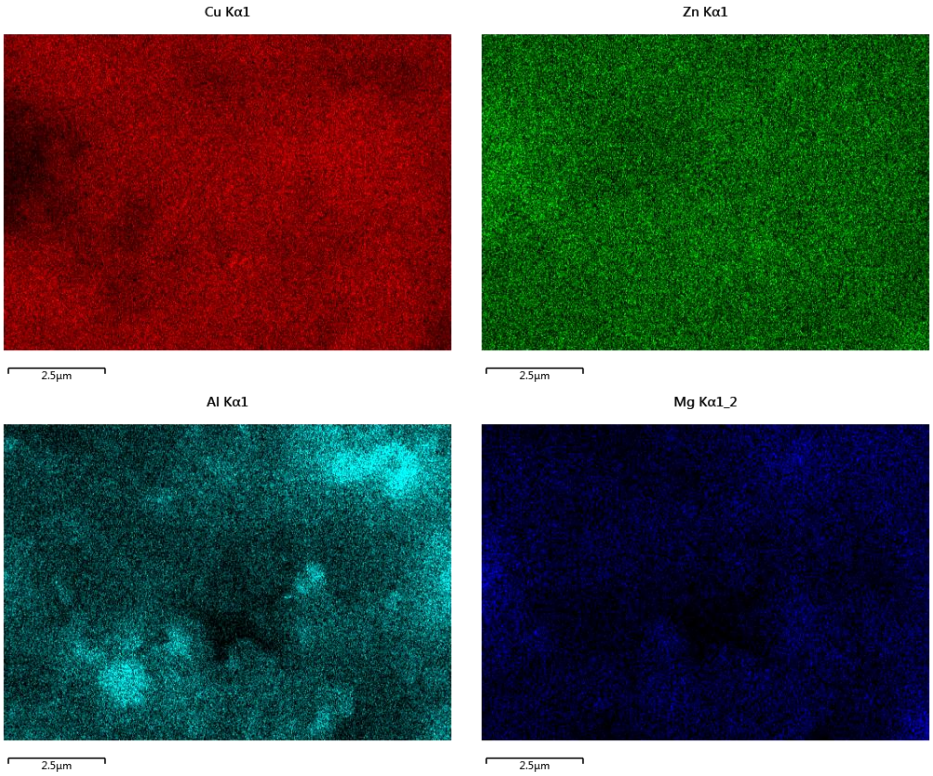

Figure A3. Elemental maps of commercial catalyst.

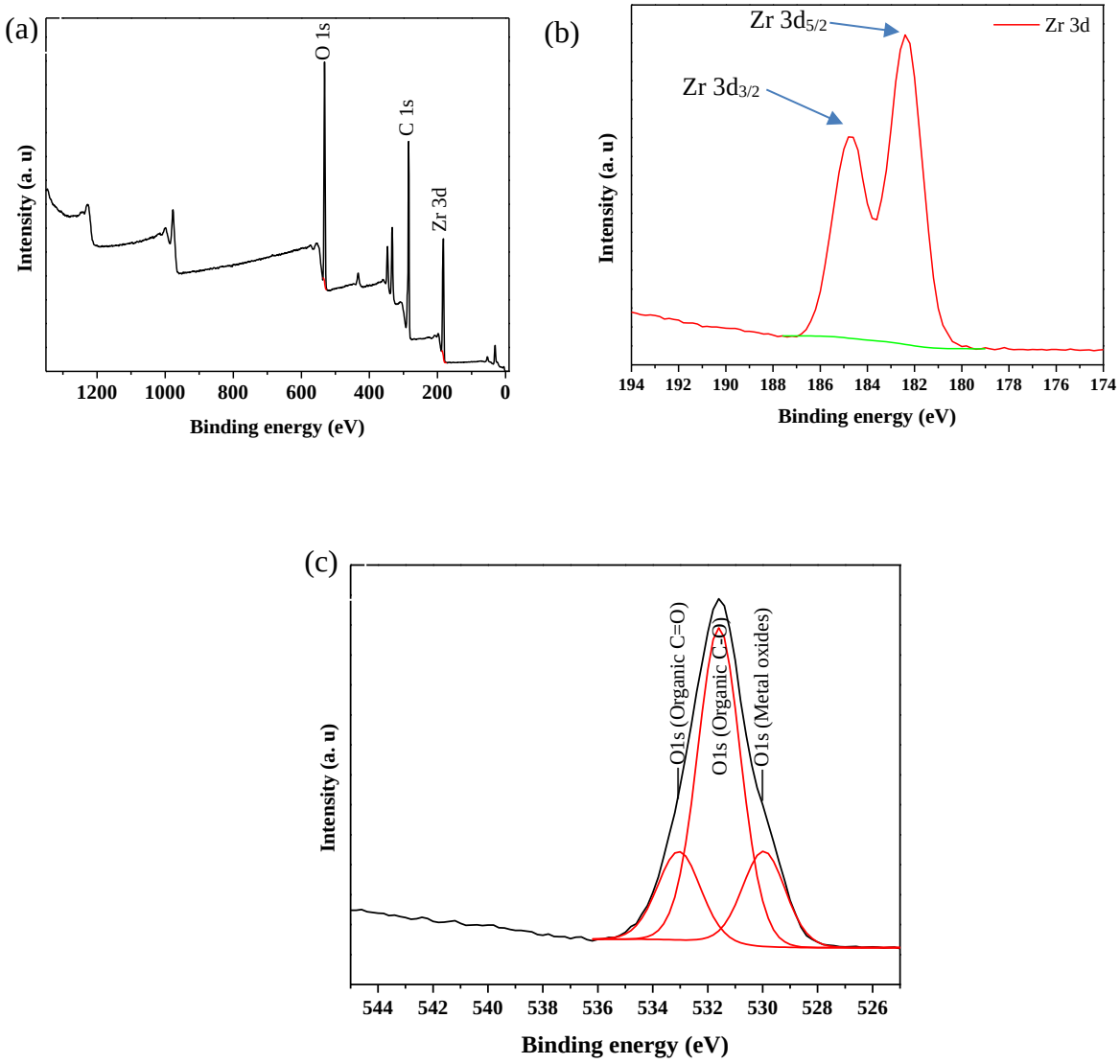

Figure A4. XPS results of UiO-66. (a) Full survey, (b) Zr3d, and O1s scan.

Appendix B

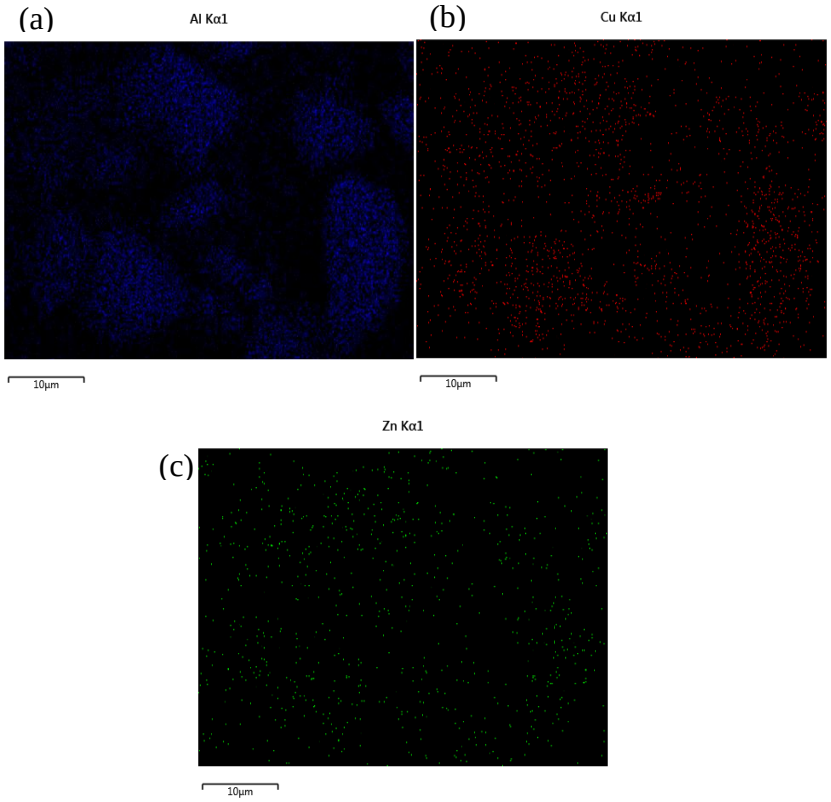

Figure A5. Individual elemental maps of 7Cu/3Zn/AlFum MOF. **(a)** Al Kα1; **(b)** Cu Kα1; and **(c)** Zn Kα1.

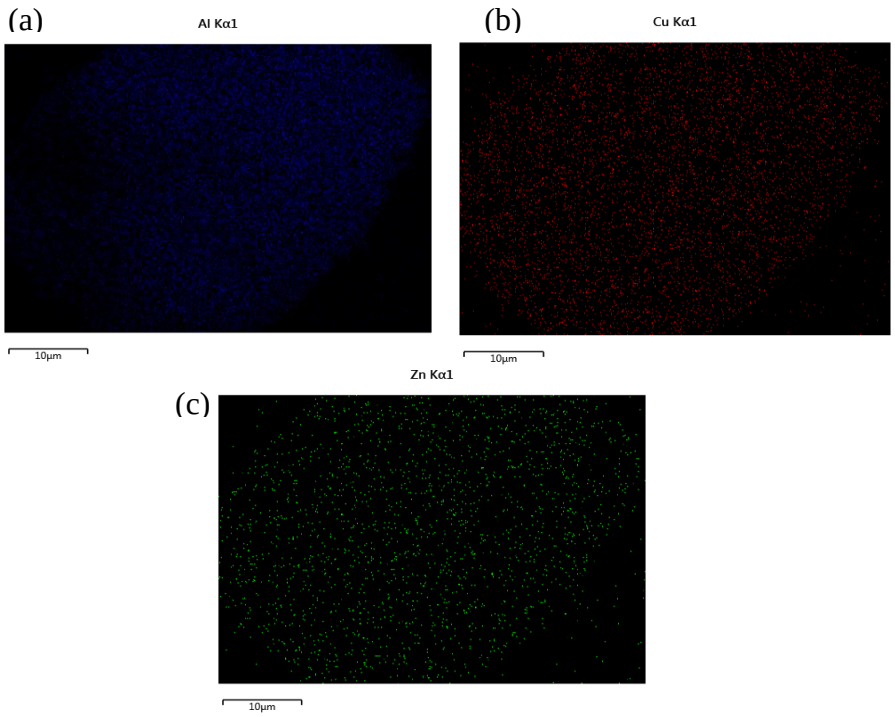

Figure A6. Individual elemental maps of 15Cu/6.4Zn/AlFum MOF. **(a)** Al Kα1; **(b)** Cu Kα1; and **(c)** Zn Kα1.

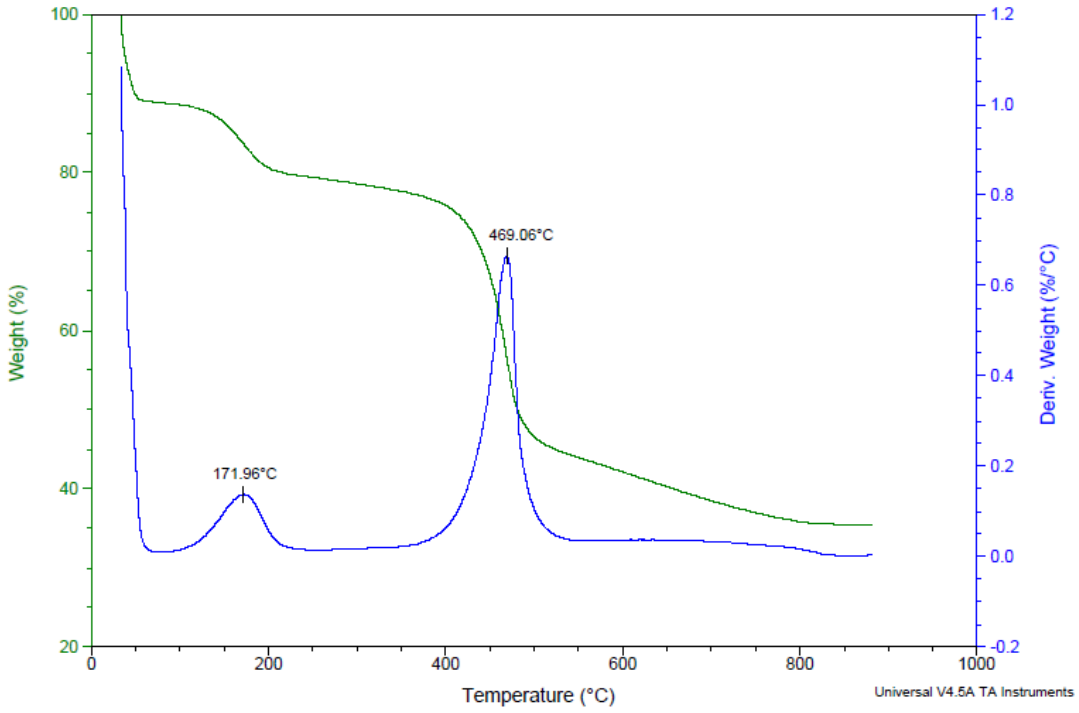

Figure A7. Derivative TGA plot of AlFum MOF.

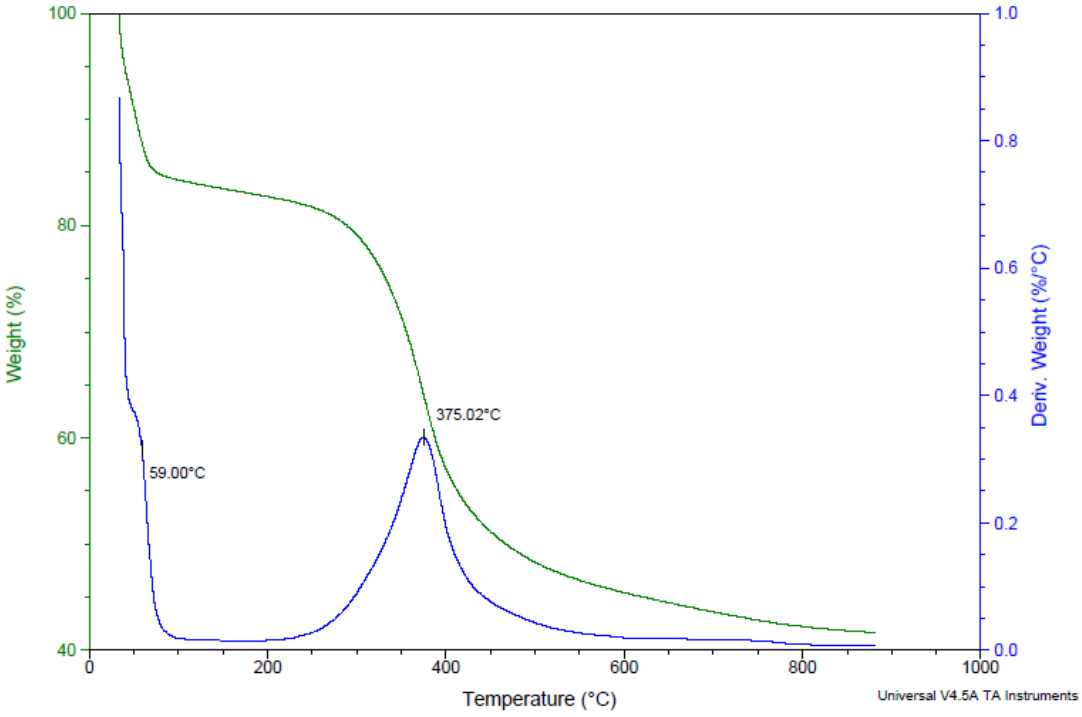

Figure A8. Derivative TGA plot of 7Cu/3ZnO/AlFum MOF.

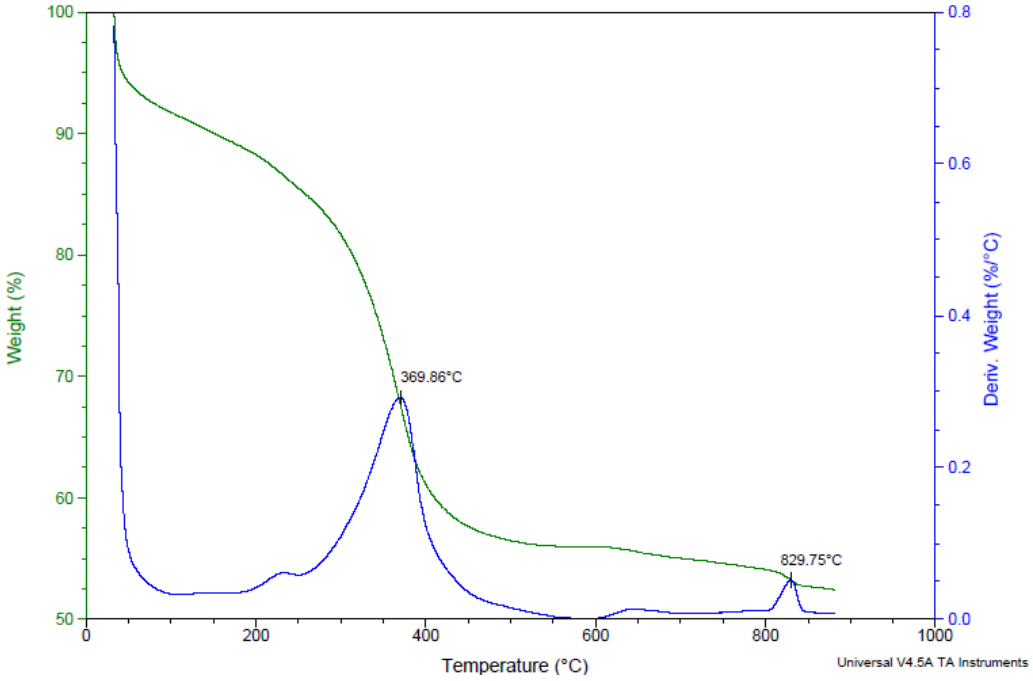

Figure A9. Derivative TGA plot of 15Cu/6.4ZnO/AlFum MOF.

References

1. Karmakar, S.; Dechnik, J.; Janiak, C.; De, S., Aluminium fumarate metal-organic framework: A super adsorbent for fluoride from water. *J Hazard Mater* **2016,** *303*, 10-20.
2. Winarta, J.; Shan, B.; McIntyre, S. M.; Ye, L.; Wang, C.; Liu, J.; Mu, B., A Decade of UiO-66 Research: A Historic Review of Dynamic Structure, Synthesis Mechanisms, and Characterization Techniques of an Archetypal Metal–Organic Framework. *Crystal Growth & Design* **2020,** *20* (2), 1347-1362.
3. Tursunov, O.; Kustov, L.; Kustov, A., A Brief Review of Carbon Dioxide Hydrogenation to Methanol Over Copper and Iron Based Catalysts. *Oil & Gas Science and Technology - Rev. IFP Energies nouvelles* **2017,** *72* (5), 30.
4. Laude, A.; Ricci, O.; Bureau, G.; Royer-Adnot, J.; Fabbri, A., CO2 capture and storage from a bioethanol plant: Carbon and energy footprint and economic assessment. *International Journal of Greenhouse Gas Control* **2011,** *5* (5), 1220-1231.
5. Friedlingstein, P.; Andrew, R. M.; Rogelj, J.; Peters, G. P.; Canadell, J. G.; Knutti, R.; Luderer, G.; Raupach, M. R.; Schaeffer, M.; van Vuuren, D. P., Persistent growth of CO 2 emissions and implications for reaching climate targets. *Nature geoscience* **2014,** *7* (10), 709-715.
6. Raza, A.; Gholami, R.; Rezaee, R.; Rasouli, V.; Rabiei, M., Significant aspects of carbon capture and storage – A review. *Petroleum* **2019,** *5* (4), 335-340.
7. Davis, S. J.; Caldeira, K., Consumption-based accounting of CO₂ emissions. *Proceedings of the National Academy of Sciences* **2010,** *107* (12), 5687-5692.
8. Simon Araya, S.; Liso, V.; Cui, X.; Li, N.; Zhu, J.; Sahlin, S. L.; Jensen, S. H.; Nielsen, M. P.; Kær, S. K., A Review of The Methanol Economy: The Fuel Cell Route. *Energies* **2020,** *13* (3).
9. Peters, G. P.; Minx, J. C.; Weber, C. L.; Edenhofer, O., Growth in emission transfers via international trade from 1990 to 2008. *Proceedings of the National Academy of Sciences* **2011,** *108* (21), 8903-8908.
10. Song, C., Global challenges and strategies for control, conversion and utilization of CO2 for sustainable development involving energy, catalysis, adsorption and chemical processing. *Catalysis Today* **2006,** *115* (1), 2-32.
11. Dai, Z.; Middleton, R.; Viswanathan, H.; Fessenden-Rahn, J.; Bauman, J.; Pawar, R.; Lee, S.-Y.; McPherson, B., An Integrated Framework for Optimizing CO2 Sequestration and Enhanced Oil Recovery. *Environmental Science & Technology Letters* **2014,** *1* (1), 49-54.
12. Alper, E.; Yuksel Orhan, O., CO2 utilization: Developments in conversion processes. *Petroleum* **2017,** *3* (1), 109-126.

13. Bertau, M.; Offermanns, H.; Menges, G.; Keim, W.; Effenberger, F. X., Methanol findet zu wenig Beachtung als Kraftstoff und Chemierohstoff der Zukunft. *Chemie Ingenieur Technik* **2010,** *82* (12), 2055-2058.
14. Ola, O.; Mercedes Maroto-Valer, M.; Mackintosh, S., Turning CO2 into Valuable Chemicals. *Energy Procedia* **2013,** *37*, 6704-6709.
15. Aresta, M.; Dibenedetto, A., Utilisation of CO2 as a chemical feedstock: opportunities and challenges. *Dalton Transactions* **2007,** (28), 2975-2992.
16. Jiang, X.; Nie, X.; Guo, X.; Song, C.; Chen, J. G., Recent Advances in Carbon Dioxide Hydrogenation to Methanol via Heterogeneous Catalysis. *Chemical Reviews* **2020,** *120* (15), 7984-8034.
17. Grabow, L. C.; Mavrikakis, M., Mechanism of Methanol Synthesis on Cu through CO2 and CO Hydrogenation. *ACS Catalysis* **2011,** *1* (4), 365-384.
18. Baena-Moreno, F. M.; Rodríguez-Galán, M.; Vega, F.; Alonso-Fariñas, B.; Vilches Arenas, L. F.; Navarrete, B., Carbon capture and utilization technologies: a literature review and recent advances. *Energy Sources, Part A: Recovery, Utilization, and Environmental Effects* **2019,** *41* (12), 1403-1433.
19. Guil-López, R.; Mota, N.; Llorente, J.; Millán, E.; Pawelec, B.; García, R.; Fierro, J. L. G.; Navarro, R. M., Structure and activity of Cu/ZnO catalysts co-modified with aluminium and gallium for methanol synthesis. *Catalysis Today* **2020,** *355*, 870-881.
20. Jiang, Z.; Xiao, T.; Kuznetsov, V. á.; Edwards, P. á., Turning carbon dioxide into fuel. *Philosophical Transactions of the Royal Society A: Mathematical, Physical and Engineering Sciences* **2010,** *368* (1923), 3343-3364.
21. Liu, Q.; Wu, L.; Jackstell, R.; Beller, M., Using carbon dioxide as a building block in organic synthesis. *Nature Communications* **2015,** *6* (1), 5933.
22. Aronu, U. E.; Svendsen, H. F.; Hoff, K. A.; Juliussen, O., Solvent selection for carbon dioxide absorption. *Energy Procedia* **2009,** *1* (1), 1051-1057.
23. Du, T.; Fang, X.; Liu, L.; Shang, J.; Zhang, B.; Wei, Y.; Gong, H.; Rahman, S.; May, E. F.; Webley, P. A., An optimal trapdoor zeolite for exclusive admission of CO 2 at industrial carbon capture operating temperatures. *Chemical Communications* **2018,** *54* (25), 3134-3137.
24. Aaron, D.; Tsouris, C., Separation of CO2 from Flue Gas: A Review. *Separation Science and Technology* **2005,** *40* (1-3), 321-348.
25. Bhown, A. S.; Freeman, B. C., Analysis and Status of Post-Combustion Carbon Dioxide Capture Technologies. *Environmental Science & Technology* **2011,** *45* (20), 8624-8632.
26. Rahman, F. A.; Aziz, M. M. A.; Saidur, R.; Bakar, W. A. W. A.; Hainin, M. R.; Putrajaya, R.; Hassan, N. A., Pollution to solution: Capture and sequestration of carbon dioxide (CO2) and its utilization as a renewable energy source for a sustainable future. *Renewable and Sustainable Energy Reviews* **2017,** *71*, 112-126.
27. Leung, D. Y. C.; Caramanna, G.; Maroto-Valer, M. M., An overview of current status of carbon dioxide capture and storage technologies. *Renewable and Sustainable Energy Reviews* **2014,** *39*, 426-443.

28. De Visser, E.; Hendriks, C.; Barrio, M.; Mølnvik, M. J.; de Koeijer, G.; Liljemark, S.; Le Gallo, Y., Dynamis CO2 quality recommendations. *International journal of greenhouse gas control* **2008,** *2* (4), 478-484.
29. Bui, M.; Adjiman, C. S.; Bardow, A.; Anthony, E. J.; Boston, A.; Brown, S.; Fennell, P. S.; Fuss, S.; Galindo, A.; Hackett, L. A.; Hallett, J. P.; Herzog, H. J.; Jackson, G.; Kemper, J.; Krevor, S.; Maitland, G. C.; Matuszewski, M.; Metcalfe, I. S.; Petit, C.; Puxty, G.; Reimer, J.; Reiner, D. M.; Rubin, E. S.; Scott, S. A.; Shah, N.; Smit, B.; Trusler, J. P. M.; Webley, P.; Wilcox, J.; Mac Dowell, N., Carbon capture and storage (CCS): the way forward. *Energy & Environmental Science* **2018,** *11* (5), 1062-1176.
30. Obersteiner, M.; Azar, C.; Kossmeier, S.; Mechler, R.; Moellersten, K.; Nilsson, S.; Read, P.; Yamagata, Y.; Yan, J., Managing climate risk. **2001**.
31. Atsbha, T. A.; Yoon, T.; Seongho, P.; Lee, C.-J., A review on the catalytic conversion of CO2 using H2 for synthesis of CO, methanol, and hydrocarbons. *Journal of CO2 Utilization* **2021,** *44*, 101413.
32. Shi, J.; Durucan, S., CO2 storage in deep unminable coal seams. *Oil & gas science and technology* **2005,** *60* (3), 547-558.
33. Szulczewski, M. L.; MacMinn, C. W.; Juanes, R., Theoretical analysis of how pressure buildup and CO2 migration can both constrain storage capacity in deep saline aquifers. *International Journal of Greenhouse Gas Control* **2014,** *23*, 113-118.
34. Mbatha, S.; Everson, R. C.; Musyoka, N. M.; Langmi, H. W.; Lanzini, A.; Brilman, W., Power-to-methanol process: a review of electrolysis, methanol catalysts, kinetics, reactor designs and modelling, process integration, optimisation, and techno-economics. *Sustainable Energy & Fuels* **2021,** *5* (14), 3490-3569.
35. Wulf, C.; Zapp, P.; Schreiber, A., Review of Power-to-X Demonstration Projects in Europe. *Frontiers in Energy Research* **2020,** *8*.
36. Rivarolo, M.; Bellotti, D.; Magistri, L.; Massardo, A. F., Feasibility study of methanol production from different renewable sources and thermo-economic analysis. *International Journal of Hydrogen Energy* **2016,** *41* (4), 2105-2116.
37. Bos, M. J.; Kersten, S. R. A.; Brilman, D. W. F., Wind power to methanol: Renewable methanol production using electricity, electrolysis of water and CO2 air capture. *Applied Energy* **2020,** *264*, 114672.
38. González-Aparicio, I.; Kapetaki, Z.; Tzimas, E., Wind energy and carbon dioxide utilisation as an alternative business model for energy producers: A case study in Spain. *Applied Energy* **2018,** *222*, 216-227.
39. Schumann, J. Cu, Zn-based catalysts for methanol synthesis. Technische Universität Berlin, 2015.
40. Bozzano, G.; Manenti, F., Efficient methanol synthesis: Perspectives, technologies and optimization strategies. *Progress in Energy and Combustion Science* **2016,** *56*, 71-105.
41. Ahouari, H.; Soualah, A.; Le Valant, A.; Pinard, L.; Magnoux, P.; Pouilloux, Y., Methanol synthesis from CO2 hydrogenation over copper based

catalysts. *Reaction Kinetics, Mechanisms and Catalysis* **2013,** *110* (1), 131-145.
42. Waugh, K. C., Methanol Synthesis. *Catalysis Letters* **2012,** *142* (10), 1153-1166.
43. Kondratenko, E. V.; Mul, G.; Baltrusaitis, J.; Larrazábal, G. O.; Pérez-Ramírez, J., Status and perspectives of CO2 conversion into fuels and chemicals by catalytic, photocatalytic and electrocatalytic processes. *Energy & Environmental Science* **2013,** *6* (11), 3112-3135.
44. Olajire, A. A., Valorization of greenhouse carbon dioxide emissions into value-added products by catalytic processes. *Journal of CO2 Utilization* **2013,** *3-4*, 74-92.
45. Olah, G. A., After Oil and Gas: Methanol Economy. *Catalysis Letters* **2004,** *93* (1), 1-2.
46. Fujita, S.-i.; Moribe, S.; Kanamori, Y.; Kakudate, M.; Takezawa, N., Preparation of a coprecipitated Cu/ZnO catalyst for the methanol synthesis from CO2 — effects of the calcination and reduction conditions on the catalytic performance. *Applied Catalysis A: General* **2001,** *207* (1), 121-128.
47. Abdel-Mageed, A. M.; Wohlrab, S., Review of CO2 Reduction on Supported Metals (Alloys) and Single-Atom Catalysts (SACs) for the Use of Green Hydrogen in Power-to-Gas Concepts. *Catalysts* **2022,** *12* (1), 16.
48. Olah, G. A.; Goeppert, A.; Prakash, G. S., *Beyond oil and gas: the methanol economy*. John Wiley & Sons: 2018.
49. Fan, R.; Kyodo, M.; Tan, L.; Peng, X.; Yang, G.; Yoneyama, Y.; Yang, R.; Zhang, Q.; Tsubaki, N., Preparation and application of Cu/ZnO catalyst by urea hydrolysis method for low-temperature methanol synthesis from syngas. *Fuel Processing Technology* **2017,** *167*, 69-77.
50. Dalena, F.; Senatore, A.; Marino, A.; Gordano, A.; Basile, M.; Basile, A., Chapter 1 - Methanol Production and Applications: An Overview. In *Methanol*, Basile, A.; Dalena, F., Eds. Elsevier: 2018; pp 3-28.
51. Bowker, M., Methanol Synthesis from CO(2) Hydrogenation. *ChemCatChem* **2019,** *11* (17), 4238-4246.
52. Richter, C., World's First Commercial CO2 to Methanol Plant. **2019**.
53. Bazaluk, O.; Havrysh, V.; Nitsenko, V.; Baležentis, T.; Streimikiene, D.; Tarkhanova, E. A., Assessment of Green Methanol Production Potential and Related Economic and Environmental Benefits: The Case of China. *Energies* **2020,** *13* (12), 3113.
54. Gu, Y.; Wang, D.; Chen, Q.; Tang, Z., Techno-economic analysis of green methanol plant with optimal design of renewable hydrogen production: A case study in China. *International Journal of Hydrogen Energy* **2022,** *47* (8), 5085-5100.
55. Frusteri, L.; Cannilla, C.; Todaro, S.; Frusteri, F.; Bonura, G., Tailoring of Hydrotalcite-Derived Cu-Based Catalysts for CO2 Hydrogenation to Methanol. *Catalysts* **2019,** *9* (12), 1058.
56. Baltes, C.; Vukojević, S.; Schüth, F., Correlations between synthesis, precursor, and catalyst structure and activity of a large set of CuO/ZnO/Al2O3 catalysts for methanol synthesis. *Journal of Catalysis* **2008,** *258* (2), 334-344.

57. Khassin, A. A.; Minyukova, T. P.; Yurieva, T. M., Genesis of catalysts for methanol synthesis. *Mendeleev Communications* **2014,** *24* (2), 67-74.
58. Li, C.; Yuan, X.; Fujimoto, K., Development of highly stable catalyst for methanol synthesis from carbon dioxide. *Applied Catalysis A: General* **2014,** *469*, 306-311.
59. Liu, X.-M.; Lu, G. Q.; Yan, Z.-F.; Beltramini, J., Recent Advances in Catalysts for Methanol Synthesis via Hydrogenation of CO and CO2. *Industrial & Engineering Chemistry Research* **2003,** *42* (25), 6518-6530.
60. Graciani, J.; Mudiyanselage, K.; Xu, F.; Baber, A. E.; Evans, J.; Senanayake, S. D.; Stacchiola, D. J.; Liu, P.; Hrbek, J.; Sanz, J. F.; Rodriguez, J. A., Highly active copper-ceria and copper-ceria-titania catalysts for methanol synthesis from CO₂. *Science* **2014,** *345* (6196), 546-550.
61. Behrens, M., Coprecipitation: An excellent tool for the synthesis of supported metal catalysts – From the understanding of the well known recipes to new materials. *Catalysis Today* **2015,** *246*, 46-54.
62. Spencer, M. S., The role of zinc oxide in Cu/ZnO catalysts for methanol synthesis and the water–gas shift reaction. *Topics in Catalysis* **1999,** *8* (3), 259.
63. Whittle, D. M.; Mirzaei, A. A.; Hargreaves, J. S. J.; Joyner, R. W.; Kiely, C. J.; Taylor, S. H.; Hutchings, G. J., Co-precipitated copper zinc oxide catalysts for ambient temperature carbon monoxide oxidation: effect of precipitate ageing on catalyst activity. *Physical Chemistry Chemical Physics* **2002,** *4* (23), 5915-5920.
64. Behrens, M.; Kasatkin, I.; Kühl, S.; Weinberg, G., Phase-Pure Cu,Zn,Al Hydrotalcite-like Materials as Precursors for Copper rich Cu/ZnO/Al2O3 Catalysts. *Chemistry of Materials* **2010,** *22* (2), 386-397.
65. Mota, N.; Guil-Lopez, R.; Pawelec, B. G.; Fierro, J. L. G.; Navarro, R. M., Highly active Cu/ZnO–Al catalyst for methanol synthesis: effect of aging on its structure and activity. *RSC Advances* **2018,** *8* (37), 20619-20629.
66. Behrens, M.; Zander, S.; Kurr, P.; Jacobsen, N.; Senker, J.; Koch, G.; Ressler, T.; Fischer, R. W.; Schlögl, R., Performance Improvement of Nanocatalysts by Promoter-Induced Defects in the Support Material: Methanol Synthesis over Cu/ZnO:Al. *J Am Chem Soc* **2013,** *135* (16), 6061-6068.
67. Thongkam, M.; Piyabunditgul, N.; Trisupakitti, S.; Rungrojchaipon, P., Effects of Zinc and Aluminum on the CuO Crystalline Size for Direct Dimethyl Ether Synthesis from Syngas. *Chemical Engineering & Technology* **2021,** *44* (9), 1623-1630.
68. Kurtz, M.; Wilmer, H.; Genger, T.; Hinrichsen, O.; Muhler, M., Deactivation of Supported Copper Catalysts for Methanol Synthesis. *Catalysis Letters* **2003,** *86* (1), 77-80.
69. Aresta, M.; Dibenedetto, A.; Angelini, A., The changing paradigm in CO2 utilization. *Journal of CO2 Utilization* **2013,** *3-4*, 65-73.
70. Kang, S.-H.; Bae, J. W.; Prasad, P. S. S.; Oh, J.-H.; Jun, K.-W.; Song, S.-L.; Min, K.-S., Influence of Ga addition on the methanol synthesis activity of Cu/ZnO catalyst in the presence and absence of alumina. *Journal of Industrial and Engineering Chemistry* **2009,** *15* (5), 665-669.

71. Chinchen, G. C.; Denny, P. J.; Jennings, J. R.; Spencer, M. S.; Waugh, K. C., Synthesis of Methanol: Part 1. Catalysts and Kinetics. *Applied Catalysis* **1988,** *36*, 1-65.
72. Chinchen, G. C.; Denny, P. J.; Parker, D. G.; Spencer, M. S.; Whan, D. A., Mechanism of methanol synthesis from CO2/CO/H2 mixtures over copper/zinc oxide/alumina catalysts: use of14C-labelled reactants. *Applied Catalysis* **1987,** *30* (2), 333-338.
73. Barbieri, G.; Marigliano, G.; Golemme, G.; Drioli, E., Simulation of CO2 hydrogenation with CH3OH removal in a zeolite membrane reactor. *Chemical Engineering Journal* **2002,** *85* (1), 53-59.
74. Din, I. U.; Shaharun, M. S.; Alotaibi, M. A.; Alharthi, A. I.; Naeem, A., Recent developments on heterogeneous catalytic CO2 reduction to methanol. *Journal of CO2 Utilization* **2019,** *34*, 20-33.
75. Sahki, R.; Benlounes, O.; Chérifi, O.; Thouvenot, R.; Bettahar, M. M.; Hocine, S., Effect of pressure on the mechanisms of the CO2/H2 reaction on a CO-precipitated CuO/ZnO/Al2O3 catalyst. *Reaction Kinetics, Mechanisms and Catalysis* **2011,** *103* (2), 391-403.
76. Bailie, J. E.; Rochester, C. H.; Millar, G. J., Spectroscopic evidence for adsorption sites located at Cu/ZnO interfaces. *Catalysis Letters* **1995,** *31* (4), 333-340.
77. Purnama, H.; Ressler, T.; Jentoft, R. E.; Soerijanto, H.; Schlögl, R.; Schomäcker, R., CO formation/selectivity for steam reforming of methanol with a commercial CuO/ZnO/Al2O3 catalyst. *Applied Catalysis A: General* **2004,** *259* (1), 83-94.
78. Ginés, M. J. L.; Marchi, A. J.; Apesteguía, C. R., Kinetic study of the reverse water-gas shift reaction over CuO/ZnO/Al2O3 catalysts. *Applied Catalysis A: General* **1997,** *154* (1), 155-171.
79. Chen, C.-S.; Cheng, W.-H., Study on the Mechanism of CO Formation in Reverse Water Gas Shift Reaction Over Cu/SiO2 Catalyst by Pulse Reaction, TPD and TPR. *Catalysis Letters* **2002,** *83* (3), 121-126.
80. Campbell, C. T.; Ernst, K.-H., Forward and Reverse Water—Gas Shift Reactions on Model Copper Catalysts. In *Surface Science of Catalysis*, American Chemical Society: 1992; Vol. 482, pp 130-142.
81. Fujitani, T.; Nakamura, I.; Uchijima, T.; Nakamura, J., The kinetics and mechanism of methanol synthesis by hydrogenation of CO2 over a Zn-deposited Cu(111) surface. *Surface Science* **1997,** *383* (2), 285-298.
82. Spadaro, L.; Santoro, M.; Palella, A.; Arena, F., Hydrogen Utilization in Green Fuel Synthesis via CO2 Conversion to Methanol over New Cu-Based Catalysts. *ChemEngineering* **2017,** *1* (2), 19.
83. Behrens, M.; Schlögl, R., How to prepare a good Cu/ZnO catalyst or the role of solid state chemistry for the synthesis of nanostructured catalysts. *Zeitschrift für anorganische und allgemeine Chemie* **2013,** *639* (15), 2683-2695.
84. Dang, S.; Yang, H.; Gao, P.; Wang, H.; Li, X.; Wei, W.; Sun, Y., A review of research progress on heterogeneous catalysts for methanol synthesis from carbon dioxide hydrogenation. *Catalysis Today* **2019,** *330*, 61-75.

85. Munnik, P.; de Jongh, P. E.; de Jong, K. P., Recent Developments in the Synthesis of Supported Catalysts. *Chemical Reviews* **2015,** *115* (14), 6687-6718.
86. Schwarz, J. A.; Contescu, C.; Contescu, A., Methods for Preparation of Catalytic Materials. *Chemical Reviews* **1995,** *95* (3), 477-510.
87. Prieto, G.; Zečević, J.; Friedrich, H.; de Jong, K. P.; de Jongh, P. E., Towards stable catalysts by controlling collective properties of supported metal nanoparticles. *Nature Materials* **2013,** *12* (1), 34-39.
88. Munnik, P.; de Jongh, P. E.; de Jong, K. P., Control and Impact of the Nanoscale Distribution of Supported Cobalt Particles Used in Fischer–Tropsch Catalysis. *J Am Chem Soc* **2014,** *136* (20), 7333-7340.
89. Saib, A. M.; Claeys, M.; van Steen, E., Silica supported cobalt Fischer–Tropsch catalysts: effect of pore diameter of support. *Catalysis Today* **2002,** *71* (3), 395-402.
90. Yoon, M.; Srirambalaji, R.; Kim, K., Homochiral Metal–Organic Frameworks for Asymmetric Heterogeneous Catalysis. *Chemical Reviews* **2012,** *112* (2), 1196-1231.
91. Hasegawa, S.; Horike, S.; Matsuda, R.; Furukawa, S.; Mochizuki, K.; Kinoshita, Y.; Kitagawa, S., Three-Dimensional Porous Coordination Polymer Functionalized with Amide Groups Based on Tridentate Ligand: Selective Sorption and Catalysis. *J Am Chem Soc* **2007,** *129* (9), 2607-2614.
92. An, B.; Zhang, J.; Cheng, K.; Ji, P.; Wang, C.; Lin, W., Confinement of Ultrasmall Cu/ZnOx Nanoparticles in Metal–Organic Frameworks for Selective Methanol Synthesis from Catalytic Hydrogenation of CO2. *J Am Chem Soc* **2017,** *139* (10), 3834-3840.
93. Introduction to Metal–Organic Frameworks. *Chemical Reviews* **2012,** *112* (2), 673-674.
94. Pascanu, V.; González Miera, G.; Inge, A. K.; Martín-Matute, B., Metal–Organic Frameworks as Catalysts for Organic Synthesis: A Critical Perspective. *J Am Chem Soc* **2019,** *141* (18), 7223-7234.
95. Li, M.; Li, D.; O'Keeffe, M.; Yaghi, O. M., Topological Analysis of Metal–Organic Frameworks with Polytopic Linkers and/or Multiple Building Units and the Minimal Transitivity Principle. *Chemical Reviews* **2014,** *114* (2), 1343-1370.
96. Kitagawa, S., Metal–organic frameworks (MOFs). *Chemical Society Reviews* **2014,** *43* (16), 5415-5418.
97. Lin, Y.; Kong, C.; Zhang, Q.; Chen, L., Metal-Organic Frameworks for Carbon Dioxide Capture and Methane Storage. *Advanced Energy Materials* **2017,** *7* (4), 1601296.
98. Yan, Q.; Lin, Y.; Kong, C.; Chen, L., Remarkable CO 2/CH 4 selectivity and CO 2 adsorption capacity exhibited by polyamine-decorated metal–organic framework adsorbents. *Chemical Communications* **2013,** *49* (61), 6873-6875.
99. Gutterød, E. S.; Lazzarini, A.; Fjermestad, T.; Kaur, G.; Manzoli, M.; Bordiga, S.; Svelle, S.; Lillerud, K. P.; Skúlason, E.; Øien-Ødegaard, S.; Nova, A.; Olsbye, U., Hydrogenation of CO2 to Methanol by Pt Nanoparticles

Encapsulated in UiO-67: Deciphering the Role of the Metal–Organic Framework. *J Am Chem Soc* **2020,** *142* (2), 999-1009.
100. Ren, J.; Langmi, H. W.; North, B. C.; Mathe, M.; Bessarabov, D., Modulated synthesis of zirconium-metal organic framework (Zr-MOF) for hydrogen storage applications. *International Journal of Hydrogen Energy* **2014,** *39* (2), 890-895.
101. Rungtaweevoranit, B.; Baek, J.; Araujo, J. R.; Archanjo, B. S.; Choi, K. M.; Yaghi, O. M.; Somorjai, G. A., Copper Nanocrystals Encapsulated in Zr-based Metal-Organic Frameworks for Highly Selective CO(2) Hydrogenation to Methanol. *Nano Lett* **2016,** *16* (12), 7645-7649.
102. Wu, H.; Yildirim, T.; Zhou, W., Exceptional Mechanical Stability of Highly Porous Zirconium Metal–Organic Framework UiO-66 and Its Important Implications. *The Journal of Physical Chemistry Letters* **2013,** *4* (6), 925-930.
103. Pan, Y.; Jiang, S.; Xiong, W.; Liu, D.; Li, M.; He, B.; Fan, X.; Luo, D., Supported CuO catalysts on metal-organic framework (Cu-UiO-66) for efficient catalytic wet peroxide oxidation of 4-chlorophenol in wastewater. *Microporous and Mesoporous Materials* **2020,** *291*, 109703.
104. Stawowy, M.; Ciesielski, R.; Maniecki, T.; Matus, K.; Łużny, R.; Trawczynski, J.; Silvestre-Albero, J.; Łamacz, A., CO2 Hydrogenation to Methanol over Ce and Zr Containing UiO-66 and Cu/UiO-66. *Catalysts* **2020,** *10* (1).
105. Alvarez, E.; Guillou, N.; Martineau, C.; Bueken, B.; Van de Voorde, B.; Le Guillouzer, C.; Fabry, P.; Nouar, F.; Taulelle, F.; De Vos, D., The structure of the aluminum fumarate metal–organic framework A520. *Angewandte Chemie* **2015,** *127* (12), 3735-3739.
106. Jeremias, F.; Fröhlich, D.; Janiak, C.; Henninger, S. K., Advancement of sorption-based heat transformation by a metal coating of highly-stable, hydrophilic aluminium fumarate MOF. *RSC Advances* **2014,** *4* (46), 24073-24082.
107. Teo, H. W. B.; Chakraborty, A.; Kitagawa, Y.; Kayal, S., Experimental study of isotherms and kinetics for adsorption of water on Aluminium Fumarate. *International Journal of Heat and Mass Transfer* **2017,** *114*, 621-627.
108. Xu, C.; Chen, G.; Zhao, Y.; Liu, P.; Duan, X.; Gu, L.; Fu, G.; Yuan, Y.; Zheng, N., Interfacing with silica boosts the catalysis of copper. *Nature Communications* **2018,** *9* (1), 3367.
109. Yang, X.; Chen, D.; Liao, S.; Song, H.; Li, Y.; Fu, Z.; Su, Y., High-performance Pd–Au bimetallic catalyst with mesoporous silica nanoparticles as support and its catalysis of cinnamaldehyde hydrogenation. *Journal of Catalysis* **2012,** *291*, 36-43.
110. Huang, W.; Kuhn, J. N.; Tsung, C.-K.; Zhang, Y.; Habas, S. E.; Yang, P.; Somorjai, G. A., Dendrimer Templated Synthesis of One Nanometer Rh and Pt Particles Supported on Mesoporous Silica: Catalytic Activity for Ethylene and Pyrrole Hydrogenation. *Nano Letters* **2008,** *8* (7), 2027-2034.

111. Huang, K.-W.; Hengne, A. M.; Bhatte, K. D.; Ould-Chikh, S.; Saih, Y.; Basset, J.-M., Selective production of oxygenates from CO2 hydrogenation over mesoporous silica supported Cu-Ga nanocomposite catalyst. **2018**.
112. Zhu, Y.; Wang, S.; Ge, X.; Liu, Q.; Luo, Z.; Cen, K., Experimental study of improved two step synthesis for DME production. *Fuel Processing Technology* **2010,** *91* (4), 424-429.
113. Herranz, T.; Rojas, S.; Pérez-Alonso, F. J.; Ojeda, M.; Terreros, P.; Fierro, J. L. G., Carbon oxide hydrogenation over silica-supported iron-based catalysts: Influence of the preparation route. *Applied Catalysis A: General* **2006,** *308*, 19-30.
114. Lee, S.-S.; Park, B.-K.; Byeon, S.-H.; Chang, F.; Kim, H., Mesoporous Silica-Supported Pd Nanoparticles; Highly Selective Catalyst for Hydrogenation of Olefins in Supercritical Carbon Dioxide. *Chemistry of Materials* **2006,** *18* (24), 5631-5633.
115. Pandey, D.; Deo, G., Promotional effects in alumina and silica supported bimetallic Ni–Fe catalysts during CO2 hydrogenation. *Journal of Molecular Catalysis A: Chemical* **2014,** *382*, 23-30.
116. Mohammed, A. A. A.; Saad, M. A. H. S.; Kumar, A.; Al-Marri, M. J., Synthesis of fumed silica supported Ni catalyst for carbon dioxide conversion to methane. *Greenhouse Gases: Science and Technology* **2020,** *10* (4), 715-724.
117. Wang, L.; Guan, E.; Wang, Y.; Wang, L.; Gong, Z.; Cui, Y.; Meng, X.; Gates, B. C.; Xiao, F.-S., Silica accelerates the selective hydrogenation of CO2 to methanol on cobalt catalysts. *Nature Communications* **2020,** *11* (1), 1033.
118. Min, B. K.; Santra, A. K.; Goodman, D. W., Understanding silica-supported metal catalysts: Pd/silica as a case study. *Catalysis Today* **2003,** *85* (2), 113-124.
119. Maniecki, T. P.; Mierczyński, P.; Jóźwiak, W. K., Copper-supported catalysts in methanol synthesis and water gas shift reaction. *Kinetics and Catalysis* **2010,** *51* (6), 843-848.
120. Gesmanee, S.; Koo-Amornpattana, W., Catalytic hydrogenation of CO2 for methanol production in fixed-bed reactor using Cu-Zn supported on gamma-Al2O3. *Energy Procedia* **2017,** *138*, 739-744.
121. Wan, H.; Wang, Z.; Zhu, J.; Li, X.; Liu, B.; Gao, F.; Dong, L.; Chen, Y., Influence of CO pretreatment on the activities of CuO/γ-Al2O3 catalysts in CO+O2 reaction. *Applied Catalysis B: Environmental* **2008,** *79* (3), 254-261.
122. Sun, K.; Liu, J.; Browning, N. D., Direct atomic scale analysis of the distribution of Cu valence states in Cu/γ-Al2O3 catalysts. *Applied Catalysis B: Environmental* **2002,** *38* (4), 271-281.
123. Luo, M.-F.; Fang, P.; He, M.; Xie, Y.-L., In situ XRD, Raman, and TPR studies of CuO/Al2O3 catalysts for CO oxidation. *Journal of Molecular Catalysis A: Chemical* **2005,** *239* (1-2), 243-248.
124. Ren, H.; Xu, C.-H.; Zhao, H.-Y.; Wang, Y.-X.; Liu, J.; Liu, J.-Y., Methanol synthesis from CO2 hydrogenation over Cu/γ-Al2O3 catalysts modified by ZnO, ZrO2 and MgO. *Journal of Industrial and Engineering Chemistry* **2015,** *28*, 261-267.

125. Bligaard, T.; Nørskov, J. K., Chapter 4 - Heterogeneous Catalysis. In *Chemical Bonding at Surfaces and Interfaces*, Nilsson, A.; Pettersson, L. G. M.; Nørskov, J. K., Eds. Elsevier: Amsterdam, 2008; pp 255-321.
126. Tagawa, T.; Nomura, N.; Shimakage, M.; Goto, S., Effect of supports on copper Catalysts for Methanol Synthesis from CO2 + H2. *Research on Chemical Intermediates* **1995,** *21* (2), 193-202.
127. Liu, C.; Guo, X.; Guo, Q.; Mao, D.; Yu, J.; Lu, G., Methanol synthesis from CO2 hydrogenation over copper catalysts supported on MgO-modified TiO2. *Journal of Molecular Catalysis A: Chemical* **2016,** *425*, 86-93.
128. Guo, X.; Mao, D.; Lu, G.; Wang, S.; Wu, G., The influence of La doping on the catalytic behavior of Cu/ZrO2 for methanol synthesis from CO2 hydrogenation. *Journal of Molecular Catalysis A: Chemical* **2011,** *345* (1), 60-68.
129. Gao, P.; Li, F.; Zhan, H.; Zhao, N.; Xiao, F.; Wei, W.; Zhong, L.; Wang, H.; Sun, Y., Influence of Zr on the performance of Cu/Zn/Al/Zr catalysts via hydrotalcite-like precursors for CO2 hydrogenation to methanol. *Journal of Catalysis* **2013,** *298*, 51-60.
130. Wu, G.; Wang, X.; Wei, W.; Sun, Y., Fluorine-modified Mg–Al mixed oxides: a solid base with variable basic sites and tunable basicity. *Applied Catalysis A: General* **2010,** *377* (1-2), 107-113.
131. Xaba, B. S.; Mahomed, A. S.; Friedrich, H. B., The effect of CO2 and H2 adsorption strength and capacity on the performance of Ga and Zr modified Cu-Zn catalysts for CO2 hydrogenation to methanol. *Journal of Environmental Chemical Engineering* **2021,** *9* (1), 104834.
132. Zhang, L.-x.; Zhang, Y.-c.; Chen, S.-y., Effect of promoter TiO2 on the performance of CuO-ZnO-Al2O3 catalyst for CO2 catalytic hydrogenation to methanol. *Journal of Fuel Chemistry and Technology* **2011,** *39* (12), 912-917.
133. Tokay, K. C.; Dogu, T.; Dogu, G., Dimethyl ether synthesis over alumina based catalysts. *Chemical Engineering Journal* **2012,** *184*, 278-285.
134. Fischer, H.; Wahlen, M.; Smith, J.; Mastroianni, D.; Deck, B., Ice core records of atmospheric CO2 around the last three glacial terminations. *Science* **1999,** *283* (5408), 1712-1714.
135. Wang, W.; Wang, S.; Ma, X.; Gong, J., Recent advances in catalytic hydrogenation of carbon dioxide. *Chemical Society Reviews* **2011,** *40* (7), 3703-3727.
136. Xiaoding, X.; Moulijn, J. A., Mitigation of CO2 by Chemical Conversion: Plausible Chemical Reactions and Promising Products. *Energy & Fuels* **1996,** *10* (2), 305-325.
137. Natesakhawat, S.; Lekse, J. W.; Baltrus, J. P.; Ohodnicki, P. R.; Howard, B. H.; Deng, X.; Matranga, C., Active Sites and Structure–Activity Relationships of Copper-Based Catalysts for Carbon Dioxide Hydrogenation to Methanol. *ACS Catalysis* **2012,** *2* (8), 1667-1676.
138. Agarwal, A. S.; Rode, E.; Sridhar, N.; Hill, D., Conversion of CO2 to Value-Added Chemicals: Opportunities and Challenges. In *Handbook of Climate Change Mitigation and Adaptation*, Chen, W.-Y.; Suzuki, T.; Lackner, M., Eds. Springer New York: New York, NY, 2014; pp 1-40.

139. Etim, U. J.; Song, Y.; Zhong, Z., Improving the Cu/ZnO-Based Catalysts for Carbon Dioxide Hydrogenation to Methanol, and the Use of Methanol As a Renewable Energy Storage Media. *Frontiers in Earth Science* **2020,** *8*.
140. Qaderi, J., A brief review on the reaction mechanisms of CO2 hydrogenation into methanol. *International Journal of Innovative Research and Scientific Studies* **2020,** *3* (2), 53-63.
141. An, X.; Li, J.; Zuo, Y.; Zhang, Q.; Wang, D.; Wang, J., A Cu/Zn/Al/Zr Fibrous Catalyst that is an Improved CO2 Hydrogenation to Methanol Catalyst. *Catalysis Letters* **2007,** *118* (3), 264-269.
142. Dalebout, R.; Visser, N. L.; Pompe, C. E. L.; de Jong, K. P.; de Jongh, P. E., Interplay between carbon dioxide enrichment and zinc oxide promotion of copper catalysts in methanol synthesis. *Journal of Catalysis* **2020,** *392*, 150-158.
143. Fisher, I. A.; Bell, A. T., In Situ Infrared Study of Methanol Synthesis from H2/CO over Cu/SiO2and Cu/ZrO2/SiO2. *Journal of Catalysis* **1998,** *178* (1), 153-173.
144. Jiao, Y.; Liu, Y.; Zhu, G.; Hungerford, J. T.; Bhattacharyya, S.; Lively, R. P.; Sholl, D. S.; Walton, K. S., Heat-Treatment of Defective UiO-66 from Modulated Synthesis: Adsorption and Stability Studies. *The Journal of Physical Chemistry C* **2017,** *121* (42), 23471-23479.
145. Farrusseng, D.; Aguado, S.; Pinel, C., Metal–organic frameworks: opportunities for catalysis. *Angewandte Chemie International Edition* **2009,** *48* (41), 7502-7513.
146. Liang, J.; Liang, Z.; Zou, R.; Zhao, Y., Heterogeneous catalysis in zeolites, mesoporous silica, and metal–organic frameworks. *Advanced Materials* **2017,** *29* (30), 1701139.
147. Rambau, K. M.; Musyoka, N. M.; Panek, R.; Franus, W.; Wdowin, M.; Manyala, N., Preparation of coal fly ash derived metal organic frameworks and their carbon derivatives. *Materials Today Communications* **2021,** *27*, 102433.
148. Wang, Y.; Qu, Q.; Liu, G.; Battaglia, V. S.; Zheng, H., Aluminum fumarate-based metal organic frameworks with tremella-like structure as ultrafast and stable anode for lithium-ion batteries. *Nano Energy* **2017,** *39*, 200-210.
149. Teo, B.; Chakraborty, A.; Kitagawa, Y.; Kayal, S., Experimental study of isotherms and kinetics for adsorption of water on Aluminium Fumarate. *International Journal of Heat and Mass Transfer* **2017,** *114*, 621-627.
150. Kobayashi, H.; Taylor, J. M.; Mitsuka, Y.; Ogiwara, N.; Yamamoto, T.; Toriyama, T.; Matsumura, S.; Kitagawa, H., Charge transfer dependence on CO2 hydrogenation activity to methanol in Cu nanoparticles covered with metal–organic framework systems. *Chemical Science* **2019,** *10* (11), 3289-3294.
151. Smyrnioti, M.; Ioannides, T., Dimethyl Ether Hydrolysis over WO3/γ-Al2O3 Supported Catalysts. *Catalysts* **2022,** *12* (4), 396.

152. Felgueiras, M. B. S.; Restivo, J.; Sousa, J. P. S.; Pereira, M. F. R.; Soares, O. S. G. P., Copper Supported on Mesoporous Structured Catalysts for NO Reduction. *Catalysts* **2022,** *12* (2), 170.
153. Kayal, S.; Chakraborty, A.; Teo, H. W. B., Green synthesis and characterization of aluminium fumarate metal-organic framework for heat transformation applications. *Materials Letters* **2018,** *221*, 165-167.
154. Coelho, J. A.; Ribeiro, A. M.; Ferreira, A. F. P.; Lucena, S. M. P.; Rodrigues, A. E.; Azevedo, D. C. S. d., Stability of an Al-Fumarate MOF and Its Potential for CO2 Capture from Wet Stream. *Industrial & Engineering Chemistry Research* **2016,** *55* (7), 2134-2143.
155. Kamyar, N.; Khani, Y.; Amini, M. M.; Bahadoran, F.; Safari, N., Copper-based catalysts over A520-MOF derived aluminum spinels for hydrogen production by methanol steam reforming: The role of spinal support on the performance. *International Journal of Hydrogen Energy* **2020,** *45* (41), 21341-21353.
156. Avgouropoulos, G.; Ioannides, T., Effect of synthesis parameters on catalytic properties of CuO-CeO2. *Applied Catalysis B: Environmental* **2006,** *67* (1), 1-11.
157. Djinovic, P.; Batista, J.; Levec, J.; Pintar, A., Influence of morphological, redox and surface acidity properties on WGS activity of CuO–CeO2 catalysts. *Journal of Chemical Engineering of Japan* **2009,** *42* (Supplement.), s3-s9.
158. Peng, B.; Feng, C.; Liu, S.; Zhang, R., Synthesis of CuO catalyst derived from HKUST-1 temple for the low-temperature NH3-SCR process. *Catalysis Today* **2018,** *314*, 122-128.
159. Ye, Q.; Wang, L.; Yang, R. T., Activity, propene poisoning resistance and hydrothermal stability of copper exchanged chabazite-like zeolite catalysts for SCR of NO with ammonia in comparison to Cu/ZSM-5. *Applied Catalysis A: General* **2012,** *427-428*, 24-34.
160. Farrusseng, D.; Daniel, C.; Hamill, C.; Casaban, J.; Didriksen, T.; Blom, R.; Velte, A.; Fueldner, G.; Gantenbein, P.; Persdorf, P.; Daguenet-Frick, X.; Meunier, F., Adsorber heat exchanger using Al-fumarate beads for heat-pump applications – a transport study. *Faraday Discussions* **2021,** *225* (0), 384-402.
161. Shi, Z.; Tan, Q.; Tian, C.; Pan, Y.; Sun, X.; Zhang, J.; Wu, D., CO2 hydrogenation to methanol over Cu-In intermetallic catalysts: Effect of reduction temperature. *Journal of Catalysis* **2019,** *379*, 78-89.
162. Stangeland, K.; Kalai, D.; Li, H.; Yu, Z., CO2 Methanation: The Effect of Catalysts and Reaction Conditions. *Energy Procedia* **2017,** *105*, 2022-2027.
163. Joo, O.-S.; Jung, K.-D.; Moon, I.; Rozovskii, A. Y.; Lin, G. I.; Han, S.-H.; Uhm, S.-J., Carbon Dioxide Hydrogenation To Form Methanol via a Reverse-Water-Gas-Shift Reaction (the CAMERE Process). *Industrial & Engineering Chemistry Research* **1999,** *38* (5), 1808-1812.
164. Bonura, G.; Cordaro, M.; Cannilla, C.; Arena, F.; Frusteri, F., The changing nature of the active site of Cu-Zn-Zr catalysts for the CO2 hydrogenation reaction to methanol. *Applied Catalysis B: Environmental* **2014,** *152-153*, 152-161.

165. Joo, S. H.; Park, J. Y.; Tsung, C.-K.; Yamada, Y.; Yang, P.; Somorjai, G. A., Thermally stable Pt/mesoporous silica core–shell nanocatalysts for high-temperature reactions. *Nature materials* **2009,** *8* (2), 126-131.